UNIVERSIDAD POLITÉCNICA DE MADRID
Escuela Técnica Superior de Ingenieros Navales

Numerical tools for the assessment of offshore wind platforms

D O C T O R A L T H E S I S

Submitted for the degree of Doctor by:

Irene Berdugo Parada
Master's degree in Hydrodynamics for Ocean Engineering

Madrid, 2025

UNIVERSIDAD POLITÉCNICA DE MADRID
Escuela Técnica Superior de Ingenieros Navales

Doctoral Degree in Naval Architecture, Marine and Ocean Engineering

Numerical tools for the assessment of offshore wind platforms

DOCTORAL THESIS

Submitted for the degree of Doctor by:

Irene Berdugo Parada
Master's degree in Hydrodynamics for Ocean Engineering

Under the supervision of:
Dr. Julio García Espinosa
Dr. Borja Serván Camas

Madrid, 2025

Title: Numerical tools for the assessment of offshore wind platforms

Author: Irene Berdugo Parada

Doctoral Programme: Naval Architecture, Marine and Ocean Engineering

Thesis Supervision:

Prof. Julio García Espinosa (Supervisor). Full professor. Universidad Politécnica de Madrid.

Dr. Borja Serván Camas (Co-supervisor). Associate Research Professor. Centro Internacional de Métodos Numéricos en la Ingeniería (CIMNE).

External Reviewers:

Thesis Defense Committee:

Thesis Defense Date:

This work was financially supported by the International Centre for Numerical Methods in Engineering (CIMNE) as part of the Severo Ochoa program. The present research has been carried out within the scope of the European program Horizon 2020 Research and Innovation, with grant numbers 101006860 (FIBRE4YARDS project) and 952966 (FIBREGY project). In addition, this work was partially supported by the "Ministerio de Ciencia e Innovación" under grant agreement MLAMAR (ref. PID2021-126561OB-C31). All this support is gratefully acknowledged.

Acknowledgement

In the first place, I would like to thank my thesis supervisors, Dr. Borja Serván Camas, and Prof. Julio García Espinosa, for guiding me throughout this journey. Their experience and support have been fundamental to complete this research. Thank you for the time and trust you placed in me from the very beginning. I am honored to have had the opportunity to learn from you and your commitment to academic excellence.

I would like to extend my gratitude to the International Centre for Numerical Methods in Engineering for giving me the opportunity to develop a professional career as a researcher. Additionally, I am grateful for the help provided by Compass Ingeniería y Sistemas and its entire team. Furthermore, I am deeply thankful to the National Renewable Energy Laboratory for their warm welcome and the support provided by their team during my stay in Colorado. Their experience contributed significantly to this work.

This project also belongs, to all those who have been part of my academic journey. Thanks to my colleagues from the NT3 building, especially to the CAMMS group. Your daily support during the long days of research made this work much simpler and more enjoyable.

To my friends, who remain indispensable to me no matter how much time passes. Without a doubt, the good times we have spent together have been a constant source of strength and motivation. I cannot forget my family, especially my sister Sandra, for the support received.

Finally, I have a lot to be grateful for to Nacho, for his patience and understanding. Thank you for your encouragement and for believing in me.

Abstract

Floating offshore wind turbines (FOWT) are a promising solution to capture the wind energy potential found in the oceans. However, these structures face aggressive environmental conditions that can jeopardize their structural integrity. In that account, their design relies on the use of modeling tools that can simulate the entire coupled system behavior. To address this challenge, this doctoral thesis presents a comprehensive numerical framework for the simulation of floating offshore wind turbines. The developed tool allows for their integrated load analysis (ILA) by obtaining their structural response under combined wind-wave excitation.

Efforts to reduce the levelized cost of energy produced by FOWTs are driving the development of larger and lightweight platforms. This upscaling increases their energy production capacity, but also might introduce significant elastic deformations, which makes them prone to fatigue damage. Research is now focused not only on optimizing energy generation but also on extending the operational lifespan of these platforms. In this context, the present framework incorporates a reduced order solution for detailed structural analysis. A novel hydroelastic strategy based on the Modal Matrix Reduction (MMR) technique is proposed and tested. This approach allows for the simulation of the elastic behavior of floating turbines, capturing local stresses and identifying potential hotspots for fatigue failure.

The marine energy field is a sector undergoing exponential growth, open to diverse incoming structural designs and bringing with it new engineering challenges. Among these, multi-rotor concepts stand out as an interesting alternative to the upscaling of wind turbines. Due to the innovative nature of these systems, the numerical solvers for their assessment are at a lower level of maturity. In this regard, within this dissertation, a methodology is proposed to extend the present tool allowing for the simulation of multi-turbine systems.

The core idea of this research is to design a tool aligned with the advances in the marine wind energy sector, promoting its growth while overcoming current numerical limitations. As a result, this work provides a robust numerical solution for the simulation of FOWTs, combining high-fidelity models with affordable computational costs.

Resumen

Las plataformas eólicas flotantes son una solución prometedora para capturar el potencial energético del viento que se encuentra en los océanos. Sin embargo, estas estructuras están sujetas a condiciones ambientales agresivas que podrían poner en peligro su integridad estructural. En este sentido, su diseño depende del uso de herramientas de modelado que puedan simular el comportamiento de todo el sistema acoplado. Para abordar este desafío, esta tesis doctoral presenta un marco numérico completo para la simulación de turbinas flotantes. La herramienta desarrollada permite realizar análisis acoplados obteniendo su respuesta estructural bajo cargas combinadas de viento y oleaje.

Los esfuerzos por reducir el coste nivelado de la energía producida por la eólica flotante están impulsando el desarrollo de plataformas cada vez más grandes y ligeras. Como consecuencia del aumento estructural destinado a mejorar la capacidad de producción energética, también podrían generarse deformaciones elásticas significativas, siendo propensas a daños por fatiga. La investigación actual se centra no solo en optimizar la generación de energía, sino también en extender la vida útil operativa de estas plataformas. En este contexto, la herramienta desarrollada incorpora una solución de orden reducido para poder realizar análisis estructurales de detalle. Se propone y verifica una nueva estrategia hidroelástica basada en la técnica de Reducción de la Matriz Modal. Esta metodología permite simular el comportamiento elástico de las turbinas flotantes, capturando tensiones locales e identificando posibles puntos críticos para fallos por fatiga.

El campo de la energía marina es un sector en desarrollo exponencial, abierto a diversos diseños estructurales emergentes, lo que trae consigo nuevos desafíos para la ingeniería. Entre estos, los conceptos multi-rotor destacan como una alternativa interesante frente al escalado de turbinas eólicas. Debido al carácter innovador de estos sistemas, los códigos numéricos para su evaluación están en un nivel de madurez inferior. En consecuencia, dentro de esta disertación, se propone una metodología para extender la herramienta actual permitiendo la simulación de sistemas con múltiples turbinas.

La idea central de esta investigación es diseñar una herramienta alineada con los avances en el sector de la energía eólica marina, promoviendo su crecimiento y superando las limitaciones numéricas actuales. Como resultado, este trabajo proporciona una solución numérica robusta para la simulación de turbinas eólicas flotantes, combinando modelos de alta fidelidad con costes computacionales asequibles.

Table of Contents

List of Figures

List of Tables

Acronyms

FOWT Floating Offshore Wind Turbine

HAWT Horizontal Axis Wind Turbine

AHSE Aero-Hydro-Servo-Elastic

LCOE Levelized Cost of Energy

BEMT Blade Element Momentum Theory

FVM Free Vortex Method

ILA Integrated Load Analysis

FEM Finite Element Method

BEM Boundary Element Method

GDW Generalized Dynamic Wake

DS Dynamic Stall

RANS Reynolds-Averaged Navier-Stokes

LES Large Eddy Simulation

SPH Smoothed-Particle Hydrodynamics

R-B Rigid-Body

M-B Multi-Body

LBT Linear Beam Theory

3D-FEM 3D Finite Element Method

PF Potential Flow

ME Morison Equation

QS Quasi Static

LM Lumped Mass

FE Finite Element

IEA International Energy Agency

OC3 Offshore Code Comparison Collaboration

OC4 Offshore Code Comparison Collaboration Continuation

MMR Modal Matrix Reduction

ROM Reduced Order Model

CFD Computational Fluid Dynamics

RAO Response Amplitude Operator

SF SeaFEM

OF OpenFAST

RK4 Runge–Kutta Method

NREL National Renewable Energy Laboratory

DLL Dynamic-Link Library

RK4 Runge–Kutta Method

FRP Fiber-Reinforced Polymer

MARIN Maritime Research Institute Netherlands

DOF Degree of Freedom

DT Digital Twin

SHM Structural Health Monitoring

RNA Rotor-Nacelle Assembly

CG Center of Gravity

DLC Design Load Case

JONSWAP Joint North Sea Wave Project

SWL Sea Water Level

C-B Craig-Bampton

NTM Normal Turbulence Model

SSS Severe Sea State

MRAO Modal Response Amplitude Operator

Symbols

C_l	Lift Coefficient
C_d	Drag Coefficient
T	Thrust
Q	Torque
B	Number of blades
U_∞	External flow velocity
α	Local flow angle
a	Axial induced velocity
a'	Angular induced velocity
ω	Rotor rotational speed
Γ	Circulation
dl	Filament length
Φ	Mode shape
q_e	Elastic motions vector
u	Displacement field
M	Mass matrix
M^a	Added mass
F	Load vector
F_I	Wave exciting force
F_B	Radiation damping force
F_D	Viscous drag force
F_M	Mooring restoring force
F_H	Hydrostatic force
q	Platform motions vector
C	Damping matrix
K	Stiffness matrix
r_i	Mooring motions vector
T_i	Mooring tension
φ	Velocity potential
ξ	Free surface elevation
Γ_B	Body wetted surface
Γ_S	Sea bottom surface
Ω	Domain
z_p	Vertical position
r_{pz}	Vertical displacement
P_P	Pressure at a point P
D	Displacements
V	Velocities
A	Accelerations
I_{ij}	Inertia terms
L	Laplacian matrix
σ	Stress tensor
b	Boundary integration vector
Ω_s	Structural domain
u	Structural displacements
t	Structural traction
S_u	Surface with displacements
S_σ	Surface with tractions
n	Normal vector
S	Tangent stiffness matrix
a_i	Eigenvectors
Ω_i	Vibration frequency
q_i	Modal amplitudes
E	Structural energy
E^D	Dynamic structural energy
η	Critical damping
c_i	Rayleigh damping
S_w	Wave energy spectrum
S_m	Structural energy spectrum
$I^{F\to S}$	Interpolation matrix

Chapter 1

Introduction

1.1 Floating wind energy background

The United Nations has called for urgent action to achieve net-zero greenhouse gas emissions by 2050, emphasizing the pivotal role of renewable energy in global decarbonization efforts. Among these, wind energy stands out for its significant contribution, as it replaces traditional fossil fuel-based energies. In particular, the floating offshore wind energy, due to the vast energy potential found in the deep seas, has seen exponential growth in recent years. However, despite this progress, the technology remains in its early stages compared to the onshore wind industry.

The renewable energy market share is growing steadily. In 2022, renewable sources accounted for 29.1% of global electricity generation. Since 2010, solar and wind energy have driven the most significant growth in renewable electricity, collectively contributing 11.7% to the global energy mix by 2022. Projections indicate that the planned installation of 6,044 GW of wind energy could supply more than one-third of the total electricity demand by 2050 [IRENA, 2024].

The offshore wind energy industry is maturing rapidly, particularly in Europe and Asia. In 2023, a total of 6,326 MW of offshore wind capacity was added worldwide, bringing the cumulative installed capacity to 68,258 MW. This represents a 10.2% increase compared to the end of 2022, with the majority being bottom-fixed installations. Nearly half (46.1%) of the new capacity was commissioned in China, followed by the United Kingdom as the next largest contributor. Technological advancements and sector development have driven a remarkable 59% reduction in the weighted-average levelized cost of offshore wind, decreasing from 0.197 to 0.081 USD per kilowatt-hour (kWh) between 2010 and 2022. Projections indicate that

global offshore wind energy will reach 492 GW by 2035 [McCoy et al., 2024].

From this offshore wind energy capacity, the floating solutions still represent a minor section. In 2023, the operating floating offshore wind capacity reached 234 MW. However, a significant growth is expected, reaching the 14 GW of floating wind to be installed globally by 2029 and 18 GW in Europe by 2035 [IRENA, 2024]. The majority of the pipeline remains in the planning phase, highlighting the early development stage of this technology. Figure 1.1 presents the cumulative floating offshore wind energy capacity by country in Europe. A detailed pie chart is shown with the installed capacity as a percentage by country in 2023.

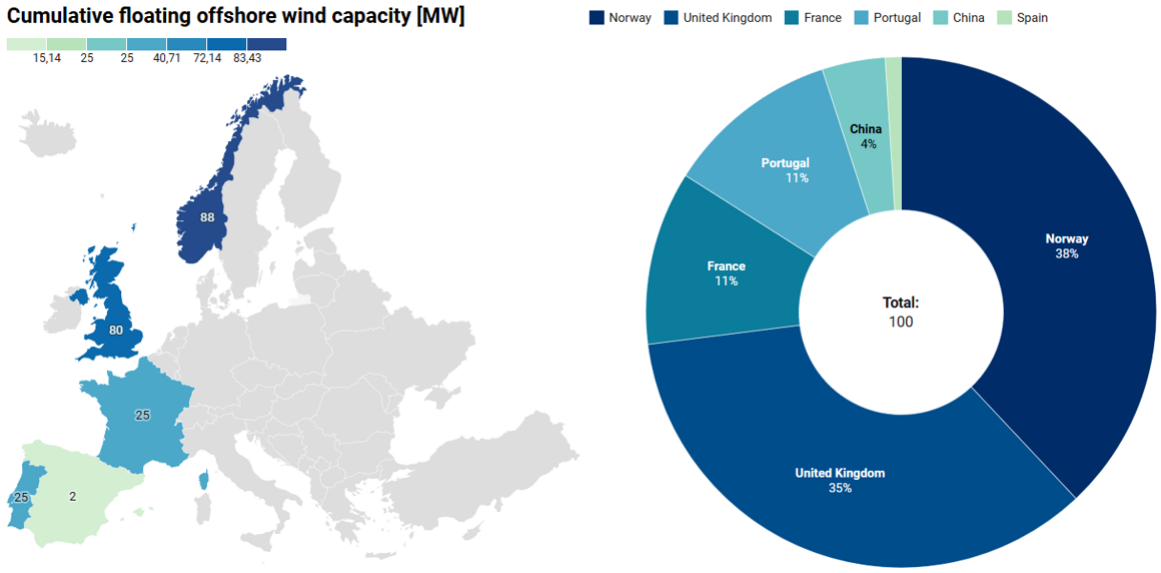

Figure 1.1: Estimated cumulative floating offshore wind capacity by country (Data from [McCoy et al., 2024]).

From the 234 MW commissioned in 2023, the largest operational floating offshore wind farm is the 88-MW Hywind Tampen in Norway. Other relevant floating farms connected to the grid are the Kincardine (United Kingdom - 50 MW), Hywind Scotland (United Kingdom - 30 MW), Windfloat Atlantic (Portugal - 25 MW) and Provence Grand Large (France - 25 MW).

The expected development in floating technology marks a transition from pilot-scale projects to full commercial-scale deployment. The majority of announced deployments through 2029 are in the United Kingdom (4,242 MW), Italy (4,160 MW), Taiwan (1,530 MW) and China (1,052 MW) [McCoy et al., 2024]. However, most of these projects remain in the planning phase, introducing a significant level of uncertainty. Figure 1.2 shows the announced floating projects classified by their size and depth for each country.

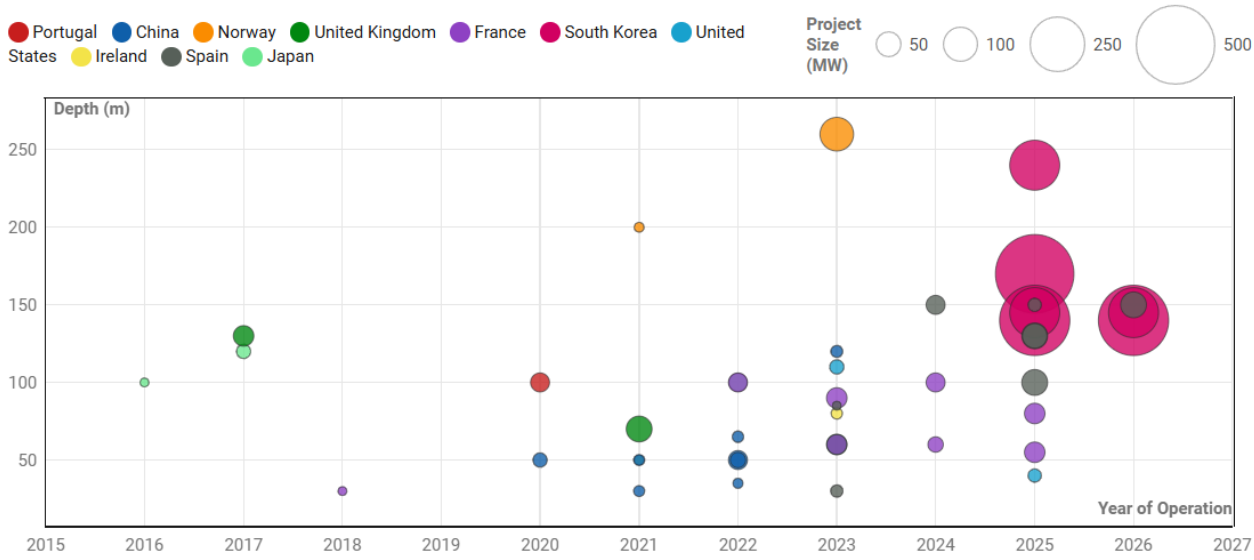

Figure 1.2: Announced floating offshore wind projects by country (Data from [Bosnjakovic et al., 2022 and Zhang et al., 2024]).

Spain is also positioning itself to integrate floating offshore wind into its energy mix, aiming to install up to 3 GW by 2030. The country's first floating offshore wind platform, the DemoSATH, started generating electricity to Spain's national grid in 2023. Its turbine capacity is 2 MW, and the project is located at the coast of Bilbao [IRENA, 2024].

The current levelized cost of electricity (LCOE) for floating wind exceeds USD 0.2/kWh, primarily due to the small scale of existing farms and early-stage developments. However, ongoing technological advancements are expected to drive a 59% reduction in costs, following the trend observed in offshore wind [McCoy et al., 2024].

1.2 Floating offshore wind technology

As highlighted in the previous section, offshore wind energy is becoming an interesting option, expecting a significant growth as a result. This is primarily due to the advantages of ocean winds, which are generally stronger, more stable, and less prone to fluctuations, resulting in a more reliable energy generation. The absence of obstructions allows the wind to flow at higher and steadier speeds. Furthermore, offshore winds experience lower turbulence and reduced wind shear compared to onshore winds, enhancing the efficiency of energy production. Additionally, this technology presents an opportunity for regions with steep seabed drops (such as Japan, China, the United States and Europe) to position wind farms much farther from the coastline.

Nearly all offshore wind turbines installed to date have been built on fixed foundations in shallow or transitional waters. Monopiles remain the most common substructure choice for announced offshore projects, accounting for more than half (55.6%). However, since fixed foundations are limited to depths of around up to 60 meters, the industry is now advancing into deeper waters with the development of floating wind technologies.

In the coming decade, the focus of wind turbine trends will be on scaling up their size. Larger rotor diameters will enable turbines to sweep a greater area, capture more wind, and consequently generate more electricity. This continuous increase of power output, reaching capacities of up to 20 MW, represents an ambitious target that is still not feasible for the onshore wind technology [Bosnjakovic et al., 2022]. The evolution of rotor size in land-based and offshore turbines is illustrated in Figure 1.3.

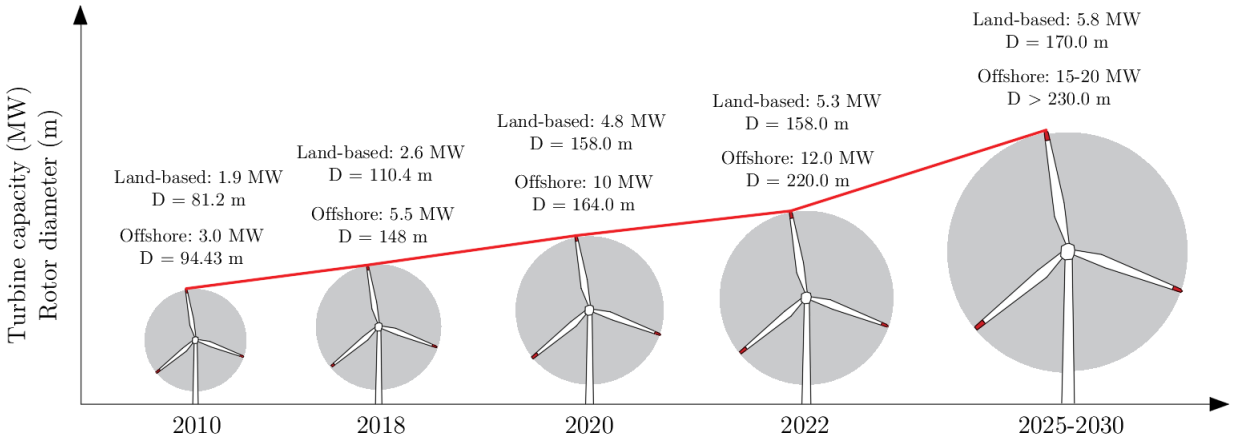

Figure 1.3: Upscaling of land-based and offshore wind turbines (Data from [Bosnjakovic et al., 2022]).

In 2023, global offshore wind installations featured turbines with an average capacity of 9.7 MW, representing a 26% year-over-year increase. The average rotor diameter reached 183.4 meters, making a 5% increase compared to the previous year. Moreover, turbine towers are becoming taller to capture more energy, since wind speeds generally increase with altitude. The average hub height in 2023 was 124.0 meters, reflecting a 6% year-over-year increase [McCoy et al., 2024].

The offshore wind sector is evolving searching for optimal solutions leading to the development new structural concepts. However, the optimal floating configuration remains uncertain, since the sector is still in its early design stages. As an emerging industry, floating offshore wind is currently in a testing and evaluation phase, with ongoing research and pilot projects to refine designs and identify the most effective technologies.

The available structural concepts are mainly classified depending on its principle to achieve stability. Spar platforms use its ballast to lower the center of mass below the center of buoyancy. In contrast, tension leg platforms (TLP) use an excess of buoyancy to generate a mooring-line tension, while barge concepts achieve stability through its water-plane area [Butterfield et al., 2007]. Other possibilities can be found, such as multi-rotors, that are platforms handling several wind turbines. The described concepts are displayed in Figure 1.4, along with a bar chart showing the global substructure capacities.

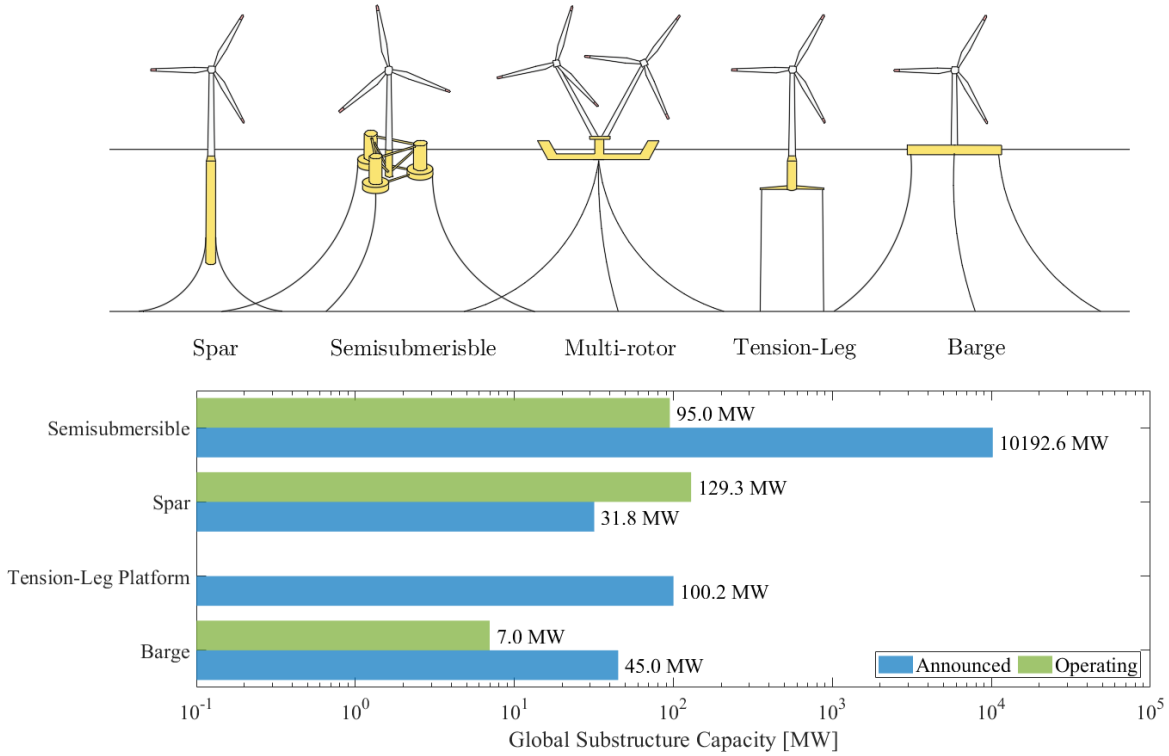

Figure 1.4: Main categories of floating offshore wind turbine foundations and global capacity (Data from [McCoy et al., 2024]).

Most of the announced floating wind farm projects are favoring semi-submersible substructures, mainly due to their relatively shallow draft and stability in terms of seakeeping. However, there is still no clear consensus on a preferred design, as the foundation choice is often made depending on the specific site conditions. Currently, 135 floating substructure concepts are competing for market share in upcoming projects [McCoy et al., 2024]. As the industry evolves, further structural innovations are expected to emerge.

1.3 Numerical simulation of FOWTs

The study of floating offshore wind turbines (FOWTs) is essential to ensure their reliability and to optimize both design and costs. Numerical simulation tools play a key role in this analysis. However, modeling floating horizontal axis wind turbines (HAWTs) is particularly challenging due to the strong coupling between wind loads acting on the turbine and wave loads on the floating platform. In order to address this complex multi-physics problem, numerical frameworks designed for the integrated load analysis of FOWTs must account for their fully coupled aero-hydro-servo-elastic (AHSE) response [He et al., 2024].

Current numerical tools for analyzing floating wind turbines are based on similar models and theoretical foundations. These tools simulate the entire multiphysics problem using interconnected modules. Below is an outline of the key physics and numerical modules relevant to this work.

Aerodynamics:

The wind loads acting over the rotor are generally modeled using the Blade Element Momentum Theory (BEMT) [Moriarty and Hansen, 2005]. This approach solves the aerodynamic effects combining the blade element theory and momentum theory, see Figure 1.5.

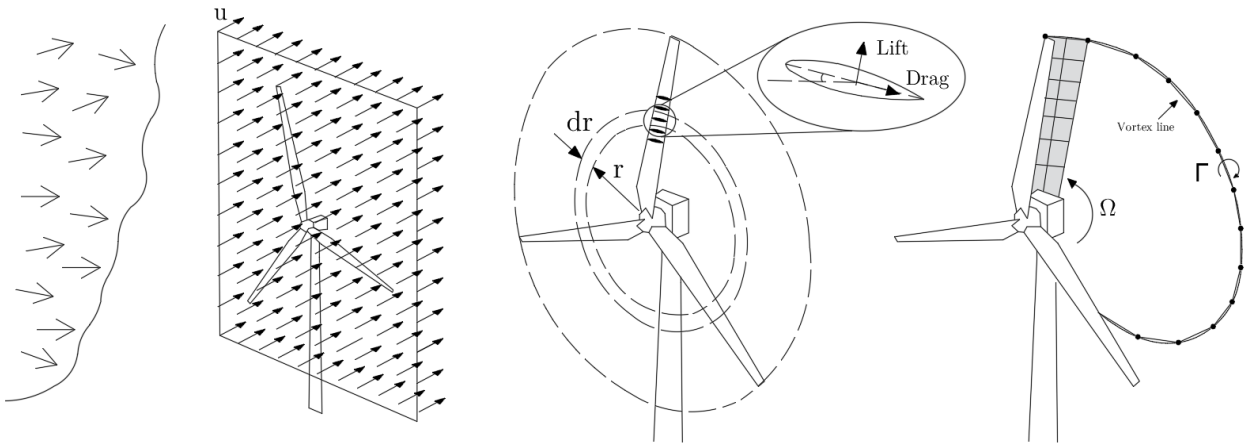

Figure 1.5: Left: turbulent wind field. Center: BEMT applied on a wind turbine. Right: FVM evolution of near-wake field.

The blade element theory divides each turbine blade into a certain number of two-dimensional airfoils along the span. Each of them is considered to operate independently based on the local flow conditions. The tables of lift and drag coefficients are included as a function of the angle of attack. Then, the thrust T and torque Q distributed around an annular segment of width dr are calculated using the drag C_d and lift C_l coefficients, as shown in Eqs. (1.1).

$$dT = B\frac{1}{2}\rho U_\infty^2 \left(C_l \cos\alpha + C_d \sin\alpha\right) c dr \qquad dQ = B\frac{1}{2}\rho U_\infty^2 \left(C_l \sin\alpha - C_d \cos\alpha\right) c r dr \tag{1.1}$$

Where B stands for the number of blades, U_∞ the external flow velocity, α the local flow angle, and c the chord length.

Meanwhile, the momentum theory is an extension of the actuator disk theory by accounting for the loss of airflow momentum as it passes through the rotor plane. Then, the thrust and torque forces can be derived from the induced velocities caused by this momentum loss. These velocities affect both the inflow and the forces received by the airfoils, hence the need to combine both methods. The thrust and torque are related to the induced velocities in Eqs. (1.2), being a and a' the axial and angular induced velocities, and Ω the rotor's rotational speed.

$$dT = 4\pi r \rho U_\infty^2 (1-a) a dr \qquad dQ = 4\pi r^3 \rho U_\infty \omega (1-a) a' dr \tag{1.2}$$

The Free Vortex Method (FVM) is an alternative to BEM theory for modeling the vortex structure in a wind turbine's wake, see Figure 1.5 (right). Based on potential flow theory, it represents the wake as vortex filaments shed from the blades trailing edges, with the turbine blades modeled as lifting lines. The wake follows a helical structure, discretized based on the rotor speed [Tian et al., 2024]. While FVM provides a more accurate approach than BEMT, it comes with a higher computational cost. The induced velocities of a line filament at a point are computed using the Biot-Savart law.

$$\mathbf{V}_{ind} = \frac{\Gamma}{4\pi}\frac{d\mathbf{l} \times \mathbf{r}}{|\mathbf{r}|^3} \tag{1.3}$$

Where Γ is the circulation, dl an elementary length along the filament and r the vector between the filament vortex and the control point.

Structural elasticity:

The structural elastic behavior of FOWTs is typically modeled using linear beam theory. This elastic solution is usually divided into two modules: one for the tower deflections and another accounting for the blade ones, as shown in Figure 1.6. These models combine a modal and multi-body dynamics formulation, where the flexibility is characterized using a linear modal representation [Branlard and Geisler, 2021].

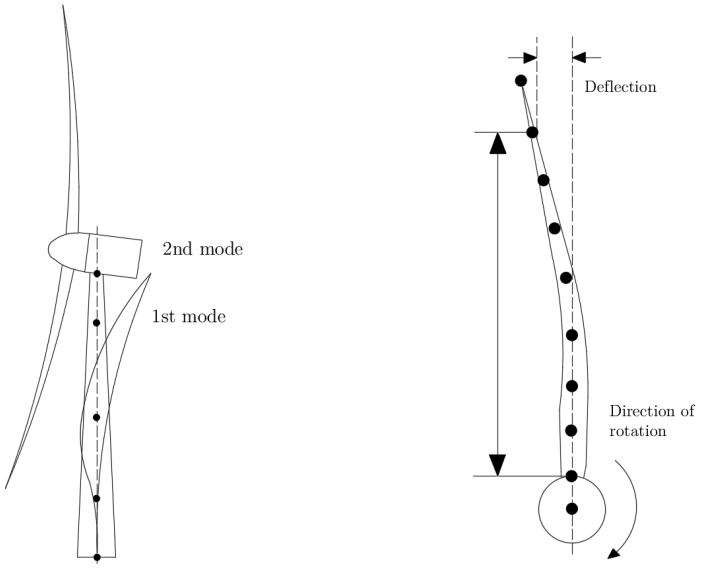

Figure 1.6: Left: Tower two fore-aft bending modes. Right: Blade beam discretization.

The elastic behavior of the beam components is defined by their material properties, including stiffness and mass, as well as their mode shapes. Usually, each blade allows for two flapwise and one edgewise bending mode, while the tower allows for two fore-aft and two side-to-side bending modes. The displacement field at a point P can then be computed as in Eq. (1.4) by modal superposition using its mode shapes $\mathbf{\Phi}$, where $\mathbf{q_e}$ are the elastic coordinates.

$$u(P,t) = \sum_{j=1}^{n_{e,i}} \mathbf{\Phi}_{ij}(P)\mathbf{q}_{\mathbf{e},ij}(t) \qquad \mathbf{M}(q_e)\ddot{\mathbf{q}}_\mathbf{e} = \mathbf{F}(q_e, \dot{q}_e, u, t) \tag{1.4}$$

Kane's method is used to obtain the multi-body dynamics by concatenating the motion equations of the individual bodies. The aero-hydro-elastic coupling is achieved by integrating the local aerodynamic and hydrodynamic loads as inputs into the structural motion equations of the flexible members. The floating platform, along with the nacelle and hub, are typically modeled as rigid bodies.

Hydrodynamics:

The hydrodynamic loads acting on the substructure are generally computed using the Morison equations and the potential flow theory [Jonkman et al., 2014]. Both methods are illustrated in Figure 1.7. Additionally, regular and irregular sea states, as well as ocean currents, can be modeled. The potential flow solution typically relies on an external code to solve the wave diffraction-radiation problem. This tool precomputes the frequency-dependent coefficients required for potential flow analysis using the Boundary Element Method (BEM), where the wet body and free surfaces are discretized using a panel method.

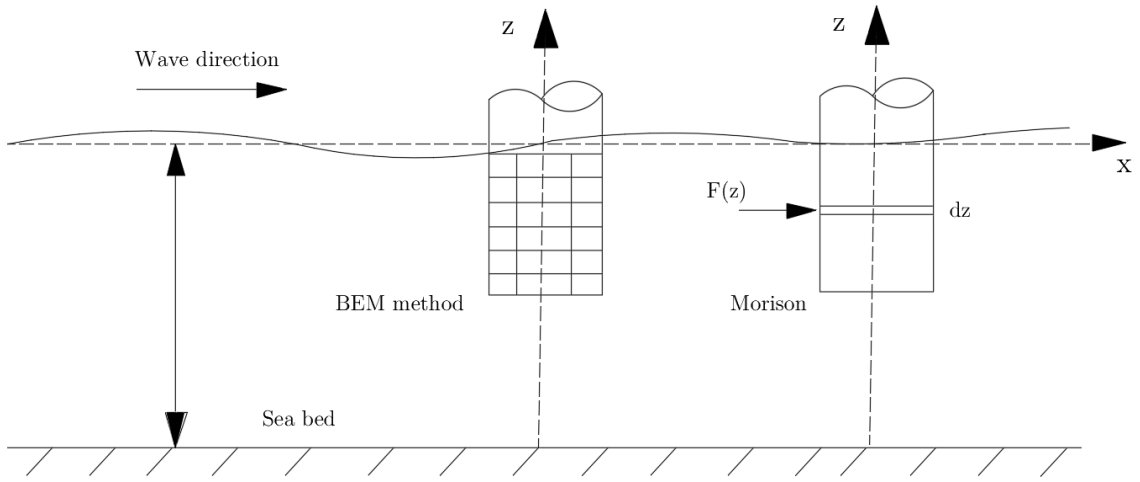

Figure 1.7: Representation of Boundary Element and Morison methods.

In the Morison approach, the structure is divided into cylindrical members, with hydrodynamic loads applied as lumped forces at the joints. The Morison approach accounts for the distributed fluid inertia, F_I, resulting from the wave pressure field acting on the structure (including Froude-Krylov and added-mass effects), as well as the viscous drag component, F_D, as expressed in:

$$F = \underbrace{\rho C_m V \dot{u}}_{F_I} + \underbrace{\frac{1}{2}\rho C_d A u|u|}_{F_D} \tag{1.5}$$

Both approaches can be combined to incorporate Morison's viscous drag within the potential diffraction-radiation solution. Then, the hydrodynamic load balance governing the motion equation of a floating body in the time domain can be expressed as:

$$[\mathbf{M} + \mathbf{M^a}]\,\ddot{\mathbf{q}} = \mathbf{F_I}(t) + \mathbf{F_B}(t, \dot{q}) + \mathbf{F_D}(t, \dot{q}) + \mathbf{F_M}(t, q) + \mathbf{F_H}(q) \tag{1.6}$$

Here, $\mathbf{q}$ is the platform motion vector, $\mathbf{F_I}$ is the wave exciting force, $\mathbf{F_B}$ is the radiation damping force, $\mathbf{F_D}$ is the nonlinear viscous drag force, $\mathbf{F_M}$ is the mooring restoring force and $\mathbf{F_H}$ is the hydrostatic force. $\mathbf{M}$ and $\mathbf{M^a}$ correspond to the floating body's mass and added mass, respectively.

Mooring dynamics:

The dynamics of mooring cables are typically modeled using either a dynamic or quasi-static approach [Hall and Goupee, 2015]. The dynamic model commonly utilizes a lumped-mass method to discretize the cable dynamics along the mooring line, as illustrated in Figure 1.8. In this method, the cable is divided into line segments connected by nodes, referred to as lumped masses.

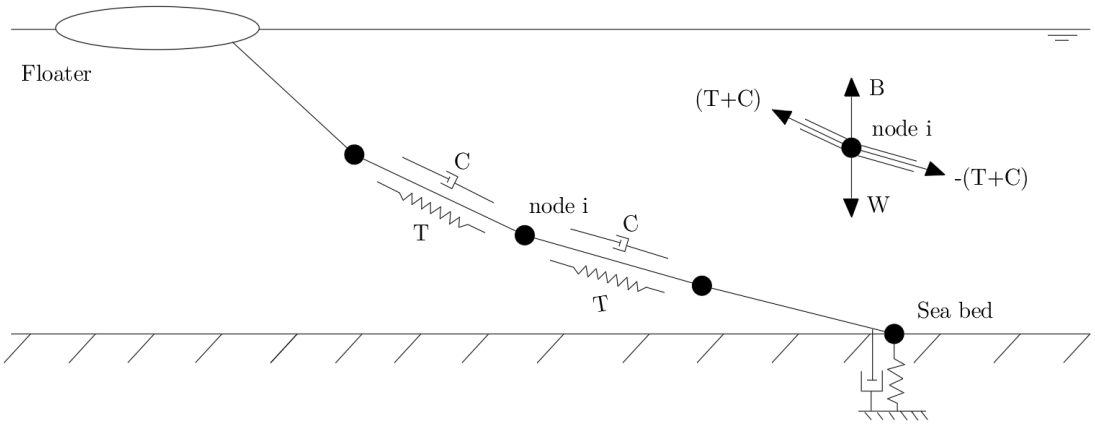

Figure 1.8: Mooring line discretization and cable loads.

This approach provides a more accurate solution by accounting for internal stiffness and damping, weight and buoyancy, hydrodynamic forces derived from Morison's equation, and vertical forces resulting from seabed contact. Hydrodynamic loads are directly computed at the nodes, where the motion equation is solved:

$$\underbrace{[m_i + a_i]}_{\text{mass and added mass}} \ddot{r}_i = \underbrace{T_{i+(1/2)} - T_{i-(1/2)} + C_{i+(1/2)} - C_{i-(1/2)}}_{\text{internal stiffness and damping}} + \underbrace{W_i + B_i}_{\text{weight and contact}} + \underbrace{D_{p_i} + D_{q_i}}_{\text{drag}} \tag{1.7}$$

The quasi-static approach solves the mooring line and tension using a set of analytical equations considering the catenary line in static equilibrium. The main limitation is that hydrodynamic and inertial loads are neglected.

Servo control:

The servo module is responsible for modeling the control systems and drivetrain dynamics of wind turbines, as shown in Figure 1.9.

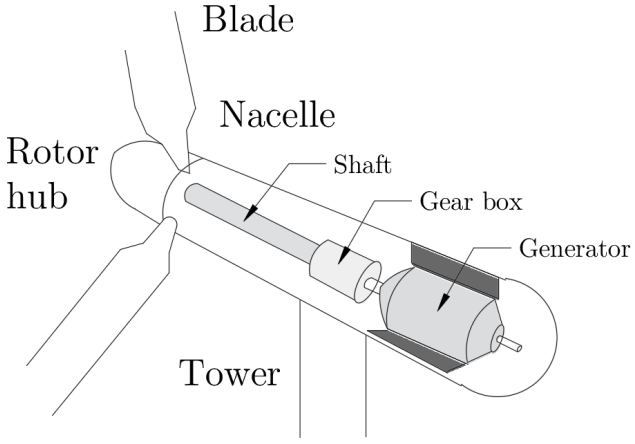

Figure 1.9: Main components of the wind turbine servo control.

It simulates the turbine's active control mechanisms, which manage blade pitch, generator torque, and yaw to optimize performance and ensure safe operation under varying wind conditions. The servo control allows simulating the blade pitch control to adjust power output and minimize aerodynamic loads. The system also includes generator torque control to manage rotor speed and maintain power stability. The yaw control system aligns the nacelle with the wind direction to maximize energy capture. Additionally, it accounts for gearbox efficiency and losses, along with the interaction between the generator and electrical systems.

1.4 Aero-hydro-servo-elastic solvers

The complexity of the multiphysics problem involving FOWTs results in less-developed simulation tools for its analysis, limiting the progress of this emerging technology. Accordingly, significant efforts are being made to improve their reliability, enabling the design of more cost-effective structural concepts [Otter et al., 2021].

The software packages used for modeling floating offshore wind turbines are typically classified as mid-fidelity or low-fidelity tools. These packages consist of interconnected modules, each dedicated to addressing a specific physical phenomenon using its own numerical technique. As a result, a wide range of numerical and physical modeling approaches are currently employed in the field, which are summarized in Table 1.1. The numerical modeling is roughly divided into four categories: hydrodynamics, aerodynamics, structural dynamics, and mooring dynamics.

Table 1.1: Fidelity of the numerical methods used for the analysis of FOWTs.

Aerodynamics			Body-Structural dynamics		
BEM	Blade Element Momentum	Mid	R-B	Rigid-Body	Mid
GDW	Generalized Dynamic Wake	Mid	M	Modal	Mid
DS	Dynamic Stall	Mid	M-B	Multi-Body	Mid
FVW	Lifting-Line Free Vortex Wake	Mid	LBT	Linear Beam Theory	High
RANS	Reynolds-Averaged Navier-Stokes	High	3D-FEM	3D Finite Element Method	High
LES	Large Eddy Simulation	High			
Hydrodynamics			Mooring dynamics		
PF	Potential Flow	Mid	QS	Quasi Static	Low
ME	Morison Equation	Mid	LM	Lumped Mass	Mid
BEM	Boundary Element Method	Mid	FE	Finite Element	High
RANS	Reynolds-Averaged Navier-Stokes	High			
SPH	Smoothed-Particle Hydrodynamics	High			

A broad range of software packages with different combinations of numerical techniques are available for the design of FOWT prototypes [Subbulakshmi et al., 2022]. These tools, referred to as aero-hydro-servo-elastic solvers, allow for the simulation of the coupled response of FOWTs to external wind and wave loads. An overview of the current state-of-the-art of simulation frameworks for FOWTs is provided in Table 1.2, where the dots indicate the numerical methods used in each framework.

Among these, OrcaFlex and OpenFAST are the most widely used options, known for their reliability. In particular, the aerodynamic solution of OpenFAST (AeroDyn) is integrated into several frameworks. Almost all of these tools rely on time-domain solutions and require input hydrodynamic coefficients from frequency-domain PF solvers, such as WAMIT, AQWA, and Nemoh to solve the radiation/diffraction problem and to include second-order effects. Solutions that require external solvers are indicated with a dash. The current available tools adapted for the solution of multi-rotors concepts are Qblade, MUST and CHARM3D.

Table 1.2: Aero-hydro-servo-elastic software packages.

	Hydrodynamics			Aerodynamics			Body-Structural dynamics					Mooring Dynamics		
	PF	ME	SO	BEMT	GDW	DS	R-B	M	M-B	LBT	FEP	QS	LM	FE
OpenFAST	-	•	-	•	•	•	•	•	•	•		•	•	•
OrcaFlex	•	•	•	OF	OF	OF	•	•	•	•			•	
Bladed-Sesam	•	•	•	•	•	•	•	•	•	•	•	•	•	•
Qblade	-	•	-	•	•	•	OF	•	OF	•		•		
Flexcom	-	•	-	OF	OF	OF	•	•	•	•		•	•	•
HAWC2	-	•	-	•	•	•	•	•	•	•		•		•
Simpack	-	OF	-	OF	OF	OF	•	•	•			•		
3DFloat	-	•	-	•		•	•			•				•
DeepLines Wind	•	•	•	•		•	•		•	•		•		•

The selection of a numerical modeling method typically involves balancing accuracy and fidelity against computational efficiency. Low-fidelity models are generally employed during the early stages of FOWT design and optimization. Mid-fidelity models, or engineering-level tools, are used to analyze operational conditions. High-fidelity models are used in the final design stages for investigations of local flow phenomena, or to accurately obtain stresses on the structure [Zhang et al., 2024]. Examples of higher-fidelity tools that are used standalone or typically combined with wind turbine simulation frameworks are given in Table 1.3.

Table 1.3: High-fidelity tools used in FOWT modeling.

Aero-hydro dynamics			Structural dynamics		
OpenFOAM	RANS	Campaña-Alonso et al., 2023	Nastran	3D-FEM	Kwangtae et al., 2021
ReFRESCO	RANS	Wang et al., 2022	Ansys	3D-FEM	Wiegard et al., 2021
Star-CCM+	RANS	Yao et al., 2023	Abaqus	3D-FEM	X. Song et al., 2024
SOWFA	LES	Chanprasert et al., 2022			
DualSPHysics	SPH	Tan et al., 2023			

Due to the complexity of these simulation codes, it is crucial to validate their accuracy with experimental data or through code-to-code comparisons [Fadaei et al., 2024]. To address this, the International Energy Agency (IEA) has launched several research initiatives, including the Offshore Code Comparison Collaboration (OC3) [Jonkman and Musial, 2010] and the Offshore Code Comparison Collaboration Continuation (OC4) [Robertson, Jonkman, Vorphal, et al., 2014] projects, which are used to confirm present work. The upcoming OC7 project will focus on the validation of CFD hydrodynamic viscous loads and structural member-level flexibility, according to the current numerical needs and trends.

1.5 Motivation and objectives

As highlighted in previous sections, the development of floating offshore wind turbines is rapidly evolving. However, the complexity and stochastic nature of marine conditions present significant challenges in their design. The development of numerical solvers for their analysis is crucial to understand the behavior of these systems, particularly for their structural assessment, in order to extend the lifespan of these structures. In this regard, reliable computational analysis models are essential for advancing FOWT technology.

Due to the coupling between the dynamics of the wind turbine under wind loads and the floater under wave and mooring loads, international standards demand the use of integrated load analysis for the certification of floating wind turbines. ILA aims to assess those interactions (i.e. aerodynamics, hydrodynamics, structural and mooring dynamics) and ensure the structure conforms with the design basis. At the moment, the certification of the structural concepts relies on coupled aero–hydrodynamic numerical simulations, being tested under several design load cases (DLCs). However, the complexity in the development and validation of high-fidelity strongly-coupled ILA models, along with the huge computational demand, are major barriers to establish reliable designs. In this context, this work aims to develop an ILA framework with a robust structural solution for the simulation of FOWTs under environmental excitation.

As outlined in previous sections, the floating wind industry is still in its early stages of development, with limited numerical tools available for performing coupled structural assessments of FOWTs. Most of the existing solvers rely on simplified numerical models due to the computational cost associated to higher-fidelity solutions, resulting in significant limitations in the available analysis technologies. Accordingly, there is a need to research more reliable aero-hydro-servo-elastic simulation tools. To address this, the present doctoral thesis aims to investigate in higher-fidelity numerical tools for the simulation of FOWTs. This research will align with current numerical trends, with a particular focus on enhancing hydrodynamic and structural solutions, without compromising the computational cost.

As offshore wind turbines continue to grow in size, their structures become more flexible. Consequently, understanding their structural-elastic behavior is becoming increasingly important. Moreover, the estimation of their fatigue damage during the design phase is essential for optimizing the structural design and ensuring a long service life. This process relies on advanced modeling tools to accurately capture local stresses. To meet this requirement, the proposed ILA framework includes a methodology to perform detailed structural assessments.

The main drawback of numerical structural solvers lies in their high computational cost. As a result, alternative techniques, such as reduced order models (ROM), are emerging. These methods reduce the solution complexity while preserving its fidelity by approximating the displacement field as a superposition of a few eigenmodes. This thesis explores the suitability of these models for the structural analysis of floating wind platforms. To do so, a ROM based on the modal matrix reduction (MMR) technique is proposed. This approach follows an energy criterion, significantly reducing the structural degrees of freedom by retaining only the most energetic eigenmodes. The method is coupled to a seakeeping solver in a whole FEM framework, enabling hydroelastic analysis.

Hydroelasticity is gaining increasing attention in the marine and offshore engineering fields. However, its application to floating offshore wind turbines is still scarce in the literature. As a result, their hydroelastic behavior remains still underexplored. In this context, the ROM is integrated into the current ILA framework, allowing for time-domain hydroelastic analyses and including two-way fluid-structure interactions. The proposed methodology also offers the flexibility to perform offline stress computations for more efficient post-processing and minimize the output data. These advanced capabilities are applied to assess the structural integrity of a floating platform in a coupled wind-wave analysis. A case study is presented in which critical conditions and hotspots are identified.

An interesting alternative to the up-scaling of wind turbines are multi-rotor concepts, which are starting to be studied. These configurations consist of a shared support structure handling smaller wind turbines. However, the lack of numerical tools for their assessment remains a challenge. To address this gap, a methodology is proposed to extend the framework for the analysis of multi-rotor concepts. This enables the simulation and evaluation of a broader range of emerging offshore wind energy designs using the proposed ILA framework.

Overall, the main objective of this work is to develop a comprehensive framework for the simulation of floating wind concepts, aligned with current research trends in the wind energy field. Forefront numerical models will be explored to enhance the reliability of structural integrity assessments. The results of this study aim at contributing to the structural evaluation of FOWTs, promoting longer service life and optimized designs. In turn, it is expected to reduce maintenance costs and overall energy generation expenses, supporting the development of this emerging sector.

The growing interest in floating wind turbines and the research lines of this dissertation are reflected in the number of recent publications, as shown in Figure 1.10.

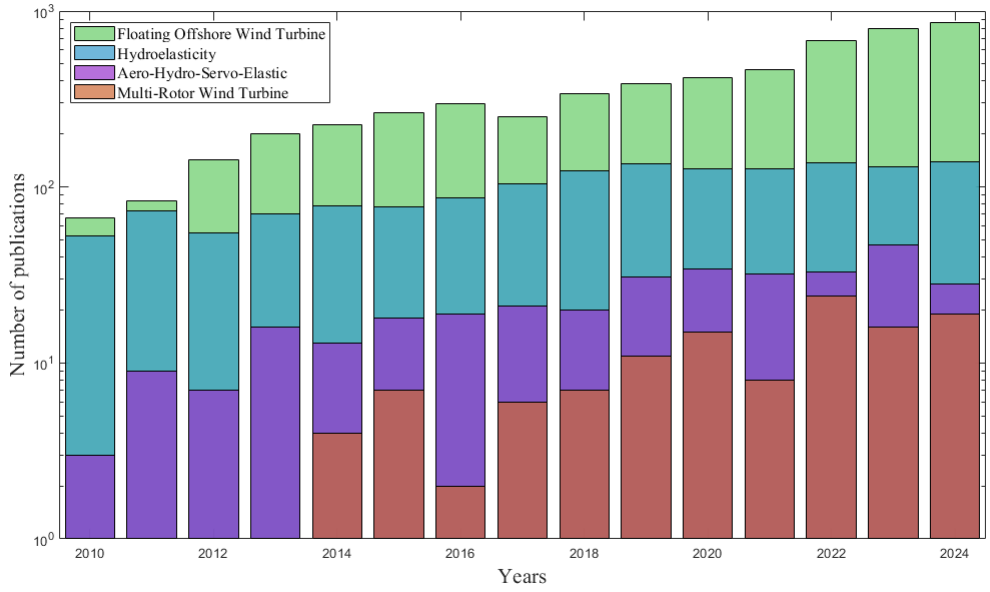

Figure 1.10: Number of publications by year found in SCOPUS database for each keywords.

To provide clarity, the main objectives of this work are summarized and listed below:

- Develop a coupled tool for the ILA of floating offshore wind turbines, enabling robust time-domain aero-hydro-servo-elastic simulations.

- Extend the framework for the solution of incoming multi-rotor concepts, providing insights into their performance, stability, and potential benefits.
- Enhance the hydrodynamic solution including second-order effects for the study of non-linear motions and resonance phenomena.
- Explore the suitability of a structural ROM for the study of the elastic behavior in FOWTs.
- Study of the interaction between hydrodynamic and structural dynamics by solving the fully coupled hydroelastic problem.
- Perform detailed structural assessments to evaluate the platform integrity during operation, with a focus on dynamic effects that contribute to fatigue damage; including methodologies for identifying potential hotspots.
- Examine the coupled response of different platform configurations under combined wind and wave loads to gain a better understanding of the whole multi-physics problem.

1.6 Thesis outline

The structure of the thesis is divided into chapters following the implementation stages of the developed tool. Chapters 2-3-4-5-6 present the methodology and results for each implementation. Whereas chapters 1 and 7 provide the global introduction and conclusions. A summary of the chapters is listed below.

- Chapter 1 presents the background of this work, starting with a general introduction to the advances in the offshore wind energy. It also includes a review of the relevant state of the art, examining previous literature. This offers an insight into the current needs in the simulation of these structures which lead to the purpose of this work. Consequently, a summary of the main objectives is defined.
- Chapter 2 introduces the environment of a numerical framework for the coupled aero-hydro simulation of FOWTs. It provides a description of the starting tools and their coupling strategy. The resulting tool allows for computing the time-domain response of a single-wind turbine platform under coupled environmental loads.
- Chapter 3 extends the previous numerical framework for the simulation of multi-turbine concepts. A methodology is proposed that enables the use of two independent turbines, accounting for their dynamic interaction through the floater. The method is evaluated through an inter-code comparison.

- In chapter 4, the developed wind turbine framework is extended to the up-to-second order seakeeping solution. The coupling strategy is demonstrated by analyzing the relevance of second-order effects in a semi-submersible wind turbine.
- Chapter 5 presents the methodology of a novel hydroelastic approach based on the MMR technique. Its capabilities are demonstrated in a static analysis. The accuracy of the reduced order approximation is proved against the classic FEM solution.
- Chapter 6 tests the consistency of the MMR hydroelastic method to perform ILAs of FOWTs under dynamic load cases of wind-waves. A methodology is proposed to identify critical conditions and potential hot-spots for fatigue failure based on the structural energy.
- Finally, chapter 7 provides a summary of the results obtained through this work and its global conclusions. Additionally, the innovation highlights are described along with their impact on the marine renewable energy field. The work concludes by discussing potential future research lines.

Chapter 2

Coupled aero-hydro framework for the analysis of FOWTs

2.1 Introduction

Floating offshore wind turbines are exposed to harsh environmental loads, including wind, waves, and ocean currents. Their study requires advanced computational methods capable of accurately simulating both structural response and power generation performance. These simulation tools must account for the dynamic interactions between various components, such as the rotor, drivetrain, nacelle, tower, support structure, and mooring system, which have a simultaneous influence on each other. The interplay of aerodynamics, hydrodynamics, structural elasticity, and mooring dynamics makes offshore wind a challenging multi-physics problem. As a developing technology, its numerical modeling and simulation still have significant potential for improvement.

The complexity of this multi-physics problem entails a lack of reliable numerical tools adapted for the analysis of this type of structures at the present time. Therefore, currently available tools for these purposes rely on lower-mid fidelity numerical solutions. Hydrodynamics are typically modeled using potential flow theory, with viscous loads introduced through Morison's equations [Jonkman and Sclavounos, 2006]. Additional solvers, such as WAMIT, are required to precompute frequency-domain coefficients [Jonkman, 2007]. In most studies, second-order loads are neglected. Meanwhile, structural elasticity is characterized by a linear modal representation using beam theory, which is not able to capture local stresses, essential to predict structural failure.

Current tools for the simulation of FOWTs share common characteristics, being conceived as a combination of modules regarding each of the physics. Those are known as aero-hydro-servo-elastic coupled frameworks, being able to solve the fully coupled dynamic solution. The main analysis tools for this purpose are OpenFAST [Jonkman and L. Buhl Jr., 2005], QBlade [Marten et al., 2022], Orcaflex ["Orcaflex Documentation." n.d.] and Sesam ["Sesam Feature Description." 2022]. However, OpenFAST is probably the most widely used, as it is a complete open-source framework. Most of the existing coupled dynamic solvers for the simulation of FOWTs are based in OpenFAST.

In the literature, it is quite common to find higher-fidelity models coupled with the OpenFAST framework. For instance, computational fluid dynamics has been integrated for aerodynamic simulations, as seen in [Campaña-Alonso et al., 2023] by coupling OpenFOAM, or in [Brown et al., 2023] by coupling a large-eddy simulation model. Similarly, for hydrodynamic modeling, as in [Tan et al., 2023], using a smoothed particle hydrodynamics method. Moreover, OpenFAST has been combined with structural FEM solvers, as demonstrated in [Kwangtae et al., 2021], where OpenFAST is used to pre-compute external loads.

The aforementioned higher-fidelity works usually restrict their use and research to detailed component analysis. Examples of localized analysis are found in [Sayed et al., 2019] to study the blade aeroelastic behavior and in [Reddy et al., 2022] to determine the viscous damping coefficients. These studies mostly perform uncoupled analyses, which focus on individual aspects such as the aerodynamics of the wind turbine or the hydrodynamics of the floating platform. In an uncoupled analysis, the dynamic performance of FOWTs are evaluated by considering one factor at a time (either wind or waves), neglecting the complex interaction among them [He et al., 2024].

In this chapter, the time-domain FEM seakeeping solver SeaFEM [Servan-Camas and Garcia-Espinosa, 2013, Garcia-Espinosa and Servan-Camas, 2018] is coupled with the wind turbine solver OpenFAST [Jonkman and L. Buhl Jr., 2005, Jonkman and Sclavounos, 2006] to improve its hydrodynamic and structural solutions. The coupling is presented and compared with other numerical strategies. This approach aims to integrate higher-fidelity solutions, overcoming current numerical limitations while maintaining computational efficiency. The resulting numerical framework is capable of performing aero-hydro-servo-elastic simulations for the analysis of floating offshore wind turbines. It enables the computation of the coupled dynamic response under combined wind-wave loads. This initial work sets the environment used as the foundation for further implementations presented in the following chapters of this thesis.

2.2 Methodology

A methodology is proposed for the numerical coupling between SeaFEM and OpenFAST (SF-OF). This involves designing a coupling strategy between the two independent tools. The framework configuration is explained in detail, given its relevance in the effective communication and synchronization between the solvers.

2.2.1 Introduction to the tools

SeaFEM:

SeaFEM is a seakeeping hydrodynamics simulation tool developed by the International Centre for Numerical Methods in Engineering (CIMNE) in collaboration with CompassIS. It is designed to perform seakeeping analysis of ships and offshore structures. This numerical tool is based on potential flow and solves the wave diffraction-radiation problem in the time-domain, providing an efficient handling of the non-linear hydrodynamic effects [Servan-Camas and Garcia-Espinosa, 2013, Garcia-Espinosa et al., 2015, Servan-Camas et al., 2018, Garcia-Espinosa and Servan-Camas, 2018]. SeaFEM can simulate up to second-order Stokes regular–irregular waves, as well as current effects. It includes a mooring solver capable of handling multi-segment lines based on springs, elastic catenaries and a dynamic mooring based on FEM [Gutierrez-Romero et al., 2016]. The use of the FEM enables the simulation of more complex geometries using unstructured meshes. Rigid-body dynamic analysis can be performed for multibody systems. Time domain simulations facilitate the coupling with other numerical solvers in a more natural way. Currently, hydro–elastic capabilities have been implemented using structural models based on FEM or the MMR.

OpenFAST:

OpenFAST is an open-source software developed by the National Renewable Energy Laboratory (NREL) for the simulation of wind turbines, including both onshore and offshore configurations [Jonkman and L. Buhl Jr., 2005, Jonkman and Sclavounos, 2006]. It supports the analysis of a variety of turbine models, including two- or three-blade horizontal-axis rotors, as well as upwind and downwind configurations. The turbines can be simulated being installed on different types of substructures, including fixed-bottom platforms, as well as floating ones. This tool allows simulating the combined response of floating wind turbines under wind and wave loads, both simultaneously influencing the platform motions and power production. It models the wind turbine multi-physics problem in the time-domain by solving the coupled aero-hydro-servo-elastic solution.

2.2.2 Seakeeping model

The seakeeping model used in this work is a time-domain wave diffraction-radiation solver based on the FEM, developed in-house and integrated in the commercial package SeaFEM.

The mathematical and numerical models implemented in SeaFEM have been extensively verified and validated. These can be found in [Servan-Camas et al., 2021, Garcia-Espinosa et al., 2023, Servan-Camas and Garcia-Espinosa, 2013, Servan-Camas, 2016, Garcia-Espinosa et al., 2015, Gutierrez-Romero et al., 2016, Serván-Camas et al., 2015, Servan-Camas et al., 2018, Garcia-Espinosa and Servan-Camas, 2018]. Using a frame of reference where the OZ axis represents the vertical direction and whose origin is located at the free surface, the governing equations are given by [Servan-Camas, 2016]:

$$\begin{aligned}
&\Delta\varphi = 0 && \text{in } \Omega,\\
&\partial_t\xi + (\boldsymbol{U} + \nabla_h\varphi)\cdot\nabla_h\xi - \partial_z\varphi = 0 && \text{on } z = 0,\\
&\partial_t\varphi + \boldsymbol{U}\cdot\nabla_h\varphi + \tfrac{1}{2}\nabla_h\varphi\cdot\nabla_h\varphi + g\xi = 0 && \text{on } z = 0,\\
&\boldsymbol{v}_\varphi\cdot\boldsymbol{n}_p = -\boldsymbol{v}_p\cdot\boldsymbol{n}_p && \text{on } P\in\Gamma_B,\\
&\boldsymbol{v}_\varphi\cdot\boldsymbol{n}_p = 0 && \text{on } P\in\Gamma_S,
\end{aligned} \tag{2.1}$$

$$P_p = -\rho g\left(z_p + r_{pz}\right) - \rho\left(\frac{\partial\varphi}{\partial t} + \boldsymbol{U}\cdot\nabla\varphi + \frac{1}{2}\nabla\varphi\cdot\nabla\varphi\right), \tag{2.2}$$

Where φ is the velocity potential ($v_\varphi = \nabla_\varphi$), ξ is the free surface elevation, Ω is the fluid domain, $z = 0$ represents the still water level, Γ_B is the wetted surface of a floating body, Γ_S is the seabed surface, $\mathbf{n_p}$ is a normal vector to a surface at point P, $\mathbf{v_p}$ is the velocity of point P, z_p is the initial vertical position of point P, ∇_h is the gradient operator in the horizontal directions, and r_{pz} is the vertical displacement of P. The solution can be split into the incident and diffracted-radiated wave components:

$$\begin{aligned}
\varphi &= \psi + \phi\\
\xi &= \zeta + \eta
\end{aligned} \tag{2.3}$$

Here, ψ and ζ represent the velocity potential and wave elevation for the incident wave field, while ϕ and η denote the velocity potential and free surface elevation for the diffracted-radiated waves. The incident wave field is described by the Airy wave analytical solution. By introducing the separation of variables into the governing equations, the wave diffraction-radiation problem is obtained in terms of ϕ and η as independent variables. Details on the wave diffraction-radiation governing equations can be found in [Servan-Camas, 2016, Garcia-Espinosa et al., 2015, Garcia-Espinosa and Servan-Camas, 2018].

2.2.3 Coupling strategy

The wind turbine simulation tool OpenFAST, with particular emphasis on its complete aerodynamic and wind turbine servo control modules, is coupled to the sekeeping solver SeaFEM. This is achieved through the combination of OpenFAST for the aero–servo–elastic computation of the rotor, with SeaFEM for the hydro–mooring computation of the platform-mooring. As seen in the previous section, the code structure of OpenFAST is composed of different numerical modules, illustrated in Figure 2.1: hydrodynamics (HydroDyn), mooring dynamics (MoorDyn), aerodynamics (AeroDyn), electrical system dynamics (ServoDyn), and structural dynamics (ElastoDyn), among others.

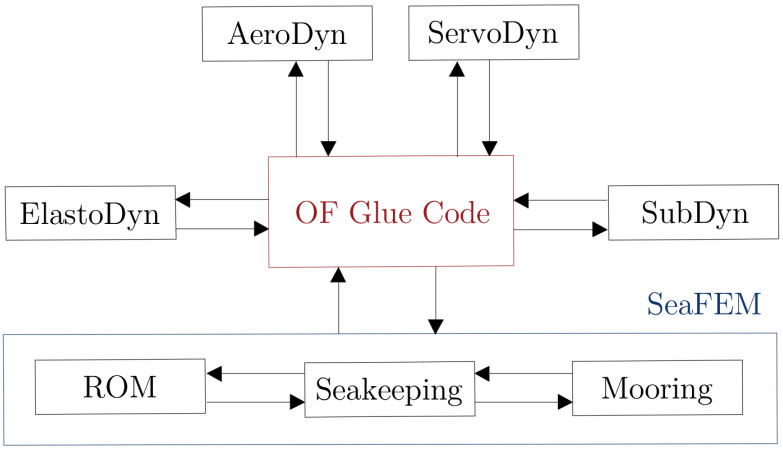

Figure 2.1: OpenFAST modularization framework.

These modules communicate with each other through a glue code, where the input-output exchange of solutions happens between them. This modular framework facilitates the replacement of the hydrodynamic and mooring dynamics modules by SeaFEM as shown in Figure 2.2. The wind field received as input in AeroDyn is defined by an external code, TurbSim, which adds turbulence to the wind profile.

The coupling strategy is performed by means of the data exchange between both solvers. SeaFEM solves the seakeeping solution, providing the sea loads acting on the substructure by direct pressure integration on the submerged body surface. Additionally, it includes the solution of the mooring dynamics. OpenFAST provides a solution for the rigid-body kinematics as well as the aerodynamic loads on the rotor blades, including the control of the servo-motor. In return, SeaFEM sends the seakeeping loads.

External loads and platform motions are related by means of the motion equation, which is solved in ElastoDyn. The dynamics of the floating wind turbine are defined by:

$$\mathbf{M}(\ddot{\mathbf{q}}^{OF}) + \mathbf{C}(\dot{\mathbf{q}}^{OF}) + \mathbf{K}(\mathbf{q}^{OF}) = \mathbf{F}^{OF}_{Turb} + \mathbf{F}^{SF}_{Hydro} \tag{2.4}$$

where **M**, **C**, **K** are the mass, damping, and stiffness matrices, respectively; **q** is the vector of the six rigid-body DoFs; and **F** represents the vector of external loads. The superscript indicates the code used to compute each variable.

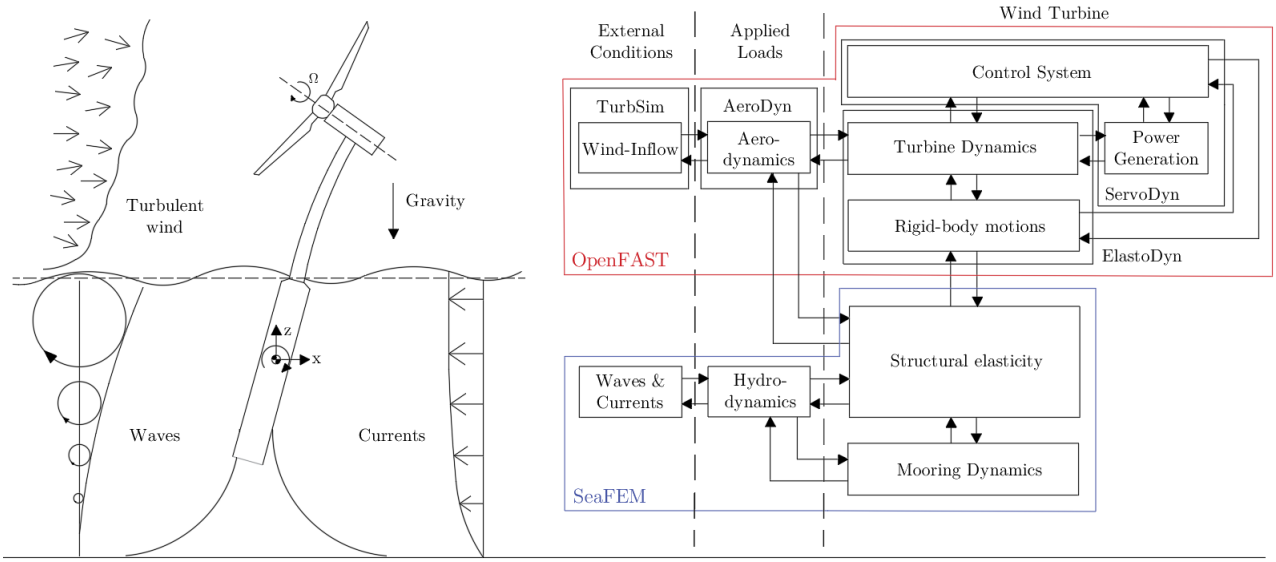

Figure 2.2: FOWT multi-physics problem and numerical framework.

This strong (two-ways) coupling is performed by imposing the rigid-body motions of the whole system obtained from OpenFAST as boundary conditions for the seakeeping hydrodynamics problem in SeaFEM. Moreover, OpenFAST aerodynamic loads on the rotor (computed by AeroDyn's module) are provided to SeaFEM to be used as an external load for its structural solver. This aero-elastic coupling is performed in one-way, the rotor loads are received at the hub reference system but the structural top-tower deflections are not transferred to the wind turbine. In Figure 2.3 is given a schema with the data exchange.

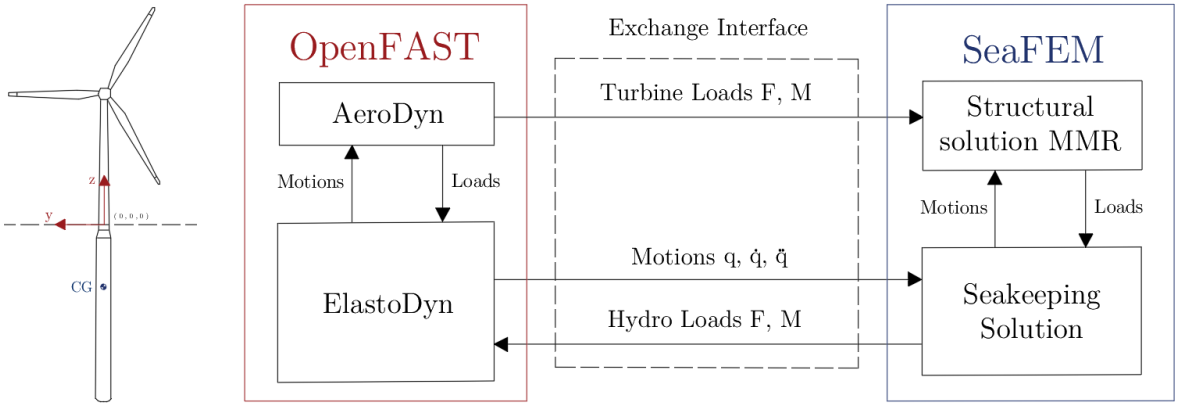

Figure 2.3: SF-OF data exchange.

The seakeeping loads are sent at the global reference point (0,0,0) placed in the mean sea level. On the other hand, SeaFEM solves with respect to the center of gravity of the platform. Since this differs from the coordinate system used in OpenFAST, the exchanged information has to be constantly translated between the sender's and receiver's coordinate systems.

This strong two-ways coupling between the kinematic motions and hydrodynamic loads requires a rigorous input-output solve between both solvers. The relationship between ElastoDyn's kinematics and SeaFEM's loads is linearized in each time step by computing a Jacobian matrix. SeaFEM is informed when this Jacobian matrix needs to be updated. The time-marching scheme is based on a fourth-order Runge–Kutta (RK4) predictor–corrector solution algorithm, with the number of correction steps defined by the user.

The linking of both codes is configured by compiling SeaFEM as an executable (.exe) and OpenFAST v.3.5.0 as a dynamic link library (.dll). The communication between executions is achieved through C++/Fortran interfaces with shared functions, see Figure 2.4.

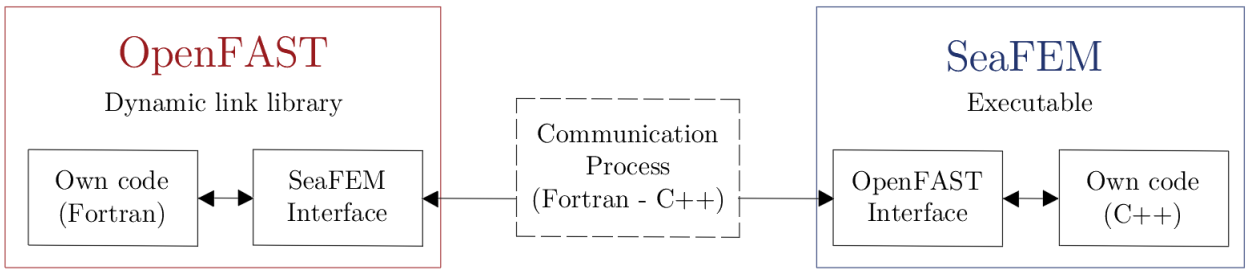

Figure 2.4: SF-OF coupling configuration.

Communication interfaces play a fundamental role when performing the coupling. In each code an interface is created that communicates with the other. Through these interfaces, information is exchanged internally and with the counterpart code. This is necessary to ensure data type compatibility in the imported procedures, since both codes do not share the same programming language. In this way, C++ arguments are passed to Fortran standardized types.

The coupling subroutines shared between the interfaces in execution order are:

- (Process 1) OpenFAST sends the turbine aerodynamic loads to SeaFEM.
- (Process 2) OpenFAST sends the kinematics to SeaFEM, which computes and returns the dynamic loads. This process is repeated in each iteration.
- (Process 3) synchronizes temporarily the two codes when the time step increases.
- (Process 4) ends the simulation when the maximum time is reached.

These subroutines for data exchange are exported from SeaFEM and imported into OpenFAST, enabling OpenFAST (DLL) to use the compiled external functions defined in SeaFEM (exe). This setup is noteworthy, as in most cases, the executable is the one that accesses functions defined in the DLL. However, in this case, this process is reversed, the DLL is the one that interacts with the executable context. This allows the code flow to jump from one tool to another and the interaction between both. Since OpenFAST takes the lead, it is the one that accesses SeaFEM when needed, as shown in the flow chart in Figure 2.5. The data exchange happens for every time step and iteration as shown in Algorithm 1.

Algorithm 1: Coupling process SF - OF

SeaFEM $\rightarrow$ Initializes OpenFAST;

for $t_{OF} < T_{max}$ **do**

  for $iter < Iter_{max}$ **do**

    Process 1 $\rightarrow$ Rotor loads received $\mathbf{F}_{Turb}$;

    Process 2 $\rightarrow$ Kinematics received $(\ddot{\mathbf{q}}, \dot{\mathbf{q}}, \mathbf{q})$ and seakeeping loads send $\mathbf{F}_{Hydro}$;

  end

  Process 3 $\rightarrow$ updates $t_{SF}++$;

end

Process 4 $\rightarrow$ ends $t_{SF} = T_{max}$

OpenFAST is initialized dominating the simulation timeline, calling SeaFEM to compute when necessary. The current calculation state in OpenFAST is communicated to SeaFEM through state tags following the simulation progress, also shown in Figure 2.5. These tags are updated depending on the subroutine executed by OpenFAST that calls SeaFEM. Based on these, SeaFEM decides which process to follow, either to proceed to the next time step or to compute seakeeping loads. In this way, SeaFEM is used as an external load calculator, being accessed only when needed by OpenFAST.

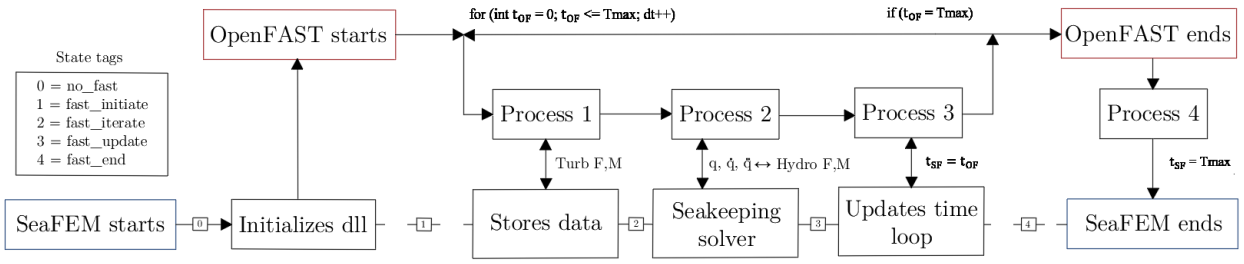

Figure 2.5: Coupling strategy and time synchronization in SeaFEM.

The coupling process is implemented in accordance with OpenFAST's programming philosophy, which follows a hierarchical structure. During the initialization phase, the set of active modules is defined. Within this stage, OpenFAST defines the data types, known as "mesh", which declare input or output variables regarding each module. A new module is defined within OpenFAST to be used as an interface with SeaFEM. This module is initialized by creating an input mesh (u_SeaFEM) to store movements, velocities and accelerations, and an output mesh (y_SeaFEM) to store seakeeping forces and moments. A more detailed diagram of the coupling flow within OpenFAST is given in Figure 2.6.

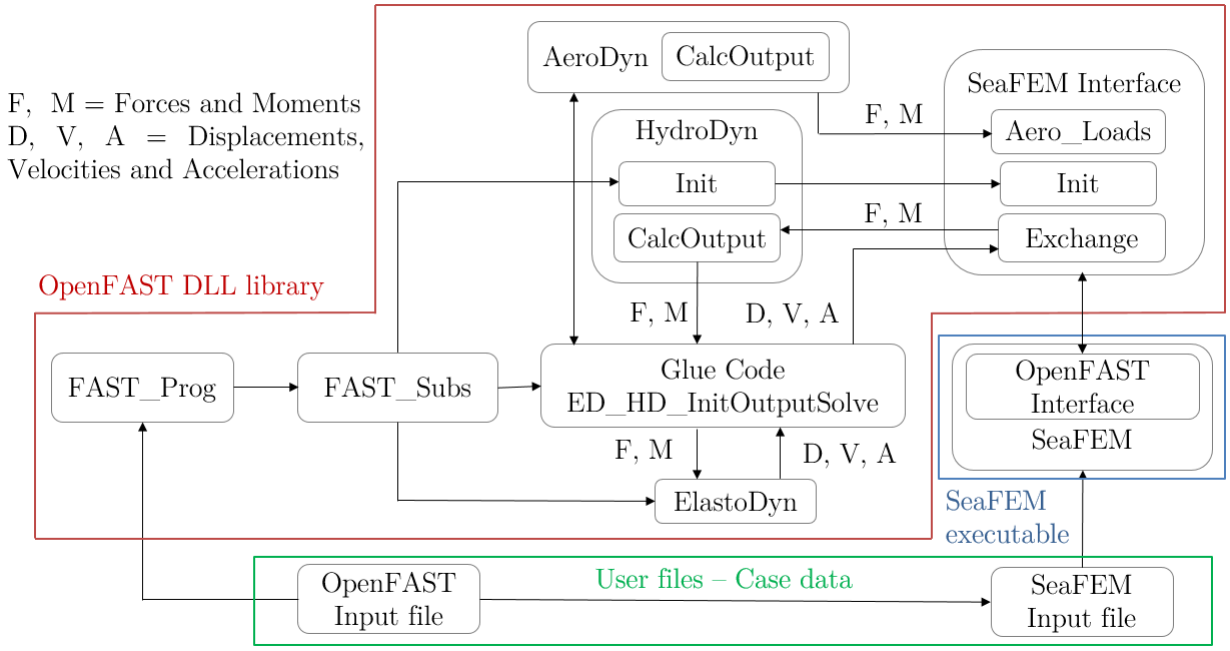

Figure 2.6: Detailed coupling flow schema in OpenFAST.

Once the modules are initialized the flow enters the glue code, where an input-output solve between modules is established. The hydrodynamic loads applied to the platform are outputs from SeaFEM (stored in y_SeaFEM) and inputs to ElastoDyn (stored in u_ED). Whereas, the platform motions are outputs from ElastoDyn (stored in y_ED) and inputs to SeaFEM (stored in u_SeaFEM).

The relationship between ElastoDyn kinematics and SeaFEM loads is linearized in each time step by computing a Jacobian matrix. This Jacobian is solved with finite differences and its matrix needs to be updated eventually. If it is necessary to be updated, SeaFEM is informed by means of the flag ("flag_SeaFEM").

The aerodynamic loads are sent from OpenFAST to be applied in the SeaFEM structural solver during hydroelastic simulations. Due to the interest of receiving them before the kinematics, they are passed into the interface through an independent exchange subroutine. SeaFEM needs to be informed about whether it has to compute the current time-step or the following one, so that its time loop is updated when necessary. When the OpenFAST computation time is greater than the current iteration time, SeaFEM is notified to temporarily update itself.

The strong coupling scheme is based on a RK4 predictor-corrector solution algorithm with the number of correction steps defined by the user. This parameter "p%Iterations" is used to inform SeaFEM when the simulation is finished. The computation ends when time equals the maximum simulation time and iterations equals the number of corrections. This happens when the predictor-corrector scheme is performed for all the correction steps.

2.3 Intercode comparison - OC3 Hywind

The floating spar–buoy concept "Hywind", belonging to the OC3 project, is used as a benchmark model to compare the numerical results against other strategies. As part of phase IV, the coupled dynamic response of the NREL 5-MW reference wind turbine installed on the Hywind platform with catenary mooring lines is analyzed. The technical descriptions of the NREL-5MW turbine and the Hywind platform are found in [Jonkman et al., 2009, Jonkman, 2010], respectively. In Table 2.1, the OC3-Hywind platform specifications are summarized.

Table 2.1: OC3-Hywind platform particulars.

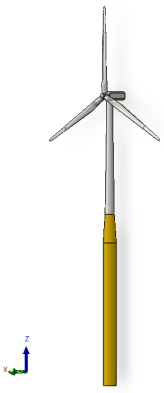

	Unit	Value
Mass (with ballast)	kg	7,466,330
Downwind distance of CM	m	0.00
Lateral distance of CM	m	0.00
Vertical distance of CM	m	-89.9155
Roll inertia about CM	$kg \cdot m^2$	4,229,230,000
Pitch inertia about CM	$kg \cdot m^2$	4,229,230,000
Yaw inertia about CM	$kg \cdot m^2$	164,230,000

The response amplitude operators (RAOs) are compared to FAST using its own hydrodynamic model and coupled with WAMIT. RAOs are transfer functions that relate the wave excitation to the platform's response. The RAOs computed solution is obtained for the rigid floating system subjected to a simplified case with no wind or currents. In the present tool, the prediction of the wave–body interaction is performed with a time–domain simulation using a white noise wave spectrum.

The extracted RAOs, referenced at the origin, are compared to those previously published by NREL [Ramachandran et al., 2013]. The RAOs comparison, for the relevant degrees of freedom is shown in Figure 2.7. Natural frequencies are well predicted in surge for 0.007 Hz, heave 0.03 Hz and pitch 0.03 Hz. Only small differences are observed in surge peak amplitude and pitch frequency at their natural frequencies. This can be due to small differences in the numerical parameters of the different analyses, which have not been reported in the consulted references.

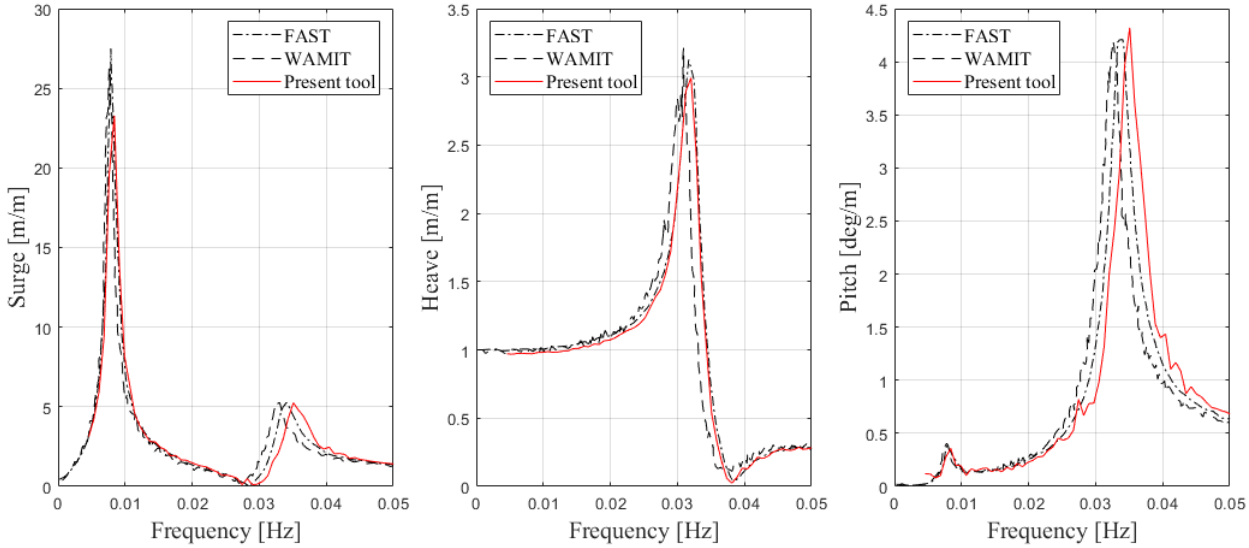

Figure 2.7: OC3-Hywind: RAO comparison (no wind, rigid turbine).

The transfer of turbine loads is confirmed against SeaFEM's own rigid-body solution. A case with a steady wind condition in the absence of waves is computed. The wind force along the upwind direction over the rotors is extracted from the present framework simulation. The same case configuration is computed in SeaFEM, where the previously extracted load is introduced as a precomputed external load. The surge motions are compared between both simulations, since this is the most excited motion. The results, shown in Figure 2.8 for the OC3-Hywind case, demonstrate that both solutions agree, confirming the reliability of the data exchange process.

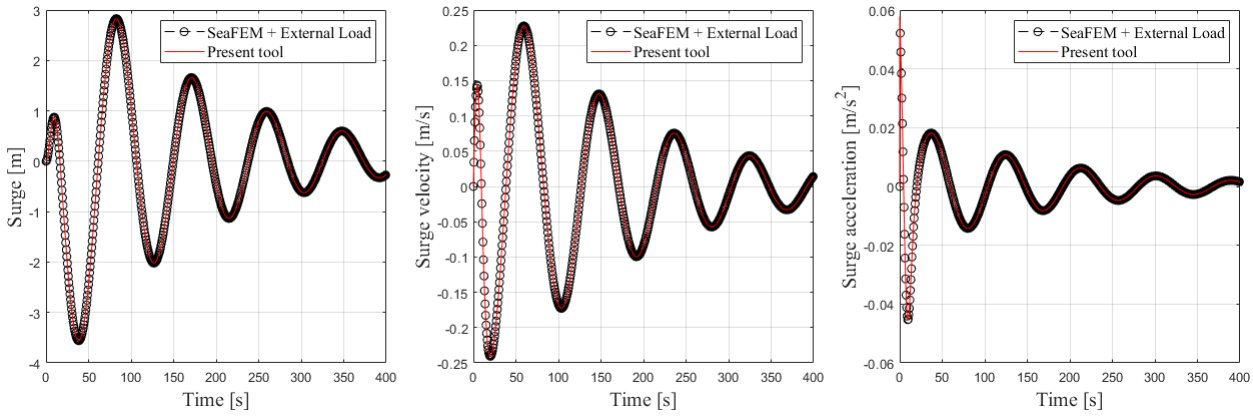

Figure 2.8: OC3-Hywind: surge motions (no waves, rigid turbine).

2.4 Conclusions

This chapter presents a strategy for the implementation of a numerical framework to simulate the dynamic behavior of floating wind turbines. The proposed tool operates in the time domain, addressing the fully coupled aero-hydro-servo-elastic problem. The resulting framework allows for the analysis of wind turbine platforms under combined environmental loads of wind and waves. The tool has proven to be consistent when compared against other numerical strategies. Agreement is observed in the RAOs and motion response under wind loads.

The combination of the numerical solvers SeaFEM and OpenFAST has shown to complement each other. OpenFAST provides the simulation of the wind turbine and SeaFEM a higher-fidelity seakeeping solution. Together, they form a unified framework without relying on additional external frequency-domain software to solve the wave diffraction-radiation problem. Since using the FEM versatility is provided in the structural concepts that can be analyzed. This coupled tool broadens the scope of analysis, making the framework suitable for emerging technologies and future developments in the offshore wind energy.

Although OpenFAST has its own hydrodynamic module, its replacement by SeaFEM brings higher-fidelity solutions and further capabilities, as demonstrated throughout this thesis. In Chapter 4, the developed tool will be combined with SeaFEM's up to second-order hydrodynamic solver, while its hydroelastic capabilities will be tested in Chapter 6 to perform detailed structural analyses of FOWTs. This last key feature will be particularly studied within this thesis. Moreover, its solution will be extended for the simulation of multi-turbine configurations in Chapter 3. The work presented in this chapter aims to set the numerical environment for a complete simulation tool of FOWTs.

Chapter 3

Extension of the coupled framework for the analysis of Multi-Turbine platforms

3.1 Introduction

The offshore wind sector is constantly growing, bringing with it new engineering challenges. Large structures with an increasing variety of concepts are under development, aiming to improve the system's efficiency while decreasing overall costs. The upscaling of wind turbines is the most common method used to increase the power production. However, enlarging the rotor diameter might imply a large increase of the components mass compared to the energy benefits [Jamieson and Branney, 2012, Xiong et al., 2023]. This offset leads to economic drawbacks, especially in offshore platforms, requiring more marine operations and higher manufacturing or installation costs [Martín-San-Román et al., 2022, Martin, 2022]. Moreover, any failure of the main components of large wind turbines will lead to long-term shutdowns and expensive repairs [Xie et al., 2023].

An interesting alternative to the up-scaling are multi-rotor concepts, which handle smaller wind turbines attached to the same support structure. In comparison with single turbines, multi-turbine systems provide several advantages. They allow for the use of smaller components while providing the same combined power [Martin, 2022], reducing manufacturing costs since the platform, mooring lines, and network connections are shared between the turbines [Bae and Kim, 2015]. The lower weight distribution leads to a better stability [Barltrop, 1993]. In addition, since they have larger support platforms, they behave more dynamically stable under sea state loads [Bae, 2013].

New multi-rotor design solutions are less well-developed, with only a few numerical tools existing for their assessment at the present time. [Bae and Kim, 2015] proposed a multiple unit floating offshore wind turbine simulation tool by coupling FAST-CHARM3D. The dynamic influences of all the turbines were included in the motion equation through a combined global coefficient matrix and by adding the rotor aerodynamics to the force vector. This was tested in a five-turbine semi-submersible system. Recently, [Martin, 2022] extended the previous approach with the integration of AeroVIEW, an aerodynamic module based on the free wake vortex method. Coupled analyses were performed in a twin-rotor configuration on the OC4 semi-submersible platform. [El Beshbichi et al., 2023] presented an alternative multi-rotor solver by coupling a FAST aerodynamic module accounting for each turbine into a Modelica framework. The rigid dynamics were analyzed in a two-rotor wind turbine concept deployed on a spar-type platform, proving significant mass saving with respect to its equivalent single-rotor configuration [El Beshbichi et al., 2021]. A recent work of [Xie et al., 2023] proposes a simulation framework composed by OpenFAST, SIMPACK and Simulink, being tested on a four-rotor platform.

The dynamic analysis of multiple rotors is frequently addressed by uncoupling the aero-hydrodynamic responses, as in [Bashetty and Ozcelik, 2022]. These studies are mainly focused on studying the benefits of wake interactions. For instance, [Martín-San-Román et al., 2021, Van der Laan et al., 2019] analyze the power increments due to the interaction of nearby rotors, while [Van der Laan et al., 2019, Ghaisas et al., 2018] study the fast wake recovery, which allows for a reduction of the wind turbine spacing in farms. Additionally, there are few studies in the literature assessing the flexible-body response in multi-rotor systems. One is the aero–hydro–elastic analysis performed in [Lamei et al., 2023] for a three-rotor semi-submersible concept, obtaining the wet natural mode shapes.

Due to the innovative character of multi-rotor systems, this chapter aims at developing a tool to perform time–domain coupled analysis of these new concepts. Although OpenFAST's current capabilities only allow to simulate single floating wind turbines, the SF-OF coupled framework is extended for the assessment of multiple turbines operating on the same platform. The proposed strategy is capable of analyzing the power generation during operation and the dynamic response interactions between the wind turbines under combined load cases of wind and waves.

3.2 Methodology

The extension for the multi-wind turbine solution is performed by coupling one execution of SeaFEM with as many OpenFAST instances as turbines placed on the platform. In this way, the aerodynamic components regarding each turbine are taken into account in the load balance. Additionally, the turbines operate with their own servo control, being possible to simulate a platform containing several turbines with different features.

3.2.1 Multi-Turbine extension

The OpenFAST instances solve each turbine independently so that the dynamic interaction is performed through the floater. In Figure 3.1, a chart with the exchanged information among the OpenFAST modules and SeaFEM is displayed. It shows how the turbine loads and rigid-body motions are provided to SeaFEM, whereas this returns the computed external loads for each turbine (including the other turbine aerodynamic loads). With this approach, the aerodynamic wake interferences between adjacent turbines are neglected. However, for turbines placed side-by-side, this interference is assumed to be a non-dominant effect.

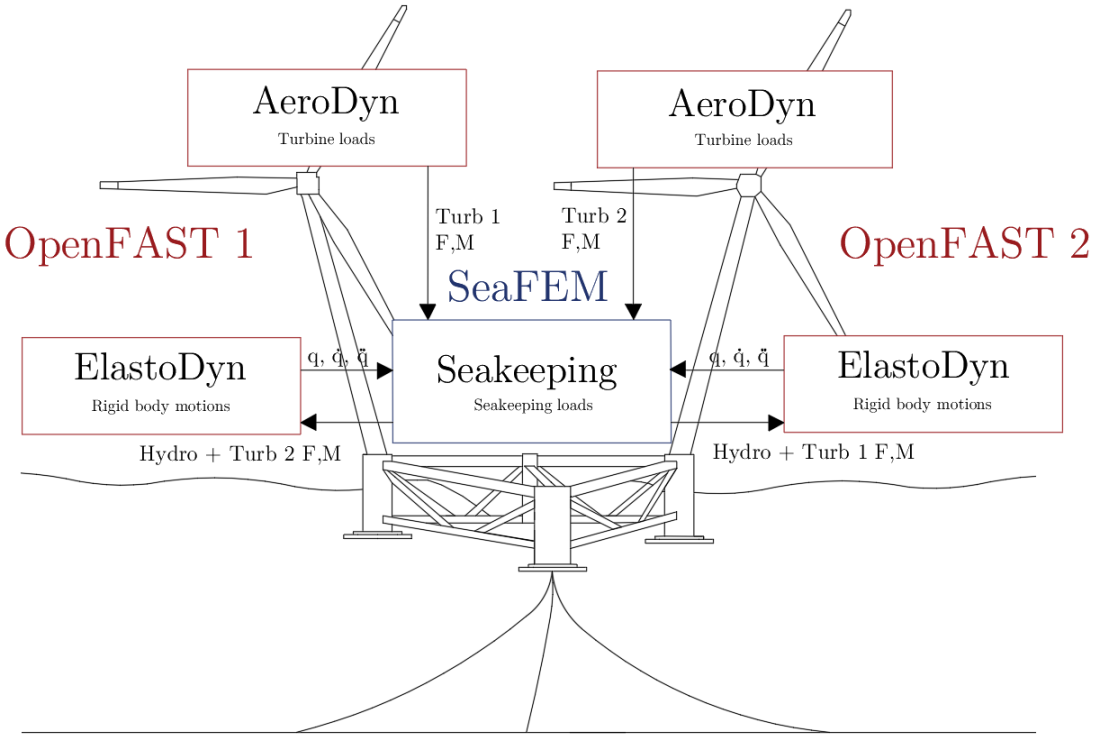

Figure 3.1: Twin-turbine extension strategy for the simulation of the W2Power platform.

Although the present methodology can be used for an arbitrary number of turbines placed on the same platform, it is presented in this work for the W2Power twin turbine concept.

As there are two OpenFAST executions coupled, one regarding each turbine, the equation of motion is solved twice, obtaining a kinematic solution for each one. Given that the entire structure is considered as a single rigid body, both kinematic solutions should be equal. To avoid small numerical differences, in every iteration, the platform motions are averaged according to Eq. (3.1):

$$\overline{(\ddot{\mathbf{q}}, \dot{\mathbf{q}}, \mathbf{q})} = \frac{\sum_{n=1}^{2} (\ddot{\mathbf{q}}_\mathbf{n}, \dot{\mathbf{q}}_\mathbf{n}, \mathbf{q}_\mathbf{n})}{2} \tag{3.1}$$

where $\overline{(\ddot{\mathbf{q}}, \dot{\mathbf{q}}, \mathbf{q})}$ are the averaged accelerations, velocities, and displacements in the platform's six DOFs, and n is the number of OpenFAST instances or turbines.

When OpenFAST solves a single floating wind turbine, it deals with the turbine, tower, and platform mass properties. For the implementation of multi-turbine capabilities, the additional tower and turbine mass components need to be included. These mass matrices are taken into account as part of the floater $\mathbf{M}_{Floater}$, which groups the platform $\mathbf{M}_{Platform}$, all the towers $\mathbf{M}_{Tower}^{1,2}$, and the additional wind turbines $\mathbf{M}_{Nacelle}$ and $\mathbf{M}_{Rotor}$. The floater definition is shown in Figure 3.2 regarding each OpenFAST instance.

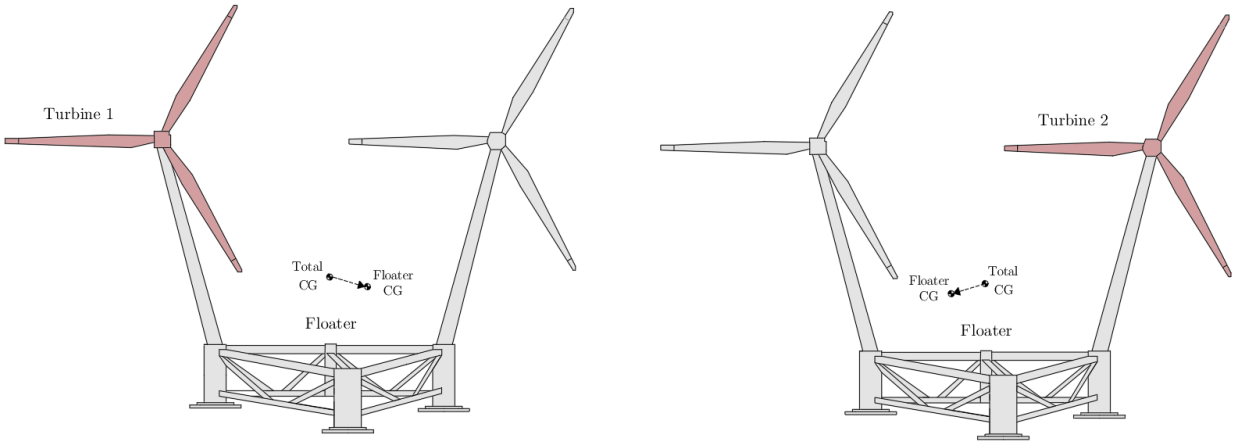

Figure 3.2: Floater mass–inertia components (left: OF1, right: OF2).

The turbine definition is kept in OpenFAST, with turbine 1 in OF1 and turbine 2 in OF2, whereas the towers are neglected. Reason found in the fact that multi-turbine concepts are generally characterized by having leaning towers, being out of ElastoDyn's simulation capabilities, which are restricted to straight towers. If SeaFEM is coupled with SubDyn, tilted towers could be modeled. The floater's gravity center is computed and defined in each OpenFAST execution. The mass matrix $\mathbf{M}$ of the floater is composed as in Eqs. (3.2) and (3.3), and it is considered within OpenFAST as the platform. The index indicates the corresponding OpenFAST instance.

$$\mathbf{M}^1_{Floater} = \mathbf{M}_{Platform} + \mathbf{M}^{1,2}_{Tower} + \mathbf{M}^2_{Nacelle} + \mathbf{M}^2_{Rotor} \tag{3.2}$$

$$\mathbf{M}^2_{Floater} = \mathbf{M}_{Platform} + \mathbf{M}^{1,2}_{Tower} + \mathbf{M}^1_{Nacelle} + \mathbf{M}^1_{Rotor} \tag{3.3}$$

The mass matrix referenced at the floater's center of mass can be defined for the six degrees of freedom of the floater, as in Eq. (3.4). Where m is the mass, I_{xx}, I_{yy}, I_{zz} are the moments of inertia with respect to the principal axis and $I_{xy}, I_{xz}, I_{yz}, I_{zx}, I_{zy}$ are the inertia products. When the mass distribution is not symmetric with respect to the principal axes, products of inertia appear. These terms indicate whether a rotation around one axis induces motion about another axis. Given the non-symmetrical mass distribution of the floater, the products of inertia become significant. Since ElastoDyn only allows the input of principal inertias, the off-diagonal terms are incorporated into SeaFEM as external loads. If it is coupled with SubDyn, the inertia products could be directly accounted for.

$$\mathbf{M}_{Floater} = \begin{bmatrix} m & 0 & 0 & 0 & 0 & 0 \\ 0 & m & 0 & 0 & 0 & 0 \\ 0 & 0 & m & 0 & 0 & 0 \\ 0 & 0 & 0 & I_{xx} & -I_{xy} & -I_{xz} \\ 0 & 0 & 0 & -I_{yx} & I_{yy} & -I_{yz} \\ 0 & 0 & 0 & -I_{zx} & -I_{zy} & I_{zz} \end{bmatrix} \tag{3.4}$$

The addition of turbines operating on the same platform implies a set of extra loads acting over the rigid-body response. These loads need to be taken into account within the total load balance. OpenFAST internally considers the aerodynamic loads of its own turbine $\mathbf{F}_{Turb}$. While the SeaFEM loads $\mathbf{F}_{SF}$ include the platform seakeeping and mooring loads.

The loads from all the additional turbines $\mathbf{F}_{Add\_Turb}$ are regarded as external loads that need to be added to the SeaFEM loads $\mathbf{F}_{SF}$, as shown in Eq. (3.5). These resulting loads are then returned to the OpenFAST executions $\mathbf{F}_{SF\rightarrow OF}$, which are added to their own turbine loads $\mathbf{F}_{Turb}$, composing the total load balance $\mathbf{F}_{Tot}$, as shown in Eq. (3.6). In this way, the additional loads acting on the other turbines are considered as external loads applied on the floater, reaching a dynamic influence between turbines.

$$\mathbf{F}^{CG,1}_{SF\rightarrow OF} = \mathbf{F}^{CG,1}_{SF} + \mathbf{F}^{CG,2}_{Add\_Turb} \qquad \mathbf{F}^{CG,2}_{SF\rightarrow OF} = \mathbf{F}^{CG,2}_{SF} + \mathbf{F}^{CG,1}_{Add\_Turb} \tag{3.5}$$

$$\mathbf{F}^{OF,1}_{Tot} = \mathbf{F}^{OF,1}_{SF\rightarrow OF} + \mathbf{F}^{OF,1}_{Turb} \qquad \mathbf{F}^{OF,2}_{Tot} = \mathbf{F}^{OF,2}_{SF\rightarrow OF} + \mathbf{F}^{OF,2}_{Turb} \tag{3.6}$$

The superscript indicates the reference system and the corresponding OpenFAST instance. SeaFEM terms are referred at the total center of gravity, and the resulting loads are translated to each OpenFAST origin. SeaFEM's origin is used as the global reference system. For the W2power platform, this origin of coordinates is located at the mean sea level and at the center of the upwind column. The X-axis is oriented along the downwind direction, with the Z-direction facing upwards. The turbine loads acting on top of the tower are received at the local hub reference systems. The reference frame layout is presented in Figure 3.3.

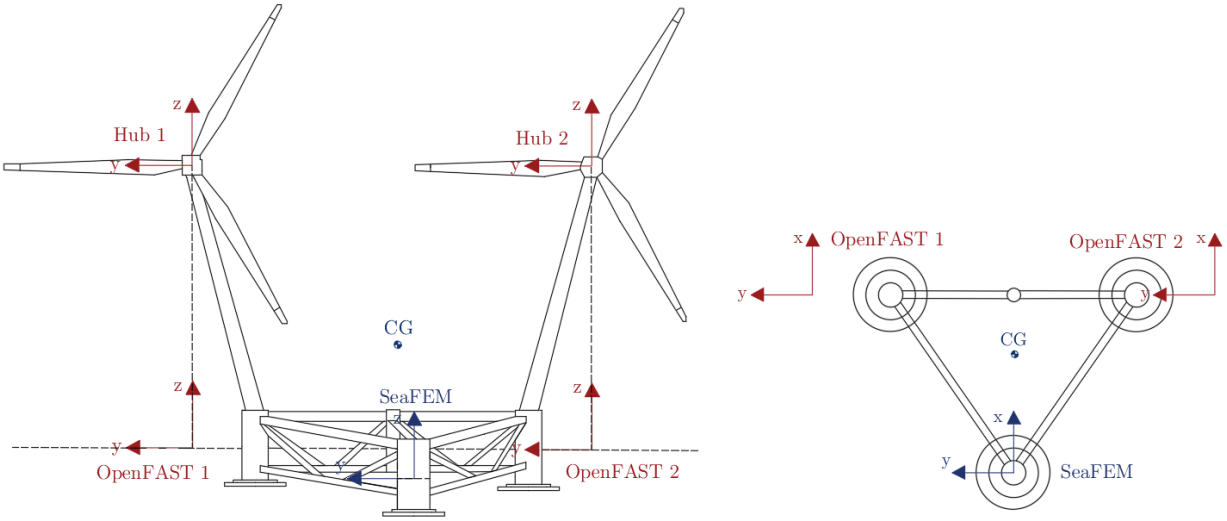

Figure 3.3: Location of the reference frames for a twin turbine solution (left: front view, right: top section view).

The kinematics are obtained through the OpenFAST global references placed at the mean sea level and on a perpendicular line passing through the yaw axis of the corresponding turbine. SeaFEM computes the seakeeping hydrodynamics and mooring loads with respect to the total center of gravity. Therefore, the exchanged data is related by constantly translating it from the coordinate system of the sender to the one at the receiver.

3.2.2 Coupling strategy

For the twin-turbine extension, two OpenFAST dlls are required to be linked with SeaFEM, as displayed in Figure 3.4. The initialization of both dlls is parallelized within the SeaFEM code using two OpenMP threads in charge of launching each OpenFAST execution. The communication between codes is performed through their 3 interfaces. There is no direct communication between the dlls, as the information flow is centralized in SeaFEM's main interface. The two OpenFAST DLLs run in parallel and interact with the same SeaFEM execution. Each code has his own user-defined package of input files, allowing the simulation to have wind turbines with different conditions or properties.

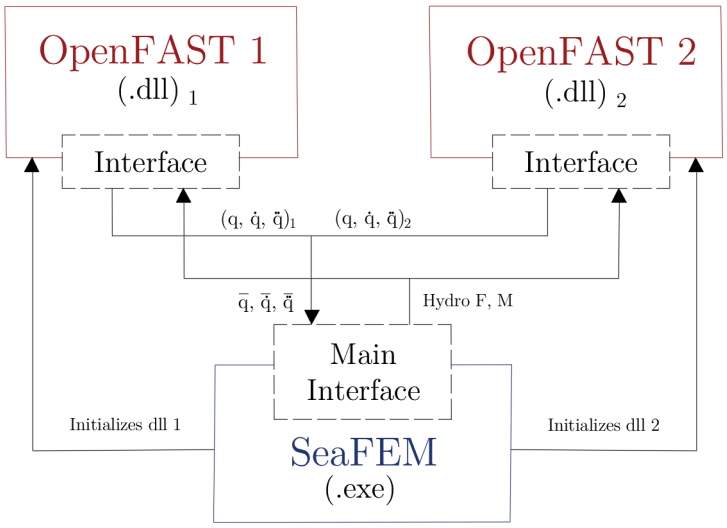

Figure 3.4: Linking configuration and interface communication.

The coupling subroutines are duplicated in the SeaFEM interface to avoid overlapping or interference between the DLLs. The first OpenFAST execution controls the time loop, while SeaFEM plays the role of a calculator, called from OpenFAST when necessary. Within the SeaFEM interface, synchronization is performed to keep both OpenFAST flows at the same point of execution, avoiding overlapping and time lags. The parallelization does not finish until the total simulation time is reached, with two mixed flows accessing SeaFEM simultaneously. To avoid interference between them, the shared processes are duplicated, as shown in the Algorithm 2.

Algorithm 2: Multi-rotor coupling process

SeaFEM → Initializes OpenFAST$_1$ and OpenFAST$_2$;

for $t_{OF} < T_{max}$ **do**

  for $iter < Iter_{max}$ **do**

    Process 1.1 → Rotor loads received $\mathbf{F}^1_{Turb}$;

    Process 1.2 → Rotor loads received $\mathbf{F}^2_{Turb}$;

    Process 2.1 → Kinematics received $(\ddot{\mathbf{q}}, \dot{\mathbf{q}}, \mathbf{q})_2$;

    Process 2.2 → Kinematics received $(\ddot{\mathbf{q}}, \dot{\mathbf{q}}, \mathbf{q})_1$ and seakeeping loads send $\mathbf{F}_{Hydro}$;

    Process 2.1 → Seakeeping loads send $\mathbf{F}_{Hydro}$;

  end

  Process 3.1 → updates $t_{SF}++$;

end

Process 4.1 → ends $t_{SF} = T_{max}$

A synchronization strategy is performed ensuring common execution points. This is implemented at the SeaFEM interface, where it is possible to identify the thread that is accessing it. State labels are associated with each thread depending on the simulation stage, as represented in the block diagram in Figure 3.5. The thread flow is stopped and waits until the other thread has finished a specific task, being informed by the state tag.

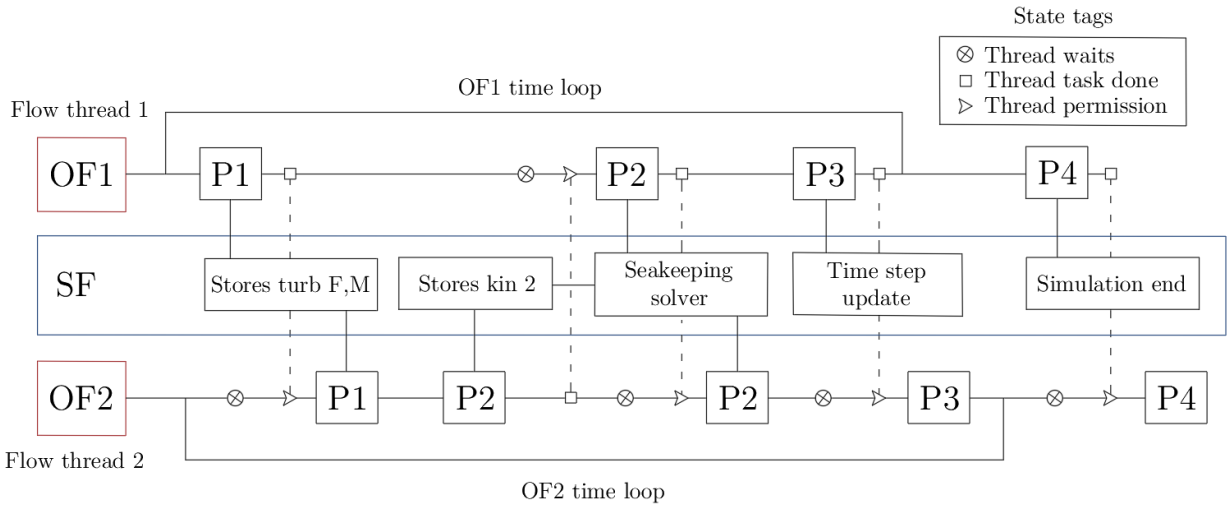

Figure 3.5: Extension strategy and thread synchronization.

OF1 controls the total timeline, giving permission to SeaFEM and OF2 to update their time step. Additionally, after each communication process is performed by OF2, its thread flow is stopped, waiting for permission to be given after the same process is finished by OF1.

Process 2 is split to gather all the kinematic solutions for its average before computing the SeaFEM loads. The tasks that need to be carried out once remain in charge of the dominant OpenFAST, while the other one waits to avoid task repetition. In this way, the temporal synchronization for the three coupled instances is achieved without interference between them.

3.3 Intercode comparison - W2Power

Existing multi-rotor solvers have not been verified or validated, given the lack of benchmark data and similar numerical strategies. In this work, the reliability of the OpenFAST extension is evaluated through an intercode comparison with the SeaFEM kinematics solver, performing a RAOs analysis and a motion study using wind loads. As part of the H2020 European Project FIBREGY [“Fibregy Project.”, 2020], the redesign of the full-scale W2Power platform concept in fiber-reinforced polymers (FRP) is tested.

The W2Power semi-submersible platform holds two towers inclined outwards, with the wind turbines placed side-by-side. The mooring system is arranged in a single point at the front column and allows the platform to align itself towards the wind. The floating structure integrates two commercial 6 MW wind turbines, achieving a total capacity of 12 MW, with the option to incorporate wave energy converters for an additional 3 MW. In 2019, it became the first wind platform deployed in Spanish waters and the world's first multi-turbine solution to undergo open-water testing. Currently, the 1:6 scale model is deployed at PLOCAN. Further details can be found in ["Enerocean", n.d.].

The W2Power concept specifications, as well as the results plot axes, cannot be shown due to confidentiality reasons. The redesigned full-scale FRP-W2Power platform, equipped with NREL 5-MW reference wind turbines on each tower, is used for the inter-code comparison of the multi-turbine extension. The dynamic response is analyzed considering a water depth of 200 m. Figure 3.6 provides a scheme of the system's platform-turbines.

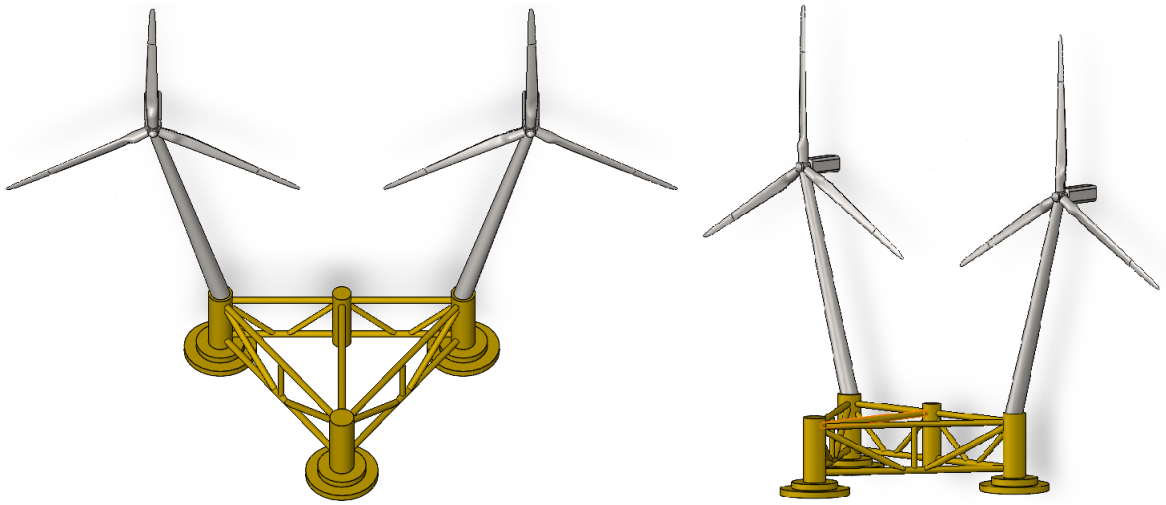

Figure 3.6: Multi-Turbine system (left: front-top view, right: front-side view).

The RAO wave are computed using the multi-turbine-extended tool in the absence of wind and compared with the SeaFEM solution. In the first approach, the rigid-body solution is computed by OpenFAST, while in the second SeaFEM uses its own rigid-body dynamics solver. A time–domain simulation using a white-noise head wave spectrum is performed. Figure 3.7 displays a comparison of the RAOs for the relevant degrees of freedom, referenced to the center of mass. A strong agreement is observed between both rigid-body solutions, confirming the reliability of the implemented tool.

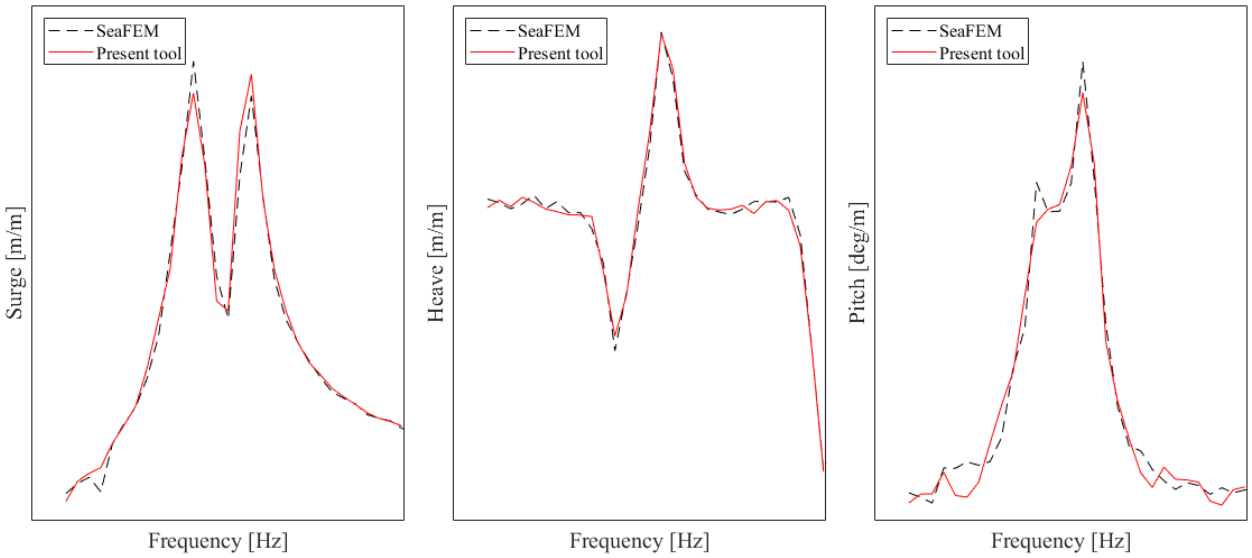

Figure 3.7: W2Power: RAOs comparison (no wind, rigid turbines).

The assessment of the turbine load exchange is carried out using the same methodology and load case conditions as for the OC3-Hywind: a constant wind velocity without waves. This load case is first computed by the present framework, from which the wind force in surge acting over the rotors is extracted. The same case is reproduced afterwards in SeaFEM, introducing the sum of the precomputed loads from both turbines as an external load. This is done to account for the wind aerodynamic loads, as SeaFEM does not include a wind turbine model. The displacement, velocity, and acceleration in surge are presented in Figure 3.8. Both solutions agree, proving that the coupling strategy is properly implemented.

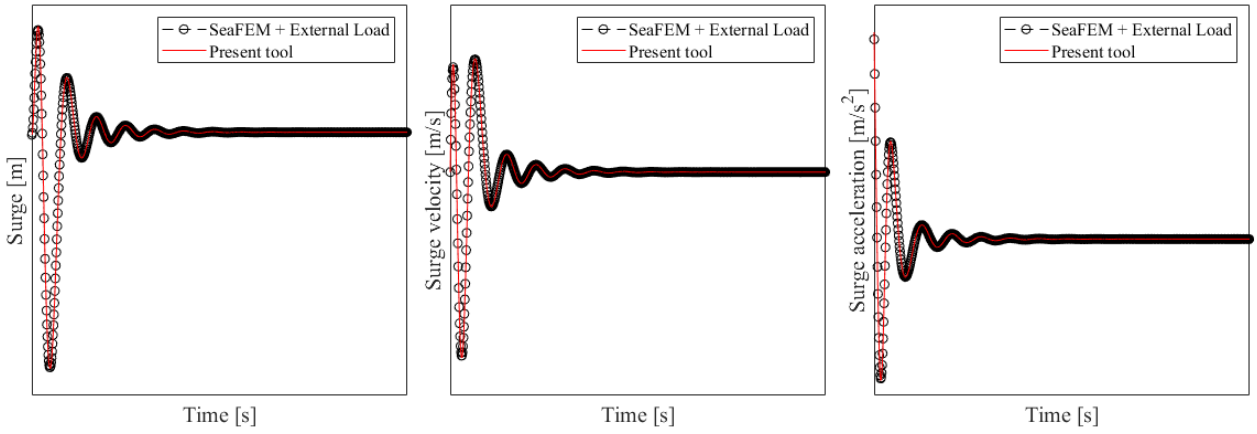

Figure 3.8: W2Power: surge motions (no waves, rigid turbines).

The coupling is further tested under a combined load case composed of a turbulent wind and an irregular sea state. The wind speed at hub height is set to 10 m/s. The wave spectrum is defined using a JONSWAP model, with a significant wave height of 5 meters and a mean wave period of 12 seconds. The minimum and maximum wave periods are 5 seconds and 25 seconds, respectively, with 50 waves used for discretization. The platform is released in surge, heave, and pitch, with the generator off.

A coupled analysis is first performed using the present SF-OF tool to extract the turbine loads. The same seakeeping condition is then simulated in SeaFEM, where the precomputed turbine loads are introduced as external loads. The extracted loads, referenced at the hub heights of their respective turbines, are translated to the total center of mass before being incorporated into SeaFEM. Figure 3.9 shows the rigid-body response for the analyzed condition, comparing both numerical strategies. The results are referenced to the center of mass.

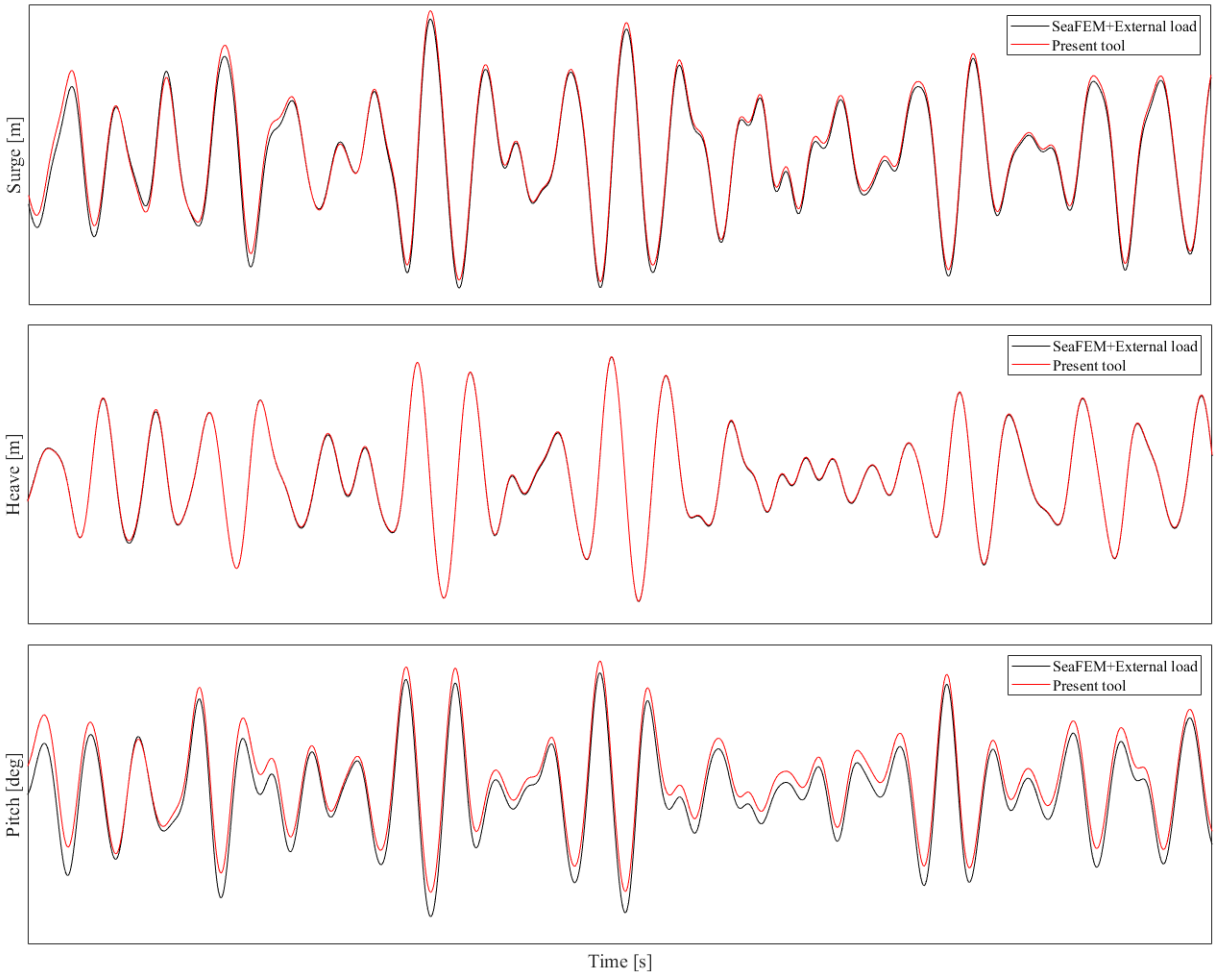

Figure 3.9: W2Power: rigid-body response in wind-waves condition.

Agreement is observed between both solutions, with slight discrepancies in pitch equilibrium, which are assumed insignificant due to their small magnitude.

3.4 Conclusions

This chapter presents a methodology for the development of a numerical solver addressed to multi-turbine offshore platforms. This tool allows the coupled analysis of these platforms, covering their combined structural response and power production. The present time–domain numerical framework computes the aero-hydro–servo–elastic solution of these structures subjected to environmental loads. It is based on the turbine dynamics simulator OpenFAST, strongly coupled with the seakeeping hydrodynamics solver SeaFEM.

The current extension is implemented for the analysis of twin turbine concepts, but can be easily extended to an arbitrary number of turbines by applying the same methodology. By using several OpenFAST executions, it is possible to analyze a platform supporting turbines with their own features and control systems in different operational conditions. Moreover, it is also able to compute structural concepts with leaning towers, which is a common feature of multi-rotor platforms. For the present application, aerodynamic wake interferences are not considered, since it is assumed to be a non-dominant effect in turbines placed side-by-side. This implies a limitation when analyzing nearby or not co-planar rotors, which is particularly relevant for the analysis of the in-field blockage effect in multi-rotor concepts or configurations with downstream turbines.

An intercode process is proposed to test the consistency of the seakeeping rigid-body response in multi-turbine platforms. The natural frequencies and peak amplitudes of the RAOs are well predicted. Moreover, the results are consistent for surge motions under wind conditions. The developed multi-rotor tool is also tested under a combined environmental condition, showing good agreement between the compared numerical strategies.

Although the structural assessment is a main concern in floating offshore platforms, current numerical solvers limit the model of multi-rotor platforms to rigid-body analysis. This approach might be inaccurate given that multi-rotor configurations are characterized by having large substructures where elastic deformations might be significant. With the hydroelastic capabilities of SeaFEM integrated into the present framework in Chapter 6, these elastic effects can be accurately captured, enabling the detailed structural assessment of these new concepts.

Chapter 4

Extension of the coupled framework including second-order hydrodynamic effects

4.1 Introduction

The mooring system attached to floating offshore wind turbines performs the function of station-keeping, providing restoring forces able to counteract environmental conditions. Its design is crucial for the safe operation of offshore floating facilities. These soft-moored platforms with catenary systems usually have high natural periods, which are outside the wave frequency range. However, although wave frequencies are generally higher, second-order effects might include low-frequency components that can also excite the slow-drift motions of the system.

This becomes even more relevant in floating wind platforms, particularly in semi-submersible concepts. Reason found in the slow-drift forces, which are usually in the range of their surge natural period. When these forces excite their resonance frequency this might lead to large platform excursions [Servan-Camas et al., 2018]. As a consequence, these large oscillations might stress the mooring system or produce vibrations causing fatigue damage to the platform. This aspect is particularly significant for FOWTs, where the sum-frequency range may excite the first tower-bending modes [Duarte et al., 2014]. Accordingly, in order to design a proper structural concept and mooring system, the second-order effects must be analyzed accurately.

Wave-tank tests conducted by the DeepCwind at the Maritime Research Institute Netherlands (MARIN) suggest that second-order effects might be more relevant than expected [Goupee et al., 2014]. In some cases, these second-order hydrodynamic loads can increase the response of a floating platform, becoming even larger than for the first-order one. Despite this, most of the existing work on floating wind turbines, such as in [Li et al., 2018 and Bjerg Thomsen et al., 2021], neglect the second-order contribution since being typically smaller and so reducing the complexity of the problem [Roald et al., 2014 and Coulling et al., 2013].

Currently, some aero-hydro-servo-elastic simulation tools for offshore wind platforms incorporate second-order hydrodynamic effects using external Boundary Element solvers. [Bayati et al., 2014] and [Matos et al., 2011] propose strategies to account for non-linear effects in OpenFAST by solving the second-order wave problem in the frequency domain with the BEM solver WAMIT. Similarly, [Mei and Xiong, 2021] integrates OpenFAST with AQWA and concludes that ignoring second-order effects leads to an underestimation of fatigue damage. CFD methods are also commonly used to evaluate non-linear hydrodynamics. For instance, [Huang et al., 2020] used OpenFOAM to analyze the hydrodynamic behavior of the DeepCwind platform. It was found that the platform response was sensitive to the low-frequency waves.

This chapter presents a strategy to upgrade the seakeeping coupling between OpenFAST and SeaFEM to account for second-order hydrodynamic effects. This is performed by using SeaFEM's up-to-second-order wave diffraction-radiation solution in the time-domain. This approach allows for a fully integrated solution of the coupled problem in the same framework.

4.2 Methodology

The first-order hydrodynamic problem for potential flow assumes that the wave amplitudes are small compared to both the wavelength and the water depth. In the case of steep waves close to the breaking limit, non-linear wave theory should be modeled, since second-order effects become noticeable.

In the first-order problem, forces and motions oscillate with the frequency of the incident waves. In contrast, the second-order problem accounts for interactions between two oscillating components, resulting in forces and motions at the sum and difference frequencies of the incident waves. These interactions might lead to: mean-drift loads, which cause an offset of the structure relative to its undisplaced position; and slow-varying loads, which can excite large amplitude resonant motions of the platform at low frequencies in irregular sea states [Roald et al., 2013].

4.2.1 Up-to-second order governing equations

The SeaFEM code allows to perform seakeeping analysis including second order effects. The governing equations used are derived from the potential flow and the wave diffraction-radiation problem. The up-to-second order equations are obtained after applying Taylor series expansion to the free surface and body boundary conditions. Then, a perturbed solution based on the Stokes wave approximation is applied to the velocity potential, the free surface elevation, and the floater motion.

Finally, by retaining the up-to-second order terms, the resulting set of equations used to solve the boundary value problem given below. The superscripts 1 and $1+2$ represent the first-order and first plus second order components. Further details and second order diffraction-radiation governing equations can be found in [Servan-Camas, 2016 and Servan-Camas et al., 2018].

- Laplace equation:

$$\Delta\varphi^{1+2} = 0 \qquad \text{in } \Omega \tag{4.1}$$

- Kinematic free surface boundary condition:

$$\frac{\partial \xi^{1+2}}{\partial t} - \frac{\partial \varphi^{1+2}}{\partial z} = \xi^1 \frac{\partial}{\partial z}\left(\frac{\partial \varphi^1}{\partial z}\right) - \frac{\partial \xi^1}{\partial x}\frac{\partial \varphi^1}{\partial x} - \frac{\partial \xi^1}{\partial y}\frac{\partial \varphi^1}{\partial y} \qquad \text{on } z = 0 \tag{4.2}$$

- Dynamic free surface boundary condition:

$$\frac{\partial \varphi^{1+2}}{\partial t} + \frac{P_{fs}}{\rho} + g\xi^{1+2} = -\xi^1 \frac{\partial}{\partial z}\left(\frac{\partial \varphi^1}{\partial t}\right) - \frac{1}{2}\nabla\varphi^1 \cdot \nabla\varphi^1 \qquad \text{on } z = 0 \tag{4.3}$$

- Body boundary condition:

$$\left(\mathbf{v_p}^1 + \mathbf{v_\varphi}^1\right) \cdot \mathbf{n_p}^1 + \left(\mathbf{v_p}^{1+2} + \mathbf{v_\varphi}^{1+2}\right) \cdot \mathbf{n_p}^0 = -\left(r_p^1 \cdot \nabla\right) \mathbf{v_\varphi}^1 \cdot \mathbf{n_p}^0 \qquad \text{on } P \in \Gamma_B \tag{4.4}$$

- Seabed boundary condition:

$$\mathbf{v_\varphi}^{1+2} \cdot \mathbf{n_p} = 0 \qquad \text{on } P \in \Gamma_S \tag{4.5}$$

The pressure at a point P of the body wet surface:

$$P_P^{1+2} = -\rho g(z_p + r_{pz}^{1+2}) - \rho\left(\frac{\partial \varphi^{1+2}}{\partial t} + r_p^1 \cdot \nabla\left(\frac{\partial \varphi^1}{\partial t}\right) + \frac{1}{2}\nabla\varphi^1 \cdot \nabla\varphi^1\right) \tag{4.6}$$

The variable definitions for the governing equations of the problem remain consistent with those provided in Chapter 2. Then, the seakeeping loads are obtained by direct pressure integration on the wet body surface.

Finally, the dynamics of the floating body are solved by the equation of motion, for each solution order independently:

$$\mathbf{M}\ddot{\mathbf{q}}^1 + \mathbf{K}\mathbf{q}^1 = \mathbf{F}^1 \qquad \mathbf{M}\ddot{\mathbf{q}}^{1+2} + \mathbf{K}\mathbf{q}^{1+2} = \mathbf{F}^{1+2} \tag{4.7}$$

The seakeeping problem is divided into first-order and up-to-second-order solutions, which can be solved separately. At each time step, the up-to-second-order solution is calculated right after the first-order solution.

4.2.2 Coupling strategy

When adapting the coupling SeaFEM - OpenFAST to account for second-order effects, the solution sequence and independence, (1st+2nd) after 1st order, needs to be respected. In other words, the first-order seakeeping analysis must be completed, within each time step, before initiating the up-to-second-order computation, as the latter relies on the results of the former. In between the first-order solution terms are transferred to the up-to-second-order problem. The Algorithm 3 details the coupling process at the interface of SeaFEM.

Algorithm 3: 2nd order coupling for single turbines

SeaFEM → Initializes OpenFAST^1 and OpenFAST^{1+2};
(SeaFEM interface);
for $t < T_{max}$ **do**
  for $iter < Iter^1_{max}$ **do**
    Rotor loads received $\mathbf{F}^1_{Rotor}$;
    Kinematics received $(\ddot{\mathbf{q}}^1, \dot{\mathbf{q}}^1, \mathbf{q}^1)$;
    Solver seakeeping 1 sends $\mathbf{F}^1_{Hydro}$;
  end
  Compute terms 1 solution → 1+2 problem;
  for $iter < Iter^{1+2}_{max}$ **do**
    Rotor loads received $\mathbf{F}^{1+2}_{\text{Rotor}}$;
    Kinematics received $(\ddot{\mathbf{q}}^{1+2}, \dot{q}^{1+2}, q^{1+2})$;
    Solver seakeeping (1+2) sends $\mathbf{F}^{1+2}_{Hydro}$;
  end
  OpenFAST^{1+2} → updates SeaFEM $t_{SF}++$;
end
OpenFAST^{1+2} → ends SeaFEM

The seakeeping solution is computed twice, corresponding to each order. Consequently, two separate OpenFAST instances are coupled, each handling the kinematic solution for its respective order. Again, since both OpenFAST solvers need to work simultaneously, the code is parallelized using two threads. The same base strategy is followed as described in Chapter 2.

A more detailed flowchart of the coupling and process synchronization is given in Figure 4.1. Once the OpenFAST DLLs are initialized by SeaFEM, the seakeeping exchange begins, involving the transfer of hydrodynamic loads and kinematic motions for the first-order solution. This process is repeated for each iteration.

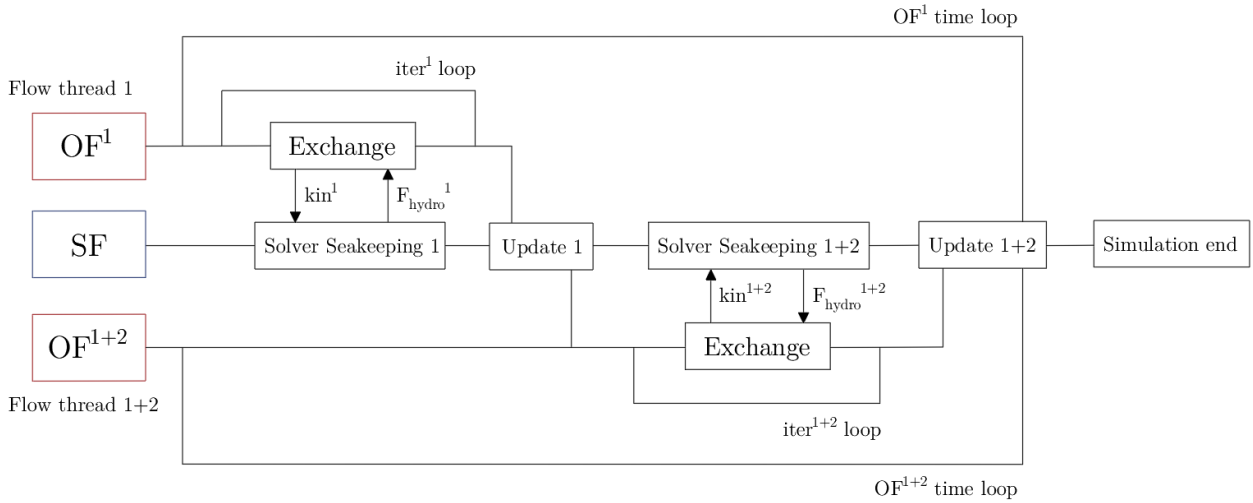

Figure 4.1: Block diagram with the 2nd order extension strategy.

When finished, the first order enters in update state enabling the seakeeping exchange for the combined first- and second-order solution. This iterative process continues until the up-to-second order solution is also updated. At this stage, the seakeeping solution for the given time step is considered complete.

SeaFEM then increments the time step and synchronizes it with the OpenFAST solvers, restarting the exchange process. This sequence repeats until the maximum simulation time is reached. The underlying concept is that at each time step, the up-to-second order solution is computed only after the first-order solution is known.

In the case of the multi-rotor solution, the same strategy would be required. Complexity is added as it requires the coupling with four OpenFAST instances. One OpenFAST for each turbine and two OpenFAST for each solution order. Accordingly, the parallelization has to be performed with four threads.

4.3 Intercode comparison - OC4 DeepCwind

The OC4-DeepCwind semi-submersible platform was selected for this study due to its design. This type of foundation was observed to be particularly sensitive to second-order effects in previous works [Servan-Camas et al., 2018 and Mei and Xiong, 2021]. The full-scale OC4-DeepCwind platform [Robertson, Jonkman, Masciola, et al., 2014] along with the NREL 5-MW reference wind turbine [Jonkman et al., 2009] and the reference mooring system is used. In Table 4.1, the OC4-DeepCwind platform specifications are summarized.

Table 4.1: OC4-DeepCwind platform particulars.

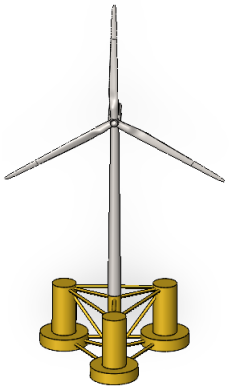

	Unit	Value
Mass (with ballast)	kg	13,473,000
Downwind distance of CM	m	0.00
Lateral distance of CM	m	0.00
Vertical distance of CM	m	-13.46
Roll inertia about CM	$kg \cdot m^2$	$6.827 \cdot 10^9$
Pitch inertia about CM	$kg \cdot m^2$	$6.827 \cdot 10^9$
Yaw inertia about CM	$kg \cdot m^2$	$1.226 \cdot 10^{10}$

The platform is subjected to an only waves loadcase, generated with an irregular sea-state using a JONSWAP spectrum. A significant wave height of 1 meter and a mean wave period of 14 seconds are considered. The number of waves used for the discretization is 100, the minimum wave period is 5 s (w_{max} = 1.25 rad/s), and the maximum wave period is 35 s (w_{min} = 0.18 rad/s). The wave spectrum used is plotted in Figure 4.2.

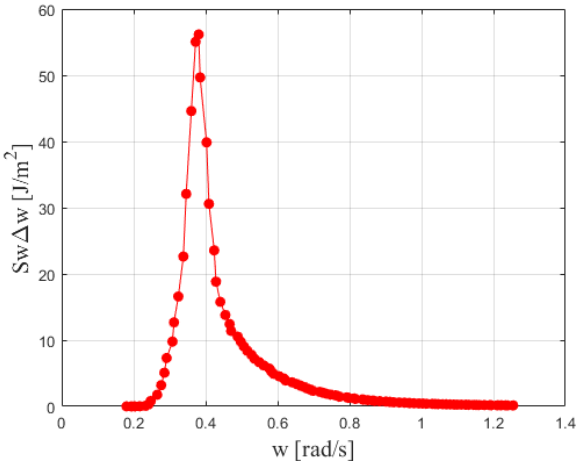

Figure 4.2: JONSWAP spectrum discretization.

The purpose of this analysis is the code-to-code comparison of the implemented extension. To do so, the rigid-body response under second-order effects of an irregular wave spectrum is studied. This frequency range is selected to represent a typical sea-state. The solution computed by only SeaFEM and the present coupled SF-OF are compared. In the coupled approach the kinematic solution is solved by OpenFAST. Figure 4.3 presents the rigid-body responses for the relevant degrees of freedom, first-order solution (left) and up-to-second-order solution (right). The first 300 seconds are omitted to exclude transient solutions.

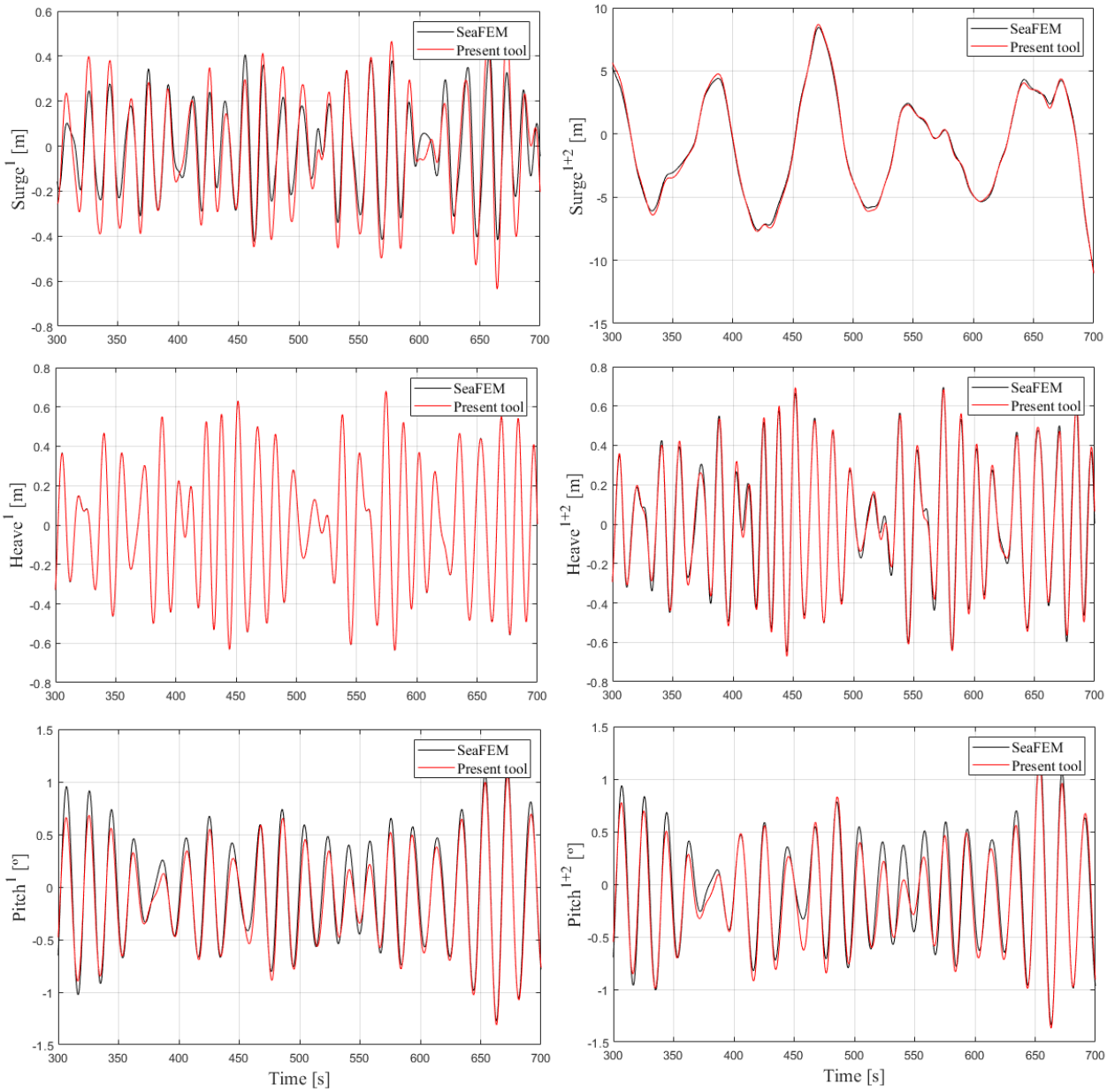

Figure 4.3: DeepCwind: rigid-body response. Left column: first-order. Right column: 1st+2nd order.

This analysis examines the impact of second-order wave excitation loads on the platform's motions. The whole solution obtained using SeaFEM alone is contrasted with the results from the combined SeaFEM (hydrodynamics) – OpenFAST (kinematics) tool. Strong agreement is observed between both methods, with discrepancies attributed to differences in the numerical schemes used for the rigid body dynamics. As expected, the surge motion is the most influenced by the non-linear wave excitation. Large excursions were obtained reaching the 10-meters amplitude in slow oscillations. In contrast, the up-to-second-order solution for heave and pitch responses exhibit only a slight impact.

Although the DeepCwind platform has a high natural period in surge (107.52 seconds), being outside the excitation range of the typical incident wave periods (5–25 seconds), the second-order resonant effects prove to be significant. This occurs despite the smaller magnitude of second-order hydrodynamic loads and the relatively low energy level of the selected wave spectrum. Difference-frequency forces, occurring at frequencies below those of the first-order forces, have the potential to excite the structure's natural frequencies. In this case, the surge motion is particularly affected, with second-order low-frequency forces inducing large excursions.

4.4 Conclusions

In the present chapter, the hydrodynamic coupling of the wind turbine framework is enhanced for the solution of the up-to-second order wave diffraction-radiation problem. Based on the methodology outlined in Chapter 2, SeaFEM computes the hydrodynamic solution, in this case including second-order effects, whereas OpenFAST provides the rigid-body kinematics. This enables the analysis of phenomena that are otherwise neglected in linear wave models, providing a more accurate representation of the platform dynamics. The coupled strategy is contrasted against the standalone SeaFEM solution. The implemented tool is applied to the DeepCwind semi-submersible concept to analyze its response under second-order effects.

This study demonstrates that neglecting higher-order terms, based on the assumption that hydrodynamic forces are relatively small, can lead to a significant underestimation in the global response of floating wind platforms. In this analysis, the semi-submersible concept was subjected to excitation within a typical wave frequency range in an irregular sea state. Large platform excursions were observed although using a low amplitude wave excitation. These resonance effects might appear during the normal operation of these floating platforms. Consequently, more research should be addressed to its study.

In particular, it was observed an excitation of the surge natural frequency leading to large excursions and oscillations. This significant influence of second-order effects on surge response is consistent with previous literature. Further studies, including aerodynamic loads, should be performed to cover the combined solution.

Given the limited research on this topic, the impact of these non-linear loads on FOWTs remains unclear. Their effects largely depend on factors such as the system's natural frequencies, structural geometry, and mooring configurations. Accordingly, studies across various platform configurations are necessary. In this context, the implemented tool can contribute to a deeper understanding of this hydrodynamic response. Furthermore, second-order wave excitations must be considered not only in the motion analysis of FOWTs but also in structural assessments. Neglecting these effect might lead to ignore the resonance of structural modes with eigen frequencies in the range of twice the wave frequencies. The hydroelastic method presented in Chapter 5 is used in Chapter 6 to capture these effects while studying the tower's structural resonance.

Chapter 5

Hydroelastic analysis using the MMR technique

5.1 Introduction

With the global exploitation of marine energy resources, a variety of offshore applications are emerging, such as floating solar systems, wind turbine platforms, and energy converters, among others. These floating structures are typically large, with complex geometries and notable flexibility due to their size. Moreover, these offshore structures might be subjected to harsh environmental conditions, making their structural assessment a critical concern. Additionally, cyclic sea-state loads subject these structures to fatigue damage limiting their useful life. A hydroelastic study could be crucial to preserve the structural integrity along its lifespan by reducing the accumulated fatigue damage. In this regard, the use of higher fidelity numerical tools becomes essential to predict the structural behavior in early design stages.

Present hydroelastic numerical solvers require the coupling between seakeeping hydrodynamics and structural dynamics solvers. The most common method involves solving the wave diffraction-radiation problem using a three-dimensional BEM, while the structural dynamics are typically modeled with a one-dimensional beam representation solved using the FEM [Jiao et al., 2018]. In order to handle hydrodynamic non-linear effects, several works have upgraded their solution by solving the Navier-Stokes equations [Xuemin et al., 2024, Jialong et al., 2024]. Although this approach comes with a higher computational cost, it may be necessary for fluid-structure interaction problems where potential flow solutions are limited to accurately capture the underlying physics. Concerning the structural solution, a few studies have proposed enhanced approaches by coupling a three-dimensional FEM model as

in [Oberhagemann et al., 2015, Kyong-Hwan et al., 2013]. However, these methods are often restricted to quasi-static approximations, which provide an accurate solution only for slow structural deformations.

In order to capture transient non-linear effects and local stresses, it is required to solve the three-dimensional fully coupled hydroelastic problem in the time-domain [Malenica, 2007]. However, this approach is quite rare in the literature due to its complexity and computational demands, mostly taken by the structural solver [Servan-Camas et al., 2025]. Current assessment methodologies rely on mid-fidelity tools inherited from the naval and offshore industries, which neglect relevant physical effects and use quasi-static approaches for structural analysis that, contrary to evidence, disregard the dynamics of structural elasticity on the overall system response. Moreover, partitioned strategies are most commonly used, solving the hydroelastic problem in several stages, but allowing only for one-way (fluid to structure) couplings. Another emerging alternative are reduced order models, which approximate the structural solution using a modal superposition method [F. Song et al., 2021].

A novel method of the latter technique is described in this chapter. The hydroelastic solver implemented in [Garcia-Espinosa et al., 2023] is able to perform fully-coupled analysis while maintaining an affordable computational cost. This model is based on the coupling of a 3D FEM seakeeping hydrodynamic solver with a 3D FEM based structural ROM. The structural degrees of freedom are significantly reduced by retaining the most energetic eigenmodes. To do so, the higher-fidelity structural solution is projected onto a reduced modal basis to obtain the modal matrix system.

Its capabilities and consistency are demonstrated in a simplified application case on the in-house semi-submersible structural design of the OC4-DeepCWind platform, named CIMNE-DeepCwind. The study performed in this chapter focuses in the structural analysis of the platform under static condition while in Chapter 6 the dynamic analysis will be performed.

5.2 Hydroelastic solver

In [Servan-Camas et al., 2021] a strategy was implemented for the coupling of seakeeping hydrodynamics and structural dynamics using solvers developed in house and integrated into the commercial packages SeaFEM and RamSeries. Both solvers are implemented under the same programming framework, allowing a direct communication between them and the use of OpenMP for its parallel execution. It was reported that most of the computational time required for fully coupled analysis is taken to solve the structural dynamics. In order to overcome this bottleneck, the authors proposed a ROM based on the MMR technique

[Garcia-Espinosa et al., 2023], where the number of degrees of freedom for the structural problem can be largely reduced alongside its computational cost.

Hydroelastic analysis can be performed by coupling this time-domain wave diffraction-radiation solver with a time-domain structural solver. Currently, two hydroelastic strategies can be used depending on their structural solution. The first one, was presented in previous published research [Servan-Camas et al., 2021], consists in the direct coupling between SeaFEM and a 3D FEM structural solver. The new implemented strategy in [Garcia-Espinosa et al., 2023] can be seen as an evolution of previous one, with the aim of reducing its computational cost. This strategy consists of using the presented structural ROM, instead of the full FEM structural solver.

In this work, the last approach will be used, needing also both codes. First, the structural solver RamSeries is used only to obtain the structural particulars such as the structural FEM matrices (mass and stiffness) and/or the modal base. Then, in a second stage, the seakeeping solver SeaFEM reads the structural particulars, building the structural dynamics equations coupled with the seakeeping hydrodynamics equations. In this way, there is no need to execute the structural solver for each hydroelastic computation.

The numerical solution using FEM of the boundary value problem presented in Chapter 2 and reported in [Servan-Camas, 2016] will be used. It requires to solve the following system of equations:

$$\mathbf{L}\boldsymbol{\phi} = \mathbf{b}^B + \mathbf{b}^R + \mathbf{b}^{Z_0} + \mathbf{b}^S \tag{5.1}$$

Where $\mathbf{L}$ is the Laplacian Matrix and $\boldsymbol{\phi}$ the velocity potential. The vectors $\mathbf{b}^B$, $\mathbf{b}^R$, $\mathbf{b}^{Z_0}$, and $\mathbf{b}^S$ result from the integration of the boundary condition terms of body surface, radiation, free surface and seabed, respectively. The above system can be written clustering the nodes lying on the body surface as:

$$\begin{bmatrix} \mathbf{L}_{II} & \mathbf{L}_{I_B} \\ \mathbf{L}_{I_B I} & \mathbf{L}_{\Gamma_B \Gamma_B} \end{bmatrix} \begin{bmatrix} \boldsymbol{\phi}_I \\ \boldsymbol{\phi}_{\Gamma_B} \end{bmatrix}^{n+1} = \begin{bmatrix} \mathbf{b}_I \\ \mathbf{b}_{\Gamma_B} \end{bmatrix}^{n+1} \tag{5.2}$$

Here, n denotes the n-th time step, while the subscripts I and Γ_B correspond to the nodes in the internal mesh and the coupling boundary between the fluid and the structure, respectively. Then, $\mathbf{b}_{\Gamma_B}$ contains the velocities of a point lying on the structure boundary. In the absence of forward speed, a fourth order compact Padé scheme is used to integrate the free surface boundary condition. The time-integration in SeaFEM is performed using the Newmark method. Additional numerical details, as well as a number of verification and validation cases, can be found in [Servan-Camas, 2016].

SeaFEM also includes a mooring solver with capabilities to simulate quasi-static and dynamic FEM multi-segment lines [Gutierrez-Romero et al., 2016]. The corresponding mooring loads can be applied to the structural solver as well.

5.2.1 Structural model

The structural dynamic model implemented in RamSeries and used in this work is based on geometrical non-linear shell finite elements. The geometrical non-linear strategy derives from the co-rotational method developed by [Felippa and Haugen, 2005]. The core element used by the co-rotational shell model is a 3-node element with three translations and three rotations per node, which is obtained by the combination of a membrane element and a plate element. The membrane element is based on the optimal triangle element with drilling rotation developed by [Felippa, 2003], while the plate element on the classical Discrete Kirchhoff Triangle (DKT) element. This element has shown better performance than the standard bilinear quadrilateral element generally used in marine applications [Felippa, 2003]. The complete model has been developed in-house and integrated within the commercial package RamSeries. The frame of reference used is the same as for the seakeeping model. The governing equations of the model are given by:

$$\begin{aligned} &\mathrm{div}(\boldsymbol{\sigma}) + \mathbf{b} = \rho\ddot{\mathbf{u}} && \text{in } \Omega_{s,}, \\ &\mathbf{u} = \overline{\mathbf{u}} && \text{on } P \in S_u, \\ &\boldsymbol{\sigma} \cdot \mathbf{n} = \overline{\mathbf{t}} && \text{on } P \in S_\sigma, \end{aligned} \tag{5.3}$$

where $\boldsymbol{\sigma}$ is the stress tensor, $\mathbf{b}$ is a vector that includes the mass force and internal damping, Ω_s is the structural domain, $\mathbf{u}$ is the structural displacement vector field, S_u is the part of the structural external surface with prescribed displacements $\overline{\mathbf{u}}$, S_σ is the part of the structural external surface with prescribed tractions $\overline{\mathbf{t}}$. The FEM version of the above system of equations can be written as:

$$\mathbf{M}\ddot{\mathbf{u}} + \mathbf{C}\dot{\mathbf{u}} + \mathbf{K}\mathbf{u} = \mathbf{f} \tag{5.4}$$

where $\mathbf{M}$ represents the mass matrix, $\mathbf{C}$ the structural damping matrix, $\mathbf{K}$ the stiffness matrix, $\mathbf{u}$ the displacement vector of the structural nodes, and $\mathbf{f}$ the boundary conditions vector containing the external loads and prescribed displacements. The time-discretized version of the above system of equations can be written as:

$$\mathbf{S}\mathbf{u}^{n+1} = \mathbf{f}^{n+1} \tag{5.5}$$

here $\mathbf{S}$ is the tangent stiffness matrix. The system above can be written clustering the nodes lying on the body surface, where $\mathbf{f}_{\Gamma_B}$ contains the body boundary condition due to the fluid pressure.

$$\begin{bmatrix} \mathbf{S}_{II} & \mathbf{S}_{I\Gamma_B} \\ \mathbf{S}_{\Gamma_B I} & \mathbf{S}_{\Gamma_B\Gamma_B} \end{bmatrix} \begin{bmatrix} \mathbf{u}_I \\ \mathbf{u}_{\Gamma_B} \end{bmatrix}^{n+1} = \begin{bmatrix} \mathbf{f}_I \\ \mathbf{f}_{\Gamma_B} \end{bmatrix}^{n+1} \tag{5.6}$$

5.2.2 Modal Matrix Reduction

The MMR technique is used to reduce the structural computational effort. In this method, the structural motion equations are projected onto the orthogonal truncated base composed of the eigenvectors. In other words, the order reduction is achieved by projecting the FEM solution onto a subspace of solutions with a smaller dimension [Garcia-Espinosa et al., 2023]. This subspace is built using the MMR technique. The displacement field is then reconstructed as a linear combination of the eigenmodes, using the modal amplitudes as scalar values for each eigenvector. In this way, the structural solution can be approximated using a less number of degrees of freedom [Patalano et al., 2019]. The detailed process is described below.

Starting from the structural dynamics Eq. (5.4), the free vibration problem $\mathbf{f} = 0$ with no damping $\mathbf{C} = 0$ can be defined by:

$$\mathbf{M}\ddot{\mathbf{u}} + \mathbf{K}\mathbf{u} = 0 \tag{5.7}$$

The solution reads $\mathbf{u}(t) = \mathbf{a}\sin(\mathbf{\Omega}t)$, where $\mathbf{a}$ is the maximum vibration amplitude and $\mathbf{\Omega}$ the vibration frequency. Then, the eigenvalue problem is obtained by introducing the solution into the Eq. (5.7):

$$(\mathbf{M}^{-1}\mathbf{K})\mathbf{a} = \mathbf{\Omega}^2\mathbf{a} \tag{5.8}$$

Physically, each mode a_i represents the shape at which the system freely vibrates at a frequency Ω_i. It can be shown that the vibration modes are orthogonal with respect to the mass matrix. Furthermore, using the eigenvalue equation (5.8), it can also be established the orthogonal property of the vibration modes with the stiffness matrix:

$$a_i^T\mathbf{M}a_j \begin{cases} = 1 \text{ if } i = j \\ = 0 \text{ if } i \neq j \end{cases} \qquad a_i^T\mathbf{K}a_j \begin{cases} = \Omega_i^2 \text{ if } i = j \\ = 0 \text{ if } i \neq j \end{cases} \tag{5.9}$$

Since the eigenmodes of the system constitute an orthonormal basis, the structural displacements can be expressed as a linear combination of the modal displacements, known as modal superposition:

$$\mathbf{u}(t) = \sum_{i=1}^{N_{DOF}} q_i(t)a_i \tag{5.10}$$

Where N_{DOF} is the number of degrees of freedom of the problem, $\mathbf{u}(t)$ is the displacement field, and q_i is the temporal variation of the modal amplitudes. By substituting Eq. (5.10) in

the structural dynamics Eq. (5.4) and projecting onto a_i, we obtain:

$$a_i^T \mathbf{M} \ddot{q}_i a_i + a_i^T \mathbf{C} \dot{q}_i a_i + a_i^T \mathbf{K} q_i a_i = a_i^T \mathbf{f}(t) \tag{5.11}$$

The structural damping, which accounts for the energy dissipation during motion due to mechanisms such as joint friction, internal heating, and interaction with the surrounding fluid, is often modeled using either Rayleigh damping or modal damping. In the Rayleigh damping approach, the damping matrix $\mathbf{C}$ is expressed as linear combination of $\mathbf{K}$ and $\mathbf{M}$, as given in $\mathbf{C} = \alpha_M \mathbf{M} + \alpha_K \mathbf{K}$. Then, by applying the orthogonal properties, the damping coefficient c_i can be defined as below, where α_M and α_K are user defined coefficients and η represents the percentage with respect to the critical modal damping.

$$c_i = \begin{cases} \alpha_M + \alpha_K \Omega_i^2 & Rayleigh \quad damping \\ 2\eta\Omega_i & Modal \quad damping \end{cases} \tag{5.12}$$

Considering the orthogonality properties in the Eq. (5.9) and the previous definition of the damping coefficient, Eq. (5.11) becomes diagonal, allowing it to be decoupled for each i_{th} mode. Here, Ω_i represents the vibration frequency of the i_{th} mode.

$$\ddot{q}_i + c_i \dot{q}_i + \Omega_i^2 q_i = f(t) \cdot a_i(x) = f_i(t) \qquad \mathbf{\Omega}^2 = \begin{bmatrix} \Omega_1^2 & 0 & 0 \\ 0 & \ddots & 0 \\ 0 & 0 & \Omega_i^2 \end{bmatrix} \tag{5.13}$$

This equation indicates that the response of a damped linear system to a given excitation can be computed from a set of N_m uncoupled equations. Once the modal amplitude evolution is known, the displacement field can be recovered as:

$$\mathbf{u}_{MMR}(t) = \sum_{i=1}^{N_m} q_i(t) a_i \tag{5.14}$$

The idea behind this order reduction approach is that, generally, only the lower frequency modes are excited and needed to obtain an accurate approximation of the structural solution. By reducing the modal basis discarding higher frequency eigenmodes, the solution is several orders of magnitudes smaller than for the structural FEM solver $N_m \sim O(10^3) \ll N_{DOF} \sim O(10^6)$.

Finally, the term elastic energy $\mathbf{E}(t)$ and $\mathbf{E}_{MMR}(t)$ are defined, being used to measure the fidelity of the MMR solution to approximate the full FEM solution.

$$\mathbf{E}(t) = \frac{1}{2} \mathbf{u}^T \mathbf{K} \mathbf{u} \qquad \mathbf{E}_{MMR}(t) = \frac{1}{2} \mathbf{u}_{MMR}^T \mathbf{K} u_{MMR} \approx \sum_{i=1}^{i=N_m} \frac{1}{2} \Omega_i^2 q_i^2 \tag{5.15}$$

5.2.3 Hydroelastic coupling

The purpose of this section is to present the strategy implemented to strongly couple the seakeeping hydrodynamics with the structural dynamics. The coupled problem is sketched in Figure 5.1.

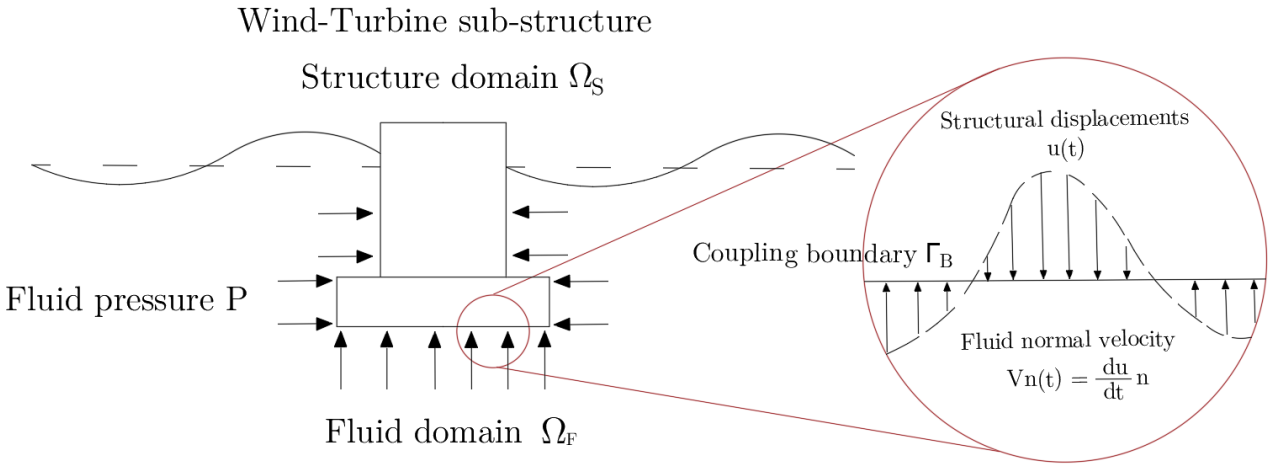

Figure 5.1: Fluid-Structure interaction in a column of a semi-submersible wind turbine.

As presented above, the seakeeping and structural problems are discretized using the FEM. However, it is not required to use identical discretization for the common boundary Γ_B, where the interaction occurs. Spatial linear interpolators are used in this work to transfer the fluid pressure to the structure boundary and to transfer the structural displacements to the fluid boundary.

$$\begin{aligned} \mathbf{P}_{S,\Gamma_B} &= \mathbf{I}^{F\to S}\mathbf{P}_{F,\Gamma_B} \\ \mathbf{u}_{F,\Gamma_B} &= \mathbf{I}^{S\to F}\mathbf{u}_{S,\Gamma_B} \end{aligned} \tag{5.16}$$

Here, $\mathbf{P}_{S,\Gamma_B}$, $\Delta\mathbf{u}_{S,\Gamma_B}$, $\mathbf{P}_{F,\Gamma_B}$, and $\Delta\mathbf{u}_{F,\Gamma_B}$ represent the fluid pressure and structural displacements at the structural and fluid discretization over Γ_B, respectively. The terms $\mathbf{I}^{F\to S}$ and $\mathbf{I}^{S\to F}$ correspond to the interpolation matrices used to transfer information between the fluid and structural domains.

The hydrodynamic and structural solvers are strongly coupled via an iterative process where the coupling variables are interpolated back and forth between the fluid and structural domains at the common boundary Γ_B. This is performed at the wet surface of the floating body, where the seakeeping solver sends the pressure loads, in return to the structural displacements computed by the structural solver. The temporal variation of the structural displacements in the surface normal direction is imposed as a boundary condition on the wet surface. Figure 5.2 shows the iterative process, which allows for one-way dynamic coupling, and strong dynamic coupling. The modified Aitken's method [Irons and Tuck, 1969] was implemented.

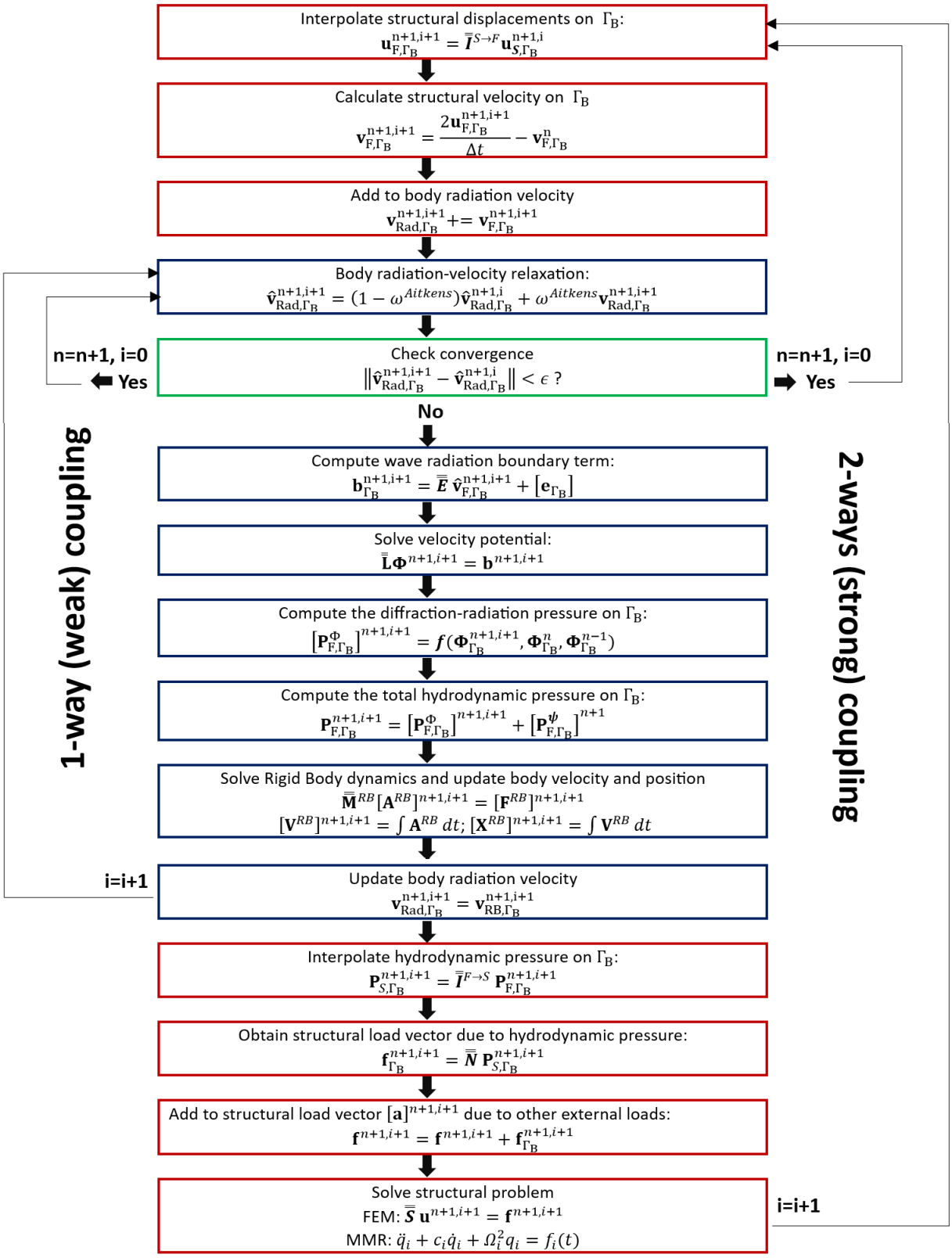

Figure 5.2: Iterative scheme of the partitioned coupling.

5.3 Structural analysis using MMR

5.3.1 Structural design: CIMNE-DeepCwind

The full-scale floating semi-submersible OC4-DeepCwind platform [Robertson, Jonkman, Masciola, et al., 2014] along with the NREL 5-MW reference wind turbine [Jonkman et al., 2009] are used as a basis to design a fully detailed structural concept named CIMNE-DeepCWind. Additionally, the reference mooring system consisting of three catenary lines, and the quadratic damping model to account for viscous effects are considered [Robertson, Jonkman, Vorphal, et al., 2014]. The details of the structural design are provided in Figure 5.3. Further details regarding the structural concept are found in the Annex.

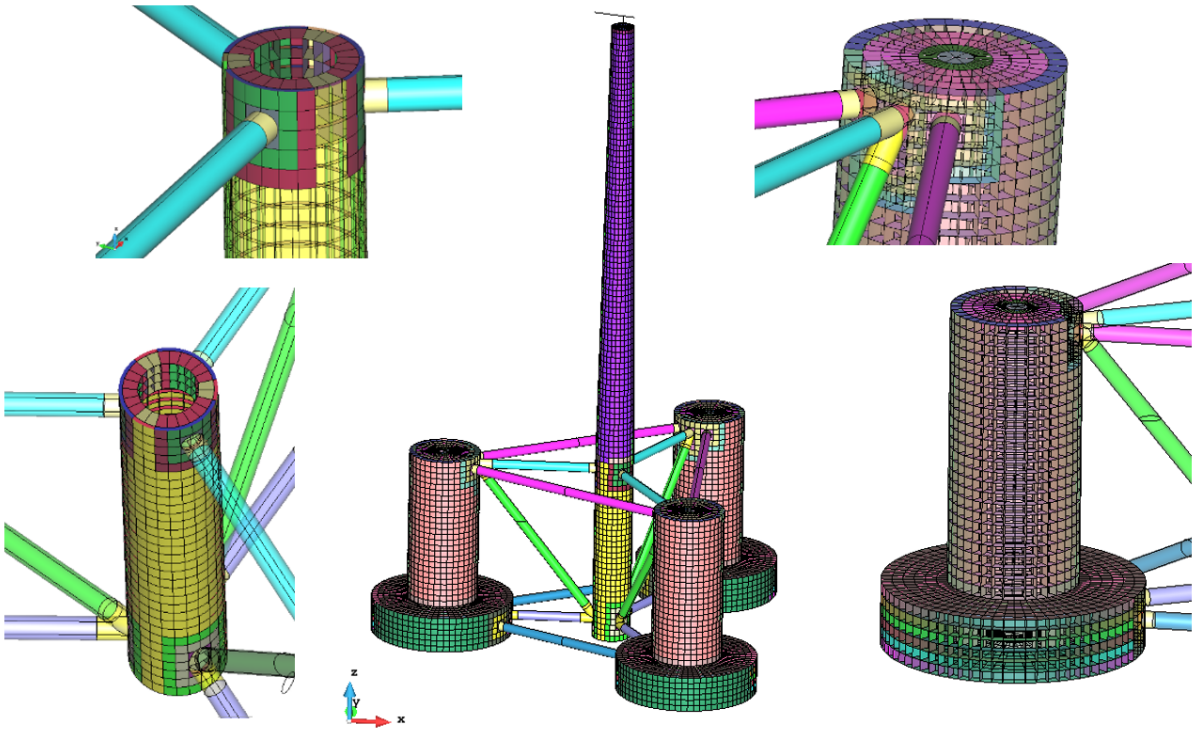

Figure 5.3: CIMNE-DeepCwind structural design and details.

It is worth mentioning that the purpose of this structural design is not to become a real structural solution, but to be used as a benchmark problem with complexity similar to a real one. Being useful as an academic benchmark case to test the capability of simulation tools for structural assessment. In order to have an equivalent global rigid-body response as the OC4-DeepCWind, an approximately similar mass matrix was intended to be preserved during its design. Table 5.1 presents a comparison of the specifications between the OC4-DeepCwind and CIMNE-DeepCwind platforms.

Table 5.1: Total turbine-tower-platform system particulars.

	Unit	OC4-DeepCwind	CIMNE-DeepCwind
Mass (with ballast)	kg	14,072,718	14,077,353
Downwind distance of CM	m	0.00	0.00
Lateral distance of CM	m	0.00	0.00
Vertical distance of CM	m	-9.888	-11.057
Roll inertia about CM	$kg \cdot m^2$	$12,581 \cdot 10^6$	$11,206 \cdot 10^6$
Pitch inertia about CM	$kg \cdot m^2$	$12,567 \cdot 10^6$	$11,140 \cdot 10^6$
Yaw inertia about CM	$kg \cdot m^2$	$12,290 \cdot 10^6$	$11,302 \cdot 10^6$
Ballast mass	kg	$9.621 \cdot 10^6$	$8.506 \cdot 10^6$

For a better agreement with the original concept, the external structural geometry and dimensions are kept similar, except for the central column which reaches 12m above the sea water level (SWL), instead of 10m as in the OC4. This implies that the tower starts at 12m above SWL. The inner structure is mainly composed of longitudinal, horizontal rings and radial reinforcements. Additional reinforcement is given in the intersections between braces and columns. The ballast is distributed within the three heave plates. An overview of the CIMNE–DeepCwind concept is presented in Figure 5.4. The scantling used for the steel plates in the different components is given in Table 5.2.

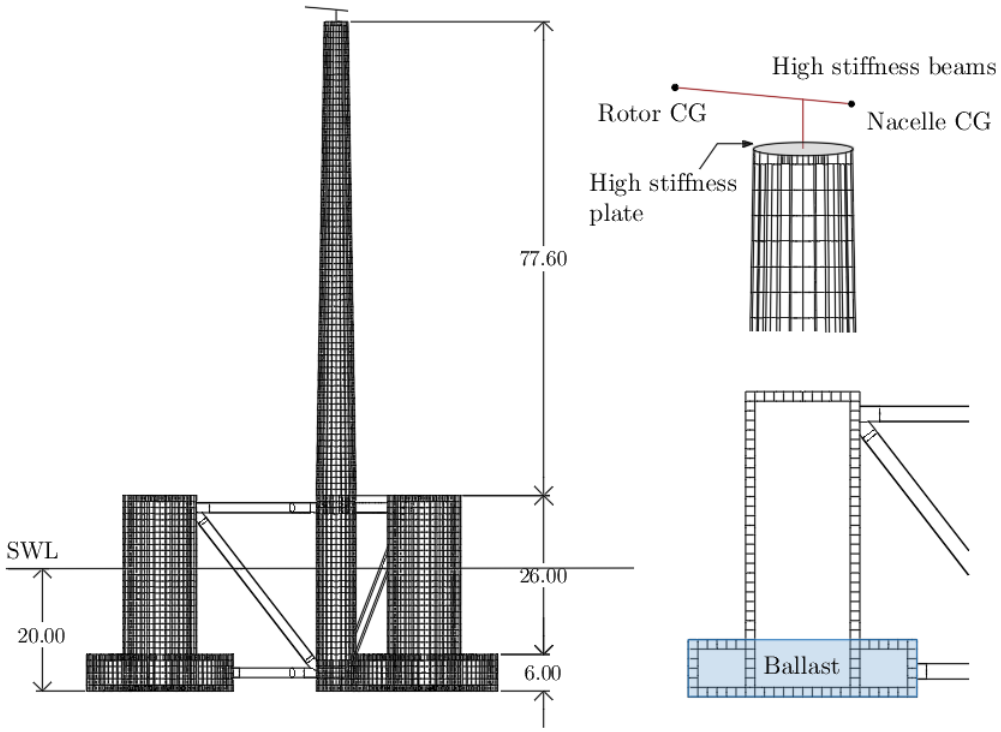

Figure 5.4: Left: main dimensions. Right: wind turbine beam model and ballast location.

Table 5.2: Structural components and steel plates properties.

	Thickness [mm]	Young modulus [GPa]	Poisson coefficient [-]	Density [kg/m^3]
Heave plates	30	210	0.3	7845
Columns	20	210	0.3	7845
Braces	17.5	210	0.3	7845
Tower	14.0	210	0.3	8500

A dynamic FEM mooring system is included in the model having as reference the defined in the OC4 project. The schema of the mooring arrangement, including anchor coordinates, is shown in Figure 5.5. Each mooring line has a length of 835.5 meters, which is discretized into 64 elements.

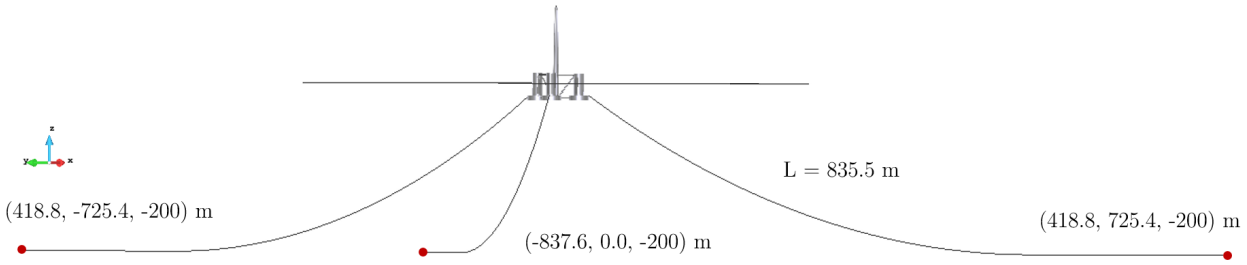

Figure 5.5: Mooring line arrangement.

The wind turbine is included in the FEM model by adding the punctual masses and inertias of the NREL-5MW components. Each mass is located at its own center of mass and reported in Table 5.3. The masses are linked to the tower-top of the model by high stiffened beams. A high-stiffness plate is used to transfer the turbine loads to the tower top.

Table 5.3: RNA data of the NREL 5-MW wind turbine.

	Mass [Kg]	CM position [m]	Ixx [kg/m^2]	Iyy [kg/m^2]	Izz [kg/m^2]
Rotor	110,000	(-5.0, 0.0, 92.0)	35,444,000	19,011,000	19,011,000
Nacelle	240,000	(1.9, 0.0, 91.35)	0.0	0.0	1,741,500

The structural mesh is composed of 380,995 shell elements and 4 beam elements (used as auxiliary elements to impose the rotor loads). The shell element consists of a linear triangle with drilling rotations and 6 DOFs per node (three translations and three rotations). There is a total of 171,025 nodes and 1,026,150 degrees of freedom.

The minimum and maximum FE sizes are 0.2 and 104.7 (cm), respectively. Figure 5.6 shows the element sizes used for the structural discretization of the mesh. The smallest FEs sizes are defined in areas where fatigue must be analyzed and are determined in accordance with fatigue assessment standards.

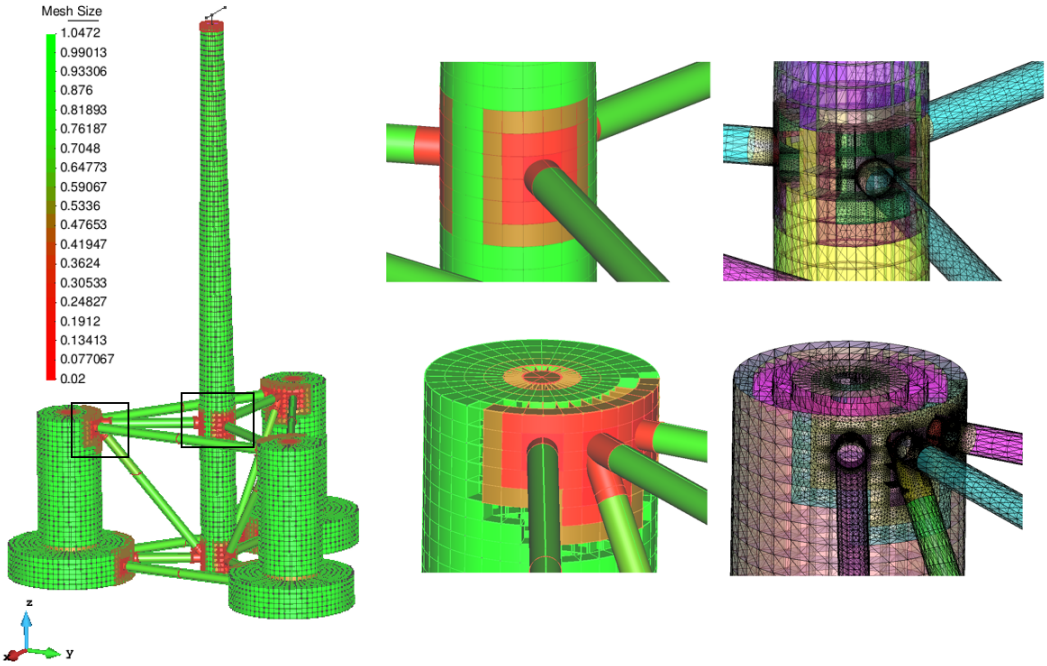

Figure 5.6: FE structural discretization in regions susceptible to fatigue damage.

The seakeeping computational domain mesh consists of 141,330 tetrahedral elements and 28,492 nodes. Minimum (near-field) FE size is 0.25 m and maximum (far-field) is 40 m. Figure 5.7 shows the discretization of the whole hydro-elastic problem (left) and the only seakeeping meshes (right). The time step used in the simulations is 0.05 s.

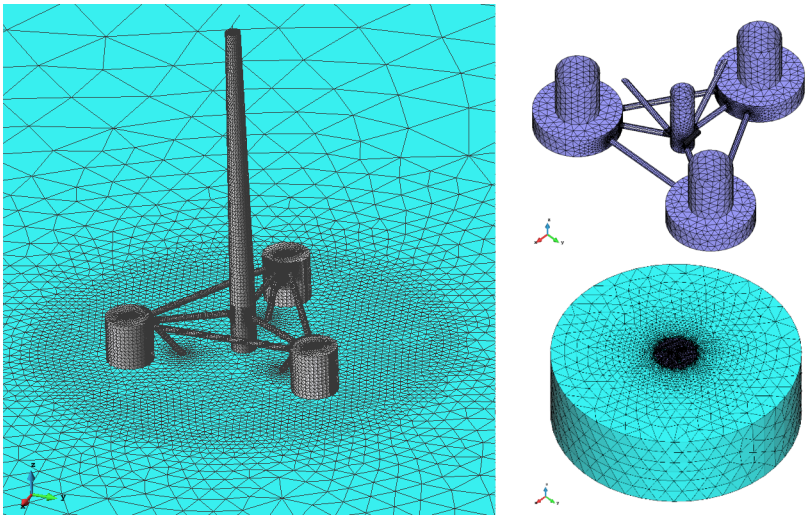

Figure 5.7: Left: whole hydroelastic mesh. Right: only seakeeping mesh.

5.3.2 Rigid-body properties

To confirm the suitability of the proposed structural model, its rigid-body response is compared with the one from the OC4-DeepCwind model. To do so, first a time–domain simulation using a white noise head wave spectrum is performed in the absence of wind and currents. The response amplitude operators are obtained for the wind turbine parked. The solution for present design is contrasted with the OC4-DeepCwind response according to the OC4 project, phase II load case 2.6 [Robertson, Jonkman, Vorphal, et al., 2014]. In Figure 5.8, the outputs for the CIMNE-DeepCwind are contrasted with the published by NREL, only the frequency band excited by the waves is shown.

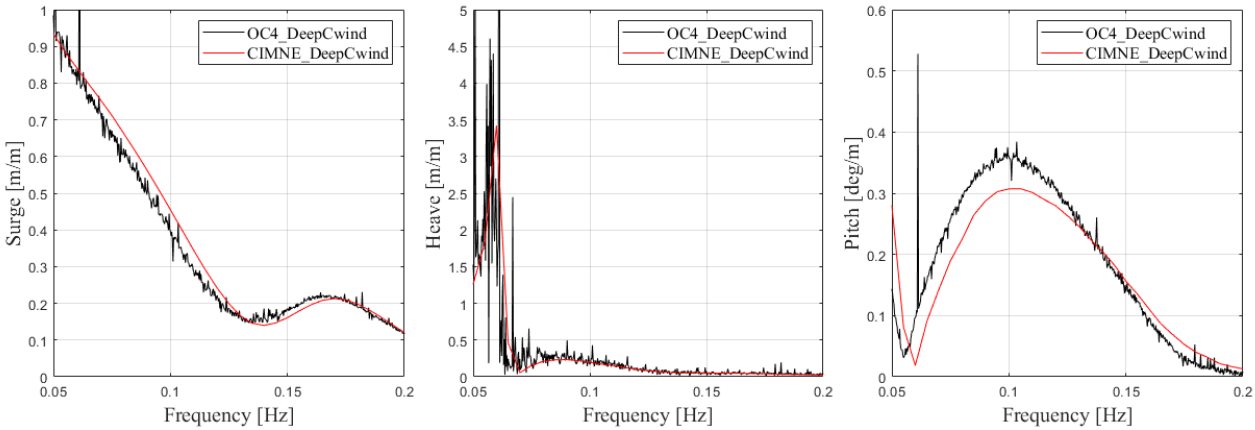

Figure 5.8: RAOs comparison without wind (OC4-DeepCwind – CIMNE-DeepCWind).

Slight discrepancies are expected due to the different characteristics of the two models. However, a reasonable agreement is observed in the rigid-body response between the OC4-DeepCwind and CIMNE-DeepCwind. Additionally, consistency is found in the natural frequencies obtained from decay tests. Table 5.4 compares the natural periods computed for the CIMNE-DeepCwind with those reported for the OC4-DeepCwind in [Robertson et al., 2013].

Table 5.4: Platform Natural periods.

	OC4-DeepCwind	CIMNE-DeepCwind
Surge	107.52 s	109.54 s
Sway	113.63 s	109.96 s
Heave	17.24 s	16.70 s
Roll	27.03 s	23.76 s
Pitch	27.02 s	23.70 s
Yaw	83.33 s	76.50 s

5.3.3 Modal analysis

The structural analysis employing the MMR technique [Garcia-Espinosa et al., 2023] begins with a modal analysis to obtain the precomputed eigenmodes. This approach requires to precompute first the vibration modes to later obtain the structural solution by the modal superposition method, see Figure 5.9. The selected range of modes establishes the structural basis to be used by the hydroelastic solver. This process is performed only once.

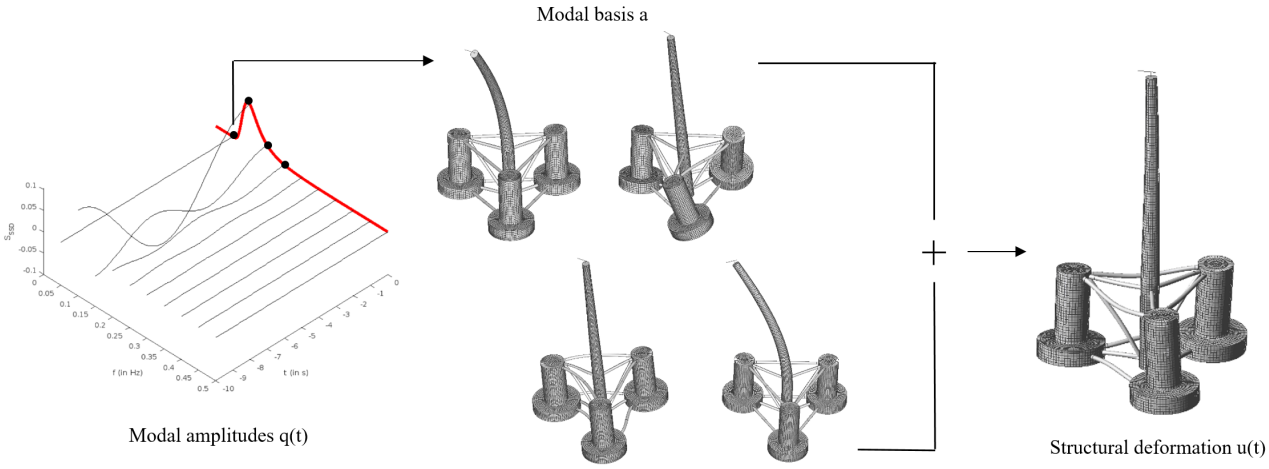

Figure 5.9: Procedure to obtain the real-time response based on the precomputed modes.

For the present study, a modal basis of 5,000 unrestricted modes is computed, accounting for only 0.48% (low-frequency modes) of the total elastic degrees of freedom. Higher-frequency modes are assumed negligible due to their localized structural response. The first 10 elastic modes are shown in Figure 5.10, with the color fill representing the structural displacements.

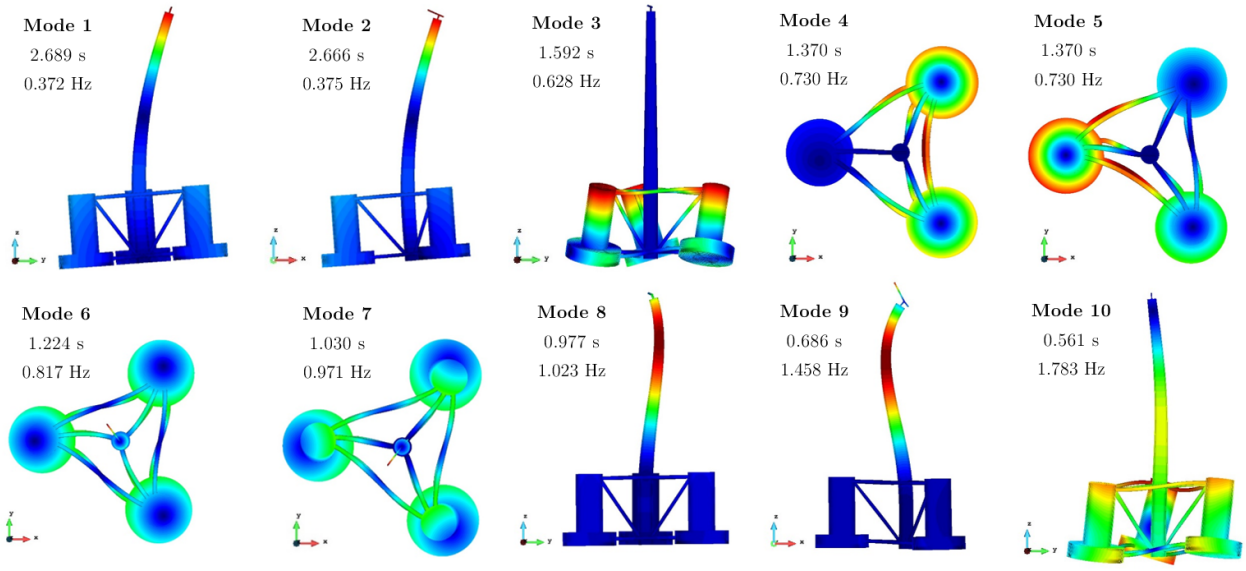

Figure 5.10: First ten elastic dry modes and modal periods.

These modes are calculated by the structural FEM solver in the absence of water and are referred to as "dry" modes. The corresponding modal frequency range goes from 0.355 Hz to 120.497 MHz. A more reduced modal basis of 1,000 modes is also tested.

When the platform is deployed in water, its structural displacements generate radiated waves, inducing dynamic fluid pressures and altering the hydrostatic pressure distribution. This implies changes in the modal frequency and introduces modal damping. To evaluate these differences, an extinction test is conducted on the platform's first elastic modes, assuming no structural damping is present. Figure 5.11 left shows the time evolution of the first elastic mode, while Figure 5.11 right shows a snapshot of the radiated waves during the extinction test.

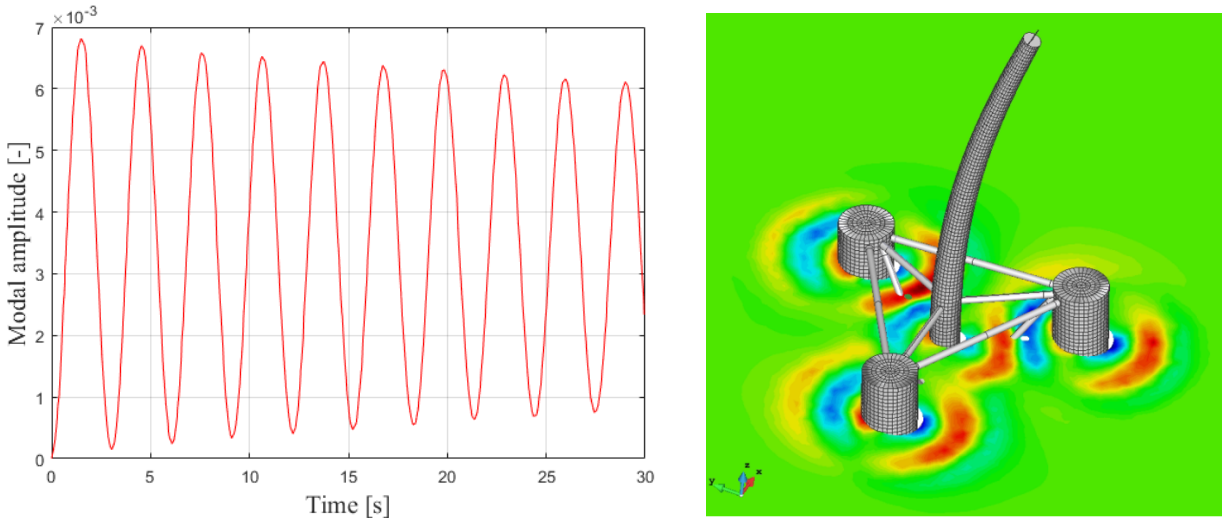

Figure 5.11: Left: extinction test for the first elastic mode. Right: snapshot of the deformed structure (x10^4) and radiated waves (colorfill).

This test is carried out using the two-ways hydroelastic coupling and the computational framework described earlier. The platform is initially placed in hydrostatic equilibrium. Then each elastic mode is released, one at a time, allowing the modal amplitudes to evolve. Meanwhile, the rest of the modes, including rigid body modes, remain fixed. Table 5.5 shows the change in the modal periods and the wave radiation damping for the first elastic modes.

Table 5.5: Modal periods and damping for the first six elastic modes.

	1st Mode	2nd Mode	3rd Mode	4th Mode	5th Mode	6th Mode
Dry period [s]	2.689	2.666	1.592	1.370	1.370	1.224
Wet period [s]	3.055	3.033	1.769	1.410	1.410	1.265
Wave radiation damping [%]	0.462	0.456	0.968	0.051	0.049	0.079

The modal periods obtained from the extinction test are referred to as "wet" periods. The damping is given as a percentage of the critical modal damping. It is observed a significant increase in the natural periods induced by the wave radiation associated to the modal vibration.

5.3.4 Verification: hydrostatic equilibrium analysis

A static load case is analyzed, where the platform is floating in hydrostatic equilibrium. In this configuration, the body is subjected to its self-weight and the vertical force from the mooring system, balanced by the hydrostatic pressure of the water. The rigid-body motions are restricted, allowing only structural deformations. The purpose of this study is to test the MMR approach under static deformation. A similar analysis is reproduced as in [Garcia-Espinosa et al., 2023]. This study also serves to demonstrate the present hydroelastic methodology to give an easy understanding of the approach and capabilities. Although the MMR has been proposed to reduce computational times of dynamic analysis, the structural solution is computed using FEM and MMR for its contrast.

The static structural energy computed using FEM is 204,851 J. The MMR approximations with 5,000 and 1,000 modes were able to recover 84.05% and 65.96% of this elastic energy, respectively. The comparison of the structural displacements between the FEM solution and the MMR solutions is presented in Figure 5.12. The consistency of the structural model order reduction solution is tested, being able to accurately approximate the high-fidelity FEM solution while capturing local deformations.

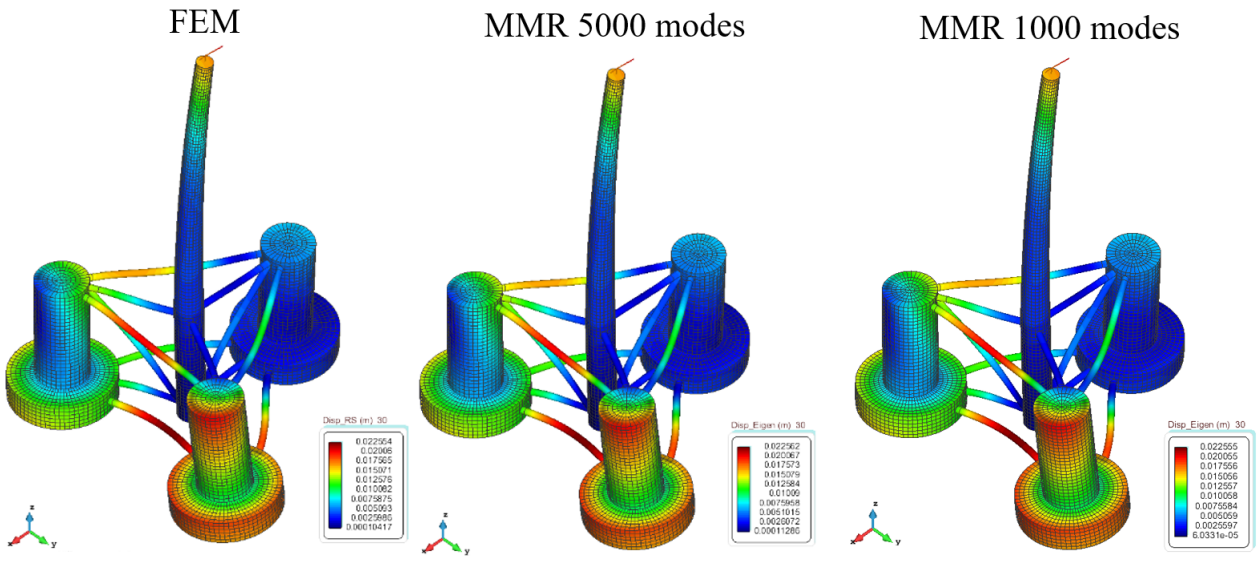

Figure 5.12: Structural displacements compared between solutions (amplified x200).

Even with 1,000 modes, representing 65.96% of the static elastic energy, the displacement field closely matches the FEM solution. As expected, the accuracy of the solution improves as the size of the modal basis increases. Figure 5.13 (left) presents the modal elastic energy distribution across the modes for this static condition, while Figure 5.13 (right) shows the color fill of modal displacements for the four most energetic eigenmodes.

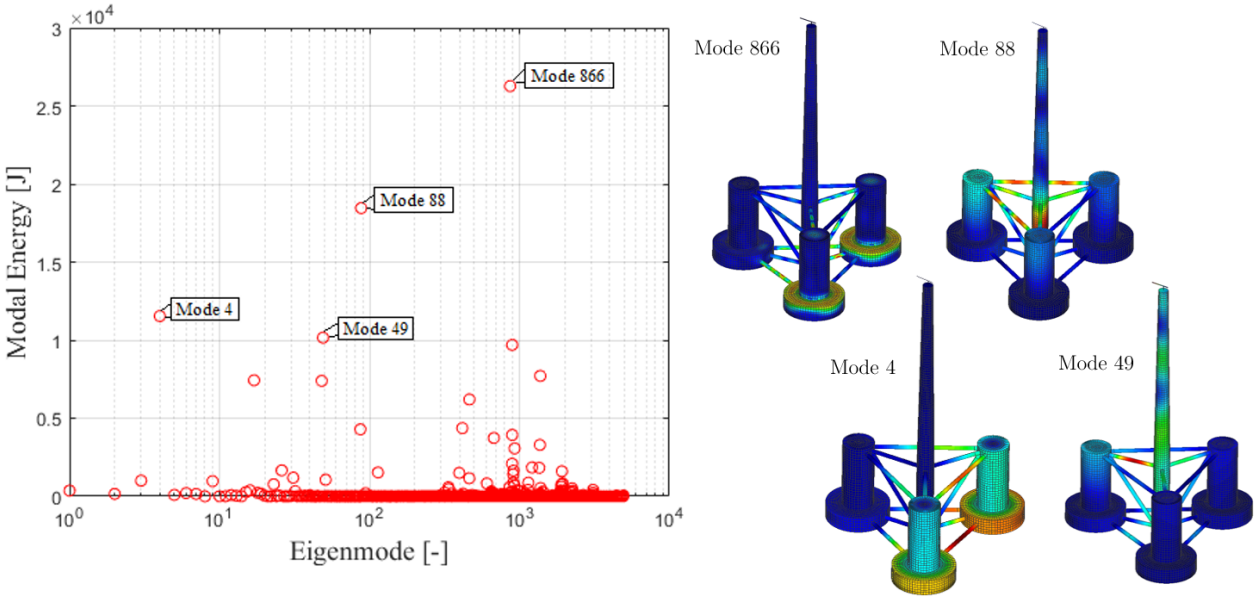

Figure 5.13: Left: modal energy distribution. Right: displacements fill of the most energetic eigenmodes.

Although most of the modal energy is concentrated in the lower-frequency eigenmodes, a significant energy distribution is observed across a wide range of modes. Table 5.6 provides the energy percentages of the ten most energetic modes.

Table 5.6: Eigenmodes with higher modal energy.

Eigenmode	Energy [J]	Energy [%]	Cumulative Energy [%]
866	26269.8	12.05	12.05
88	18457.6	8.46	20.51
4	11545.8	5.29	25.81
49	10157.9	4.66	30.47
895	9697.73	4.45	34.91
1377	7707.26	3.53	38.45
17	7426.65	3.41	41.85
48	7392.3	3.39	45.25
464	6200.78	2.84	48.09
416	4364.87	2.00	50.09

These modes retain over 50% of the elastic energy, while approximately 100 modes are needed to capture 80%. Despite using a significantly reduced basis of dynamic eigenmodes, the method provides a reasonable static approximation. However, the error introduced is not negligible. This justifies the approach taken in the next Chapter 6, where the solution will be decomposed into its static and dynamic components, as the MMR approach is expected to provide higher accuracy in solving the structure's dynamic response.

The instantaneous elastic energy is obtained as the sum of the elastic energy of all structural eigenmodes defined in the modal basis for each time instant. When knowing the most energetic eigenmodes it is also possible to reduce the modal basis even more by discarding the less energetic ones. In this way the computational effort of the hydroelastic analysis performed on the same structure can be also reduced.

5.4 Conclusions

This chapter presents the use of a novel hydroelastic approach for the structural analysis of floating wind turbines. The proposed method uses a structural ROM based on the MMR technique, being strongly coupled (two-ways) with the seakeeping solver SeaFEM. The purpose of this chapter is to showcase the methodology and capabilities of the approach, rather than to analyze the platform under operational conditions, which will be addressed in Chapter 6. The consistency of the MMR solution is tested in a static load case, being able to accurately approximate the FEM solution.

Currently, there is limited published research on the structural analysis of FOWTs, and detailed structural design parameters are often confidential. To address this gap, a benchmark structural design is defined for the DeepCwind platform. The structural details and numerical model are presented in this chapter. A motion analysis is performed to demonstrate that its global rigid-body behavior is consistent with the NREL concept.

By retaining only those eigenmodes preserving most of the structural elastic energy, the number of structural DoF is significantly reduced. The criterion used to select a basis with the dominant modes is performed using the elastic energy as main indicator.

The relevance of accounting for the two-ways (strong) hydroelastic interaction is highlighted with the study of the modes decay tests when the platform is deployed in water. A change in the modal period is observed, suggesting that while weak coupling may be sufficient for the structural assessment of stiff structures, it may be inaccurate to capture resonance in slender-flexible structures such as FOWTs.

The accuracy of the MMR approach is evaluated with the platform in hydrostatic equilibrium, recovering 80% of the structural energy. However, the method has proven to be valid when reproducing the higher-fidelity displacement field using only 0.48% of the structural degrees of freedom. The assumption of retaining only the lower-frequency modes, significantly reduces the computational effort compared to conventional FEM solvers.

The results show excitation in some higher-frequency modes, suggesting that discarding these modes could lead to a loss of structural response in static analysis. However, the MMR is primarily intended for dynamic response analysis, while static loadcases can be quickly computed solving the full FEM equations. In Chapter 6, the MMR solution is further tested in a dynamic analysis, which is its main purpose, demonstrating its accuracy in representing the dynamic response. The approach allows for the computation of local displacements resulting from distributed hydrodynamic loads. These stress distributions, obtained offline from the precomputed modal amplitudes, are studied in Chapter 6.

Chapter 6

Computational framework for the Integrated Load Analysis of FOWTs

6.1 Introduction

The efforts to lower the LCOE of floating wind turbines are leading to a new generation of larger and light-weighted floating platform concepts [Ran et al., 2023]. In order to extend the lifespan of these flexible structures withstanding the worst sea-states that might encounter, the study of its elastic behavior and fatigue damage becomes relevant. In addition, the structural design standards for FOWTs are typically derived from the oil and gas platforms, which leads to uneconomical designs and high steel consumption. Accordingly, more research is being focused to develop higher-fidelity simulation tools for the study and cost-effective optimization of the existing structural concepts.

To ensure that a floating platform is properly designed, international standards have established certification guidelines. These processes involve performing integrated load analysis under a variety of environmental conditions. The range of load cases to be analyzed for floating offshore wind turbines is significantly broader compared to those for onshore wind turbines, due to the complex interactions between wind and wave loads. Moreover, offshore certification load cases typically require longer simulations (around 3 hours), compared to the onshore turbines. Reason found in the long resonance periods of moored floating platforms and long characteristic wave periods. As a result, the computational costs associated to these numerical analyses become a critical factor.

The simultaneous wind-waves loads acting on the structure of FOWTs in addition to the mooring system, introduce strong aero-hydro-elastic interactions. These effects might cause undesirable vibrations, fatigue loads, and even instability. Its study is performed using AHSE solvers, where the hydrodynamic solution is computed generally with potential flow theory and Morison's equations, whereas the structural one is represented with simplified beam elements. ROMs have also been applied in the literature. OpenFAST uses a Craig-Bampton (C-B) reduction method [H. Song et al., 2013, Jonkman et al., 2019], where the structural deformations can be expressed as the superposition of natural modes. Another common approach is to model the elastic behavior by considering only the two relevant structural modes of the tower (fore-aft and side-to-side deflection), as seen in [Shengtao et al., 2023].

However, most research on FOWTs focuses on their motion response, with limited studies addressing their structural behavior. Existing structural analyses typically model components as beams, an approach that provides cross-sectional loads without capturing detailed stress distributions. While these methods can represent member deformations, they fail to account for local stresses, which are crucial to predict structural failure. Currently, only a few tools, such as Sesam ["Sesam Feature Description." 2022], can perform structural analysis of floating platforms including distributed hydrodynamic pressures.

When a detailed structural analysis of FOWTs is required, it is usually performed by precomputing the external loads with an AHSE solver and introducing them into a FEM structural solver. This partitioned strategy implies solving the hydroelastic problem in several stages and transforming the frequency-domain hydrodynamic loads into time-domain. However, this method is best suited for very stiff structures, as it only accounts for one-way couplings, neglecting the elastic effects on the fluid. A quasi-static approach is often used to reduce computational costs, despite hiding resonance and dynamic effects. Although these limitations, it remains the most common method for hydroelastic analysis, due to the complexity and computational cost of solving the full three-dimensional problem in the time-domain, mostly taken by the structural solver [Servan-Camas et al., 2021].

The conventional time-domain elastic analysis of wind turbines has been generally modeled by taking into account the tower and rotor blades flexibility and considering the floater as a rigid body [Cao et al., 2021, Li et al., 2018]. While this might be accurate for the analysis of small floating wind turbines, it might result in large errors on the computation of coupled natural frequencies and internal loads for larger platforms [Steinacker et al., 2022]. On this regard, the hydroelastic effects on the platform are starting to be studied as in [Bjerg Thomsen et al., 2021, Li et al., 2023] using a one-dimension beam method and in [Kwangtae et al., 2021, Park and Choung, 2023] using a FEM solver for detailed structural analysis. Recently, [Lei et al.,

2025] performed a hydroelastic study of the OC4 platform using a quasi-static approach. This analysis examines the wave-induced structural response while disregarding the turbine's aerodynamic effects, which is also a common practice in the structural analysis of FOWTs.

In this work, the structural ROM based on the MMR technique, presented in previous Chapter 5, is tested for the analysis of FOWTs. Its combination with the wind turbine solver OpenFAST, using the strategy outlined in Chapter 2, establishes a coupled areo-hydro-servo-elastic numerical framework for the ILA of floating wind concepts. The natural structural outputs are then the modal amplitudes, allowing to compute the structural displacements, strains, and stress fields offline based on the precomputed modes. This can largely reduce the computational times enabling its use for operational conditions like in a digital twin, as reported in [Pacheco-Blazquez et al., 2024], where it was implemented on the OSI4IOT [Di Capua et al., 2023] digital platform to develop a DT for structural health monitoring (SHM).

This chapter aims to consolidate the implementations presented throughout the thesis. The complete software package is applied to the structural design of the CIMNE-DeepCwind platform, focusing on the study of its structural response under dynamic conditions. Two load cases are analyzed using the proposed ILA framework: one considering only wave loads and another combining wind and wave loads for energy production. The tool capabilities are demonstrated by defining a methodology for the structural assessment of FOWTs ensuring an efficient an accurate handling of the numerical problem.

6.2 Methodology

6.2.1 Dynamic hydroelastic analysis

During the operation of floating wind turbines, the structure is subjected to external loads, which can be categorized into static and dynamic components. Static loads, which remain constant over time, include self-weight, hydrostatic pressure at the equilibrium position, mooring line pretension, and the mean wind loads. In contrast, dynamic loads vary with time and include wave-induced forces, fluctuations in mooring tension, and variations in the wind profile.

The present analysis focuses on the study of the dynamic elastic component of the structural response. This contribution is obtained by splitting the structural loads $\mathbf{f}(t)$ and displacement solution $\mathbf{u}(t)$ into a static and a dynamic part:

$$\mathbf{f}(t) = \mathbf{f}_D(t) + \mathbf{f}_S \tag{6.1}$$

$$\mathbf{u}(t) = \mathbf{u}_D(t) + \mathbf{u}_S \tag{6.2}$$

Where the subscript D denotes the dynamic component and S the static component. Then, the structural equations can be also split as:

$$\mathbf{M}\ddot{\mathbf{u}}_D(t) + \mathbf{C}\dot{\mathbf{u}}_D(t) + \mathbf{K}\mathbf{u}_D(t) = \mathbf{f}_D(t) \tag{6.3}$$

$$\mathbf{K}\mathbf{u}_S = \mathbf{f}_S \tag{6.4}$$

In the same way, $\mathbf{f}_S$ represents the static loads and $\mathbf{f}_D$ the dynamic structural loads. The dynamic component requires to solve the structural equations many times along the simulation time.

$$\mathbf{u}_{MMR}(t) = \sum_{i=1}^{N_m} q_i(t) a_i \approx \mathbf{u}_D(t) \quad N_m \ll N_{DOF} \tag{6.5}$$

When analyzing only the dynamic effects, the model reduction makes even more sense. The modal basis is composed by dynamic eigenmodes, whose lower vibration frequencies are more easily excited.

Finally, we define the term dynamic elastic energy $\mathbf{E}^D(t)$ and $\mathbf{E}^D_{MMR}(t)$ as:

$$\mathbf{E}^D(t) = \frac{1}{2}\mathbf{u}_D^{\mathrm{T}}\mathbf{K}\mathbf{u}_D \tag{6.6}$$

$$\mathbf{E}^D_{MMR}(t) = \frac{1}{2}\mathbf{u}_{MMR}^T\mathbf{K}\mathbf{u}_{MMR} \approx \sum_{i=1}^{i=N_m} \frac{1}{2}\Omega_i^2 q_i^2 \tag{6.7}$$

This dynamic energy will be used to measure the fidelity of the MMR solution to approximate the full FEM solution. Although the MMR approach is based on the FE method, the term 'FEM' in this work refers to the classic FEM structural solution.

6.2.2 ILA strategy

Due to the coupling between the dynamics of the wind turbine under transient wind loads and floater under irregular wave and mooring loads, an ILA approach is a must. The conventional way to perform ILA analysis, including the full structure analysis, is drawn in Figure 6.1.

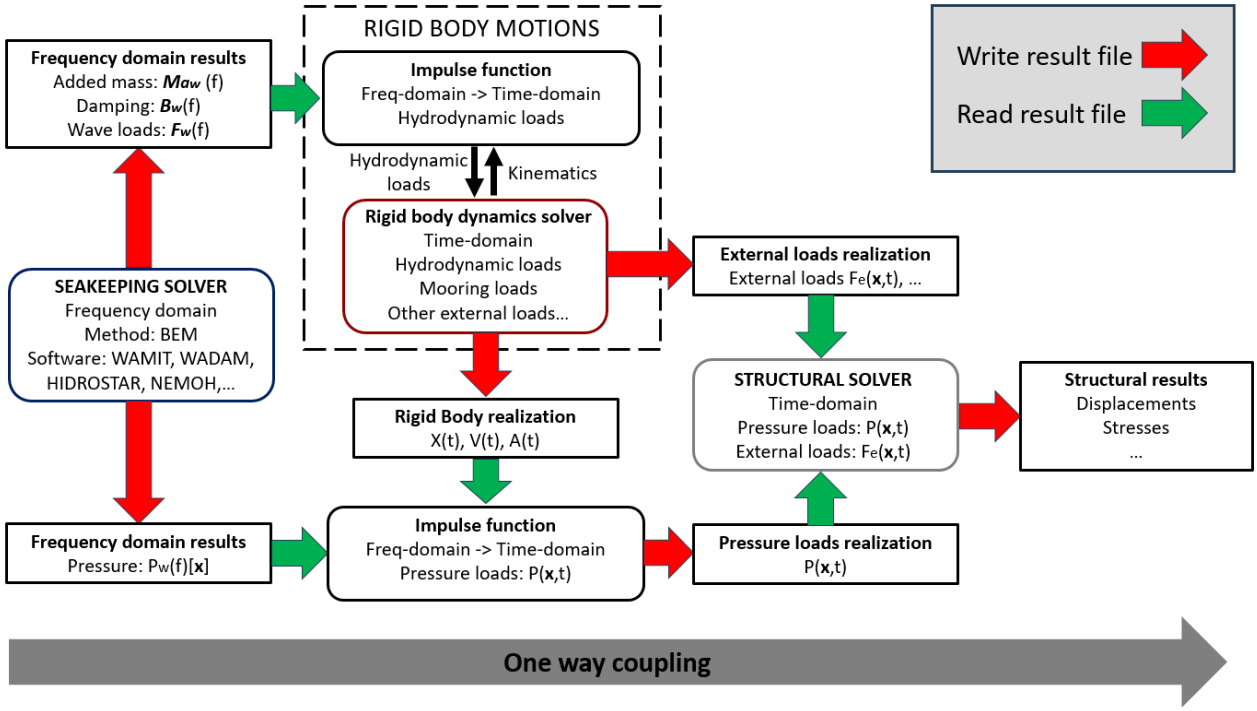

Figure 6.1: Computational flow for ILA analysis using current numerical tools.

The main steps involving this strategy are summarized as follows:

1. In the first stage, the frequency-domain seakeeping solver solves the wave diffraction-radiation problem, from where the added mass, damping, Froude-Krylov and diffraction-radiation pressure distributions and loads are obtained.
2. In order to obtain the time-dependent hydrodynamic loads, those outputs need to be transformed to the time-domain for each rigid-body dynamics realization representing a load-case.
3. Later on, all external loads and the hydrodynamic pressure must be introduced into a structural solver to obtain the structural response.
4. Finally, the structural solver computes the displacements and stresses.

Several drawbacks are drawn from this methodology:

- A number of independent computational tools must be used in a serial execution.
- A large number of files and data are generated, which must be written and read.
- The coupling is performed in only one direction, limiting its use to very stiff structures (not necessarily the case of FOWTs).

- Structural dynamic simulations are a bottleneck for ILA. A quasi-static approach is often used to reduce the computational times (hiding potential resonance/dynamic effects).

The traditional approach involves obtaining the external loads acting on the structure and then transferring them to a FEM structural solver (Figure 6.1). This results in a tedious procedure given the multiphysics nature and the number of load-cases required for structural assessment.

To overcome the exposed limitations, a different approach is taken, drawn in Figure 6.2. This method is based on a computational framework where all external loads are simultaneously computed and applied in the time domain to the dynamic structural system. By avoiding the need to write and read files between different software, it significantly improves the solution efficiency. Additionally, deformation and stress fields can be reconstructed offline, reducing computational and post-processing efforts, since they are computed on demand.

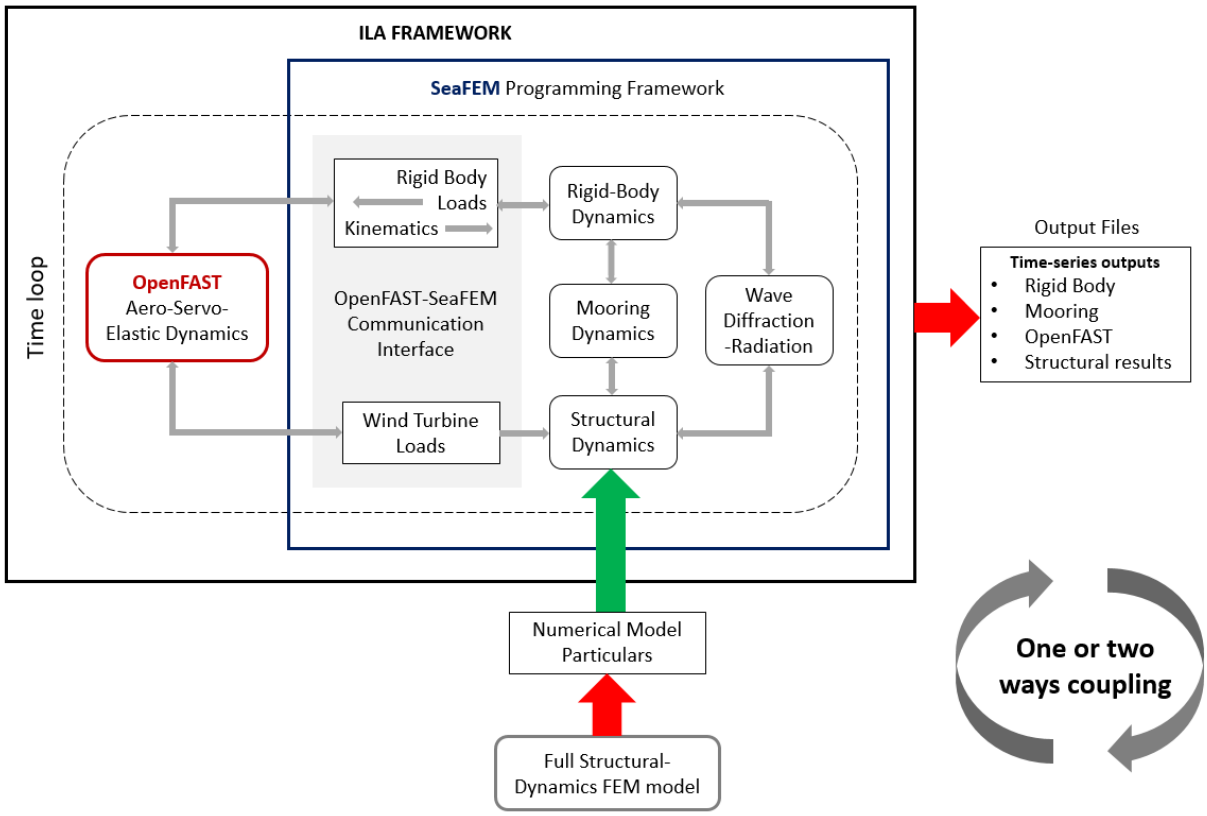

Figure 6.2: Implemented ILA computational framework.

The structural solver is only used to transfer the structural system particulars to the computational framework. Two options are available: the full FEM model, or the MMR model, see Table 6.1. In this analysis, the dynamic outputs are obtained excluding the static component.

Table 6.1: Options for structural analysis in ILA computational framework.

	Model	Inputs (structure particulars)	Outputs (structural results)
Option 1	FEM	Mass matrix: $\mathbf{M}$ Stiffness matrix: $\mathbf{K}$ Rayleigh damping: a_M and a_K	Displacements: $\mathbf{u^D}(x,t)$ Elastic Energy: $\mathbf{E^D}(t)$
Option 2	MMR	Modal displacements: $a_i(x) \quad i = 1, 2, ..., N_m$ Modal frequencies: $\mathbf{\Omega}_i \quad i = 1, 2, ..., N_m$ Rayleigh damping: α_M and α_K Modal damping: η	Modal amplitudes: $q_i(t) \quad i = 1, 2, ..., N_m$ Elastic Energy: $\mathbf{E}^D_{MMR}(t)$

The strategy represented in Figure 6.2 has a number of advantages over the one drawn in Figure 6.1:

- Reduces the number of interactions between different computational tools.
- Reduces the number of files to be written and read.
- Allows for two-ways coupling (important to account for flexibility).
- When using the MMR, the size of the structural output files is significantly reduced $\mathrm{O}(N_m/N_{DOF})$.
- All structural external loads are computed simultaneously in the time-domain (on the fly), and straightforwardly mapped onto the structural solver.
- Minimizes the communication overheads over partitioned strategies.
- Fast communication among solvers (happens at RAM memory level)
- Structural stresses can be reconstructed offline (afterwards) on demand.

When computing a large number of long structural dynamics realizations, the need of writing the time-series of the stresses leads to the problem of storing a large number of result files. These files can be large in memory size, which is not only memory demanding, but computationally demanding in terms of reading and writing tasks. The use of the MMR largely reduces the structural output file size by reporting only the time-series of the modal amplitudes. From these, various offline computations can be performed for structural assessment, including:

Ultimate load analysis:

- The structural energy can be quickly computed in order to identify those instants with maximum structural energy Eq. (6.6).

- Structural displacement field reconstruction using Eq. (6.5) for identified extreme instants.
- Structural stresses computation from structural displacements.
- Identification of hot-spots.

Fatigue damage analysis:

- Hotspots identification.
- Time-series structural displacement reconstruction using Eq. (6.5) at hot-spots.
- Time-series structural stresses computation from structural displacements at hot-spots.
- Fatigue damage computation from structural stresses time-series at hot-spots.

From these structural outputs, time-series of the stresses can be obtained offline. This optimizes the postprocessing time, by the identification of time instants with local maximums of structural energy. Also, potential hotspots for fatigue failure can be identified to obtain the stresses time history in a more localized analysis.

This ILA framework allows to compute the elastic behavior of the substructure for the coupled aero-hydrodynamic responses. The developed numerical framework, consisting of SeaFEM and OpenFAST SF-OF, introduced in Chapter 2 and published in [Berdugo-Parada et al., 2024], is used. This tool results in a time-domain aero–hydro–servo–elastic solver able to execute detailed structural analysis of FOWTs.

In its coupled solution, OpenFAST deals with the aerodynamics, blade structural response and platform rigid-body motions. Whereas SeaFEM is responsible for solving the seakeeping and mooring dynamics, as well as capturing the platform-tower elastic response through its MMR approach. The data exchange between both codes consists of the hydrodynamic loads computed by SeaFEM in return to the rigid-body kinematics computed by OpenFAST. Additionally, the wind-turbine loads computed by OpenFAST are received in the structural solver of SeaFEM. In each time step, the turbine virtually operates in OpenFAST, providing the aerodynamic wind loads to SeaFEM.

6.3 DLC 1.6: Production design

The design standards of FOWTs require a loads analysis based on site-specific external conditions. This process involves verifying its structural integrity under a series of design load cases. To do so, a site location in Morro Bay (California) is selected to obtain environmental (metocean) data. For the present study, the load case 1.6 for production operation defined in the Bureau Veritas standards ["Bureau Veritas. Rule Note NI 572 DT R02 E", 2019] is tested. The weather database used is obtained from the European project Corewind D1.2 [Vigara et al., 2019]. In Table 6.2 is given a summary with the parameters used to define the loadcase.

Table 6.2: Morro Bay location map and production DLC 1.6.

DLC	1.6 Production design
Site location	Morro Bay (California)
Depth	200 m
System condition	Intact
Wind	Speed: 14.8 m/s (hub height)
	Normal turbulence
Waves	Severe
	Spectrum: Jonswap
	Hs = 6 m
	T = 14 s
	Direction: 0^o
	Spreading: Unidirectional

The analyzed condition involves a normal turbulence wind (NTM) combined with a severe sea state (SSS), excluding current effects, with the wind turbine operating under normal conditions. According to the chosen site location, the irregular sea-state is defined with a JONSWAP wave spectrum using a significant wave height of 6 meters and a mean wave period of 14 seconds. A total of 100 waves is used for the spectrum discretization. The wave period range goes from 5s to 35s to cover the energy spectrum.

The wind parameters used for the simulation are computed according to the IEC standards ["IEC Standard. Rule Note NI 572 DT R02 E.", 2005]. The turbulent wind field is generated with TurbSim using the Kaimal spectral model. A wind speed of 14.8 m/s at the hub height and a power-law shear exponent of 0.14 are used to define the wind profile.

In order to compare the MMR and FEM model, the same structural damping must be used. Hence, the Rayleigh damping is used with $\alpha_M = 0$ and $\alpha_K = 2 \cdot 0.01 \cdot \Omega_1^{-1}$, where Ω_1 is the first elastic modal frequency. The equivalent modal damping is $c_i = 2\eta_i\Omega_i$, where $\eta_i = 0.01 \cdot \Omega_i \cdot \Omega_1^{-1}$ is the percentage of the critical damping. To quantify the relevance in the dynamics effects

its single contribution is analyzed by subtracting the static loads during the simulations. A simulation time of 800 seconds using the one-way hydro-elastic coupling is performed in only-waves and wind-wave conditions.

6.3.1 Structural assessment of FOWTs

Offshore wind turbines are subjected to cyclic excitations from wind and waves, exposing their support structures to several dynamic load sources. These include aerodynamic loads acting on the rotor and tower, hydrodynamic loads on the substructure, and forces generated by operational and control systems such as yaw, pitch, braking, and torque control mechanisms, among others [Del Pozo Gonzalez and Domínguez-García, 2022].

These loads induce fluctuating stress responses in the structure, which can lead to fatigue damage characterized by the initiation and propagation of cracks in the material. Over their operational lifespan, wind turbines are subjected to a high number of load cycles, making the fatigue limit state a critical factor that often governs their design [Partovi-Mehr et al., 2024]. To address this concern, a methodology is proposed in Figure 6.3, which identifies potential hot-spots for fatigue damage using the structural elastic energy as main indicator. This can be done simply by looking for the maximum stress points at the most energetic time instants.

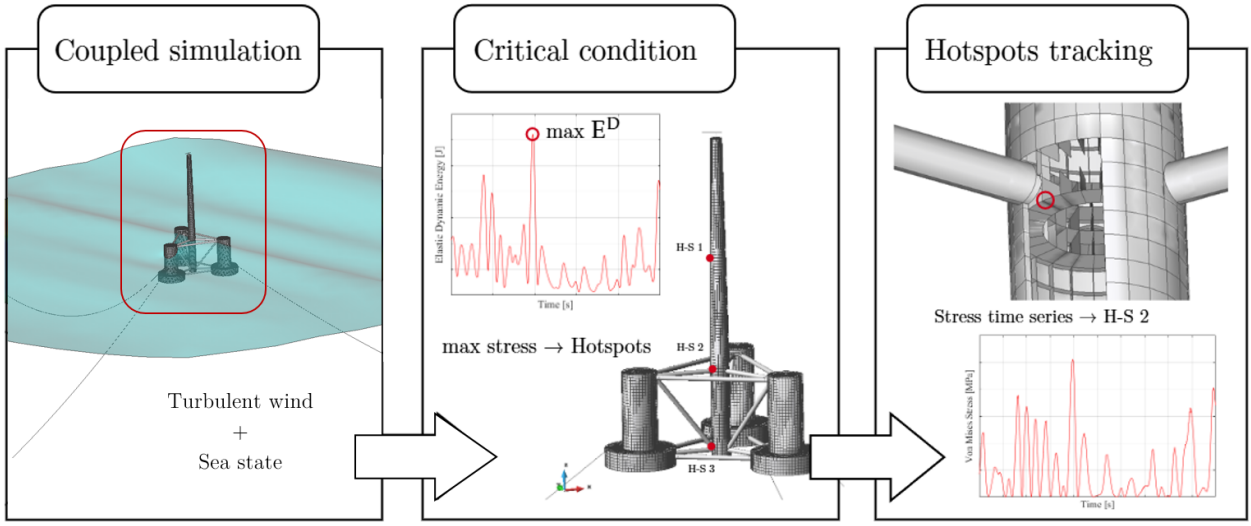

Figure 6.3: Methodology for structural assessment and hotspot detection.

The research on fatigue damage focuses on analyzing specific hotspots, structural points susceptible to potential fatigue failure. In FOWTs, one critical location is the tower base at the floater connection, which experiences significant bending moments. Consequently, previous literature has been addressed to study this area [Li et al., 2018, Kim et al., 2018].

These bending moments are influenced by the wind turbine size, as a larger rotor increases both weight and thrust forces. Additionally, a greater hub-to-tower base distance amplifies the tower deflection experienced by the structure.

To determine when the platform is in a critical excitation state, the time instants corresponding to structural energy peaks can be pinpointed. Once these moments are identified, the stress distribution across the entire mesh can be computed offline. The full displacement field is first reconstructed by a linear combination of the modal displacements, after which the strains and stresses are calculated using the material properties.

From the stress field at the critical load case condition, it is possible to identify significant stress regions on the structure. These locations are associated with the highest fatigue damage, being potential hotspots. This analysis is also presented in the scientific publication [Servan-Camas et al., 2025], which resulted from the dissemination of the present research.

6.3.2 Wave only analysis

The structure subjected to only-wave loads is analyzed using the one-way coupling strategy. The purpose of this study is to verify the consistency of the MMR approach with respect to the high-fidelity FEM solution, being the two-way coupled solution not necessary. In the next section, the study of the importance in performing two-ways coupling will be presented. An 800 seconds simulation has been carried out, where the initial 200 second are discarded due to transients/initialization effects. The same modal bases used in the static analysis, consisting of 1,000 and 5,000 eigenmodes, are tested.

Figure 6.4 compares the dynamic energy when using the full FEM and MMR solutions. Additionally, the same methods are solved using a quasi-static approach. The MMR solution agrees with the FEM one, proving that even a modal basis of 1,000 modes is enough to capture most of the structural dynamic energy. From the instantaneous energy plots, it is possible to detect the instant where the structure is most stressed.

Figure 6.4 (top), shows the different solutions in the total analysis time, and (bottom) shows the local maximums of dynamic energy for the last time range of 100 seconds. Additionally, a close-up view of the highest peak is provided, found at the time instant of 739.1 seconds. The black curve represents the dynamic FEM solution, while the red curve corresponds to the quasi-static FEM approach. The dynamic solutions obtained using the MMR approach with 5,000 and 1,000 modes are represented by green and blue dots, respectively.

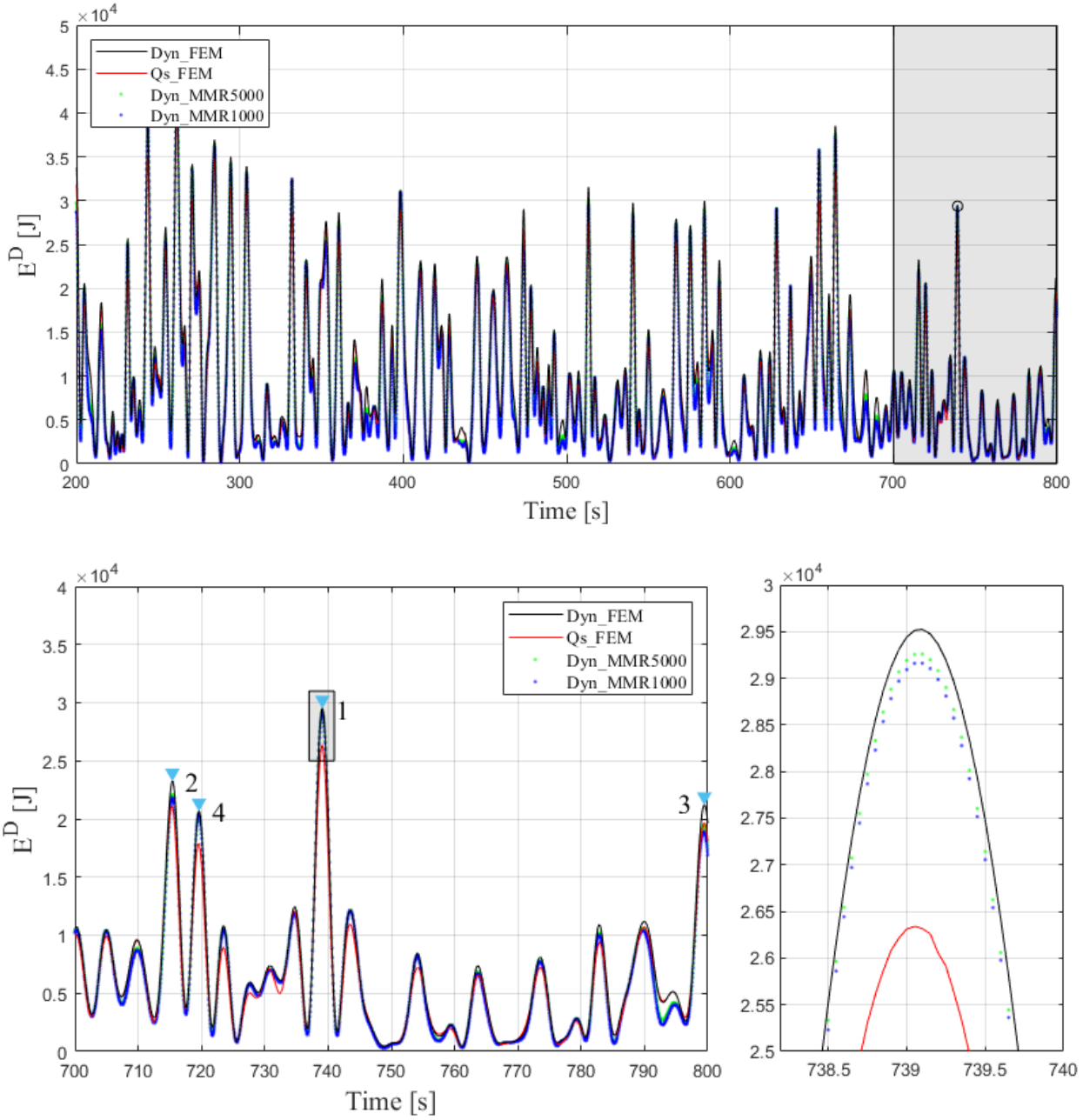

Figure 6.4: Instantaneous E^D plots, top: total time range and bottom: bounded time range.

Table 6.3 presents the dynamic energy percentages for the four highest peaks marked in the previous plot 6.4. Although the MMR quasi-static solutions are not plotted, the results are presented in Table 6.3. The percentages for the different solutions are provided relative to the dynamic FEM solution.

The signal peaks are accurately predicted with the modal approximations, retaining over 90% of the dynamic energy, even for the 1,000-mode MMR. As shown, the MMR approach provides a more accurate solution when representing a dynamic load case, in contrast to the static load case examined in Chapter 5, where only 80% was captured. A better approximation is observed with the dynamic MMR rather than with the FEM quasi-static solution. The MMR results in a closer approach since capturing the higher elastic energy concentration in the first modes when performing dynamic analysis.

Table 6.3: Percentage of the E^D with respect to the dynamic FEM analysis.

Analysis type	Dynamic			Quasistatic		
	FEM	MMR 5000	MMR 1000	FEM	MMR 5000	MMR 1000
Peak 1	100%	99.07%	98.74%	89.09%	88.19%	87.87%
Peak 2	100%	95.05%	93.87%	91.20%	86.26%	85.10%
Peak 3	100%	92.31%	89.93%	92.59%	84.90%	82.52%
Peak 4	100%	99.16%	98.83%	86.79%	85.97%	85.63%

The critical structural condition identified corresponds to a head wave with a wavelength approximately twice the length of the platform. This critical wave heading is also identified in [Lei et al., 2025], suggesting that this relationship wave-platform length should be particularly examined in the floater's design. Figure 6.5 illustrates this scenario, showing the deformation of the free surface elevation on the left and the hydrodynamic pressure distribution over the platform's wet surface on the right.

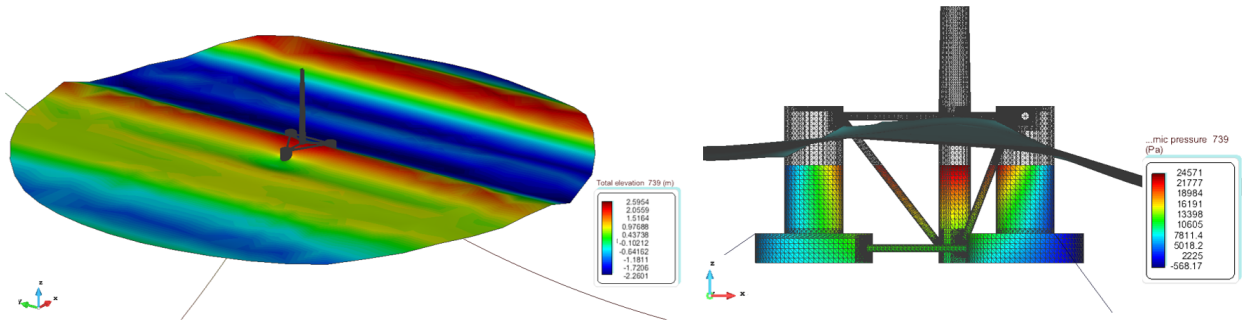

Figure 6.5: Left: wave elevation in critical condition. Right: hydrodynamic pressure.

In Figure 6.6 (left) is given a snapshot of the simulation at this maximum structural dynamic energy instant. The free surface elevation and stress field in the whole structure are shown. The structure deformations are amplified by 150. A closer view of the stress field with the location of the element with maximum stress is pointed out in Figure 6.6 (right).

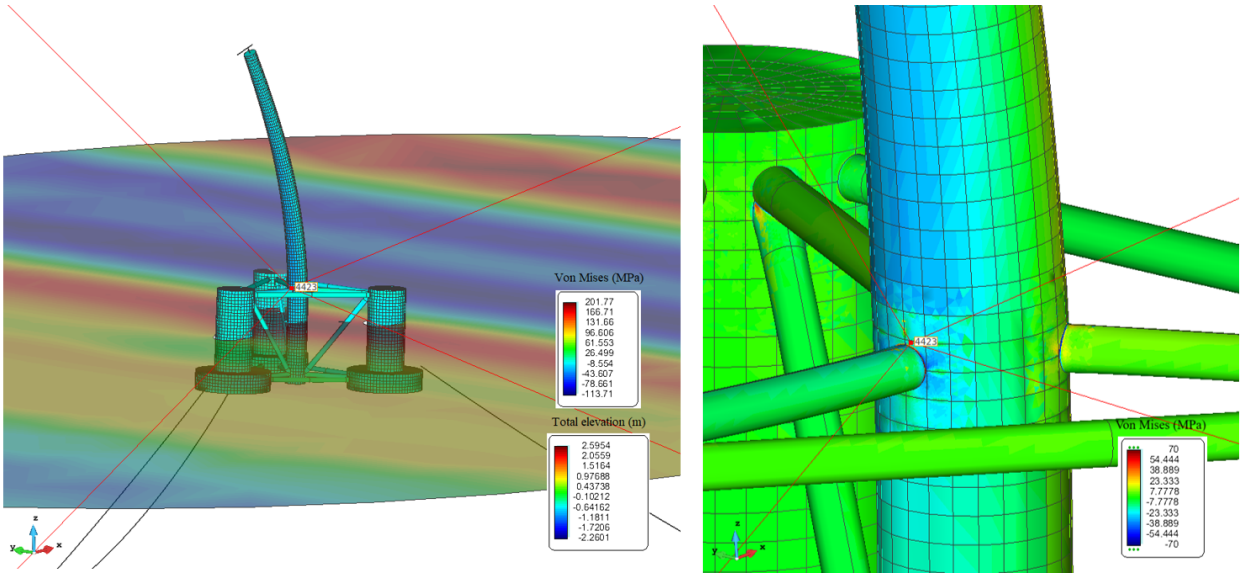

Figure 6.6: Left: stress field and deformation in critical condition (def x150). Right: close-up view of the stress field.

Table 6.4 provides the values of the five most energetic modes and their cumulative energies. The most energetic eigenmode already covers over the 70% of the FEM structural energy and only the 10 most energetic eigenmodes are needed to recover over the 90%. The fore-aft bending mode, second elastic eigenmode, retains the higher structural energy.

Table 6.4: Energy distribution and cumulative energies from the most energetic modes.

Mode	Modal E^D [J]	E^D [%]	Accumulated E^D [%]
2	6375.66	71.51 %	71.51 %
11	450.28	5.05 %	76.56 %
13	378.14	4.24 %	80.80 %
17	160.74	1.80 %	82.60 %
866	158.02	1.77 %	84.37 %

The structural stresses are then obtained offline based on the computed modal amplitudes. Figure 6.7 left shows the element of maximum stress for the time instant of maximum dynamic energy (hotspot). This is found in the reinforcement between the braces joints and the main column. The stress time-history at this hotspot is also computed offline for the time range of 100 seconds and compared to the dynamic energy.

Close correlation is observed between the stress and energy signals. The peaks and phases coincide, reflecting a relationship between these two variables. This supports the assumption that structural energy serves as an effective criterion for identifying critical instants and potential stress hotspots. It is also a good indicator of the structural performance, being

a consistent parameter to be used as a criterion to select the reduced set of modes for an accurate representation of the structural problem. To observe a better correlation, the square values of the Von Mises stresses σ^2 are shown.

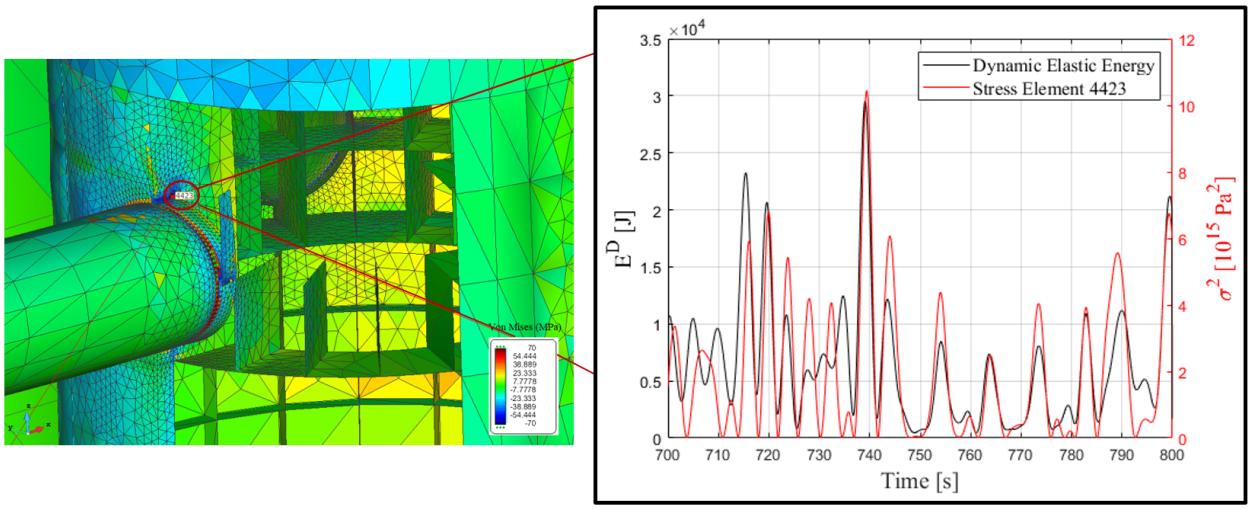

Figure 6.7: Stress filed and location of maximum stress hotspot (left). Instantaneous squared Von Mises stresses at hotspot element and structural dynamic energy (right).

The average time to compute the stresses at the hotspot in one time step is 0.0002 s. Then, for a one-hour simulation with a time step of 0.05 s, the stresses time-history at one hotspot can be computed in about 14.4 s. The computational time to obtain the stresses time history will grow/decay linearly with the number of hotspots and time steps. When computing the stresses offline the computational effort in the postprocess can be reduced. This is done by averaging the modal energy and discarding the least energetic eigenmodes.

Table 6.5 shows the computational cost of the different solvers involved in the simulation. In this case, both structural models (FEM and MMR) were used for comparison purposes. It is observed that the structural FEM is the most computationally expensive part, while MMR5000 is approximately 10 times faster than FEM. Parallel execution using OpenMP on 4 CPUs was employed, with the simulation running on an AMD Ryzen Threadripper 3970X 3.70GHz CPU unit.

Table 6.5: Computational cost breakdown.

Solver	Computational time/Simulation time
Rigid Body+Dynamic Mooring (FEM):	0.66 s/s
Wave diffraction-radiation	0.87 s/s
Structural FEM	4.6 s/s
Structural MMR 5000	0.47 s/s

For the present case study, the computational time required to compute the stresses for one time instant in all FEs is about 0.1s. This means that, for a one-hour simulation and a mean wave period of 14 seconds, the number of local maximums would be approximately 3,600/14=257 time instants. Then, it would take about 25 seconds to compute the dynamic stresses offline over the whole structure for the most critical points in time.

6.3.3 Wind-Wave analysis

The structure subjected to wind and wave loads is analyzed next. In accordance with the proposed decomposition between static and dynamic effects, the static component of the wind loads is subtracted in the simulation. This allows for a focused analysis of the dynamic component, which is the only one affecting the fatigue response of steel structures. A precomputed rigid-body simulation of the same case setup is used to extract the aerodynamic loads time-series from OpenFAST. Figure 6.8 left shows the aerodynamic wind force in surge and its average.

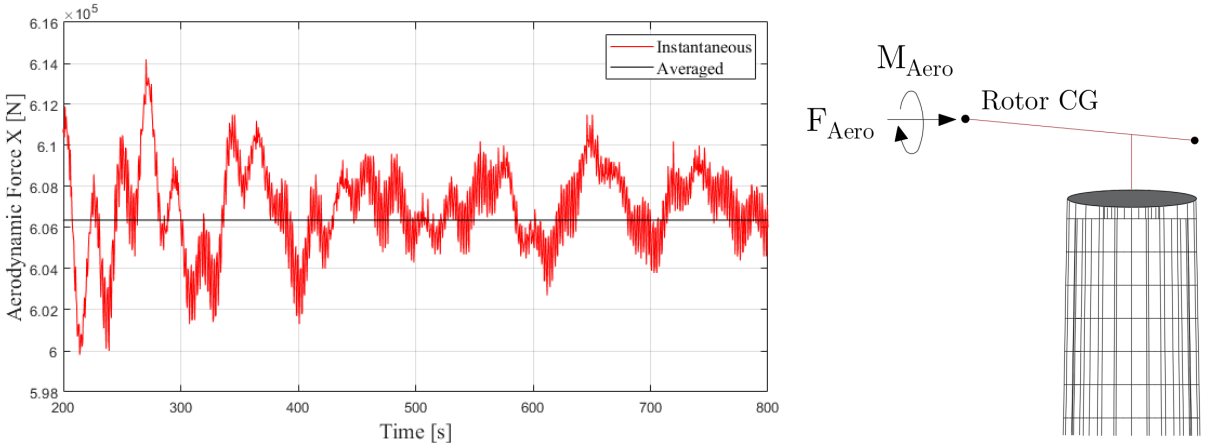

Figure 6.8: Left: wind load component in X acting on the rotor. Right: application point for the aerodynamic loads.

These set of loads are averaged and then extracted during the hydroelastic analysis. As observed, the static component (averaged) is dominant, while the dynamic part is several orders of magnitude smaller compared to the wave loads. In addition, the static component of the mooring loads is also subtracted.

Although the wind turbine is not explicitly modeled in SeaFEM, it operates virtually in OpenFAST throughout the simulation. Figure 6.8 right shows how the aerodynamic loads computed by OpenFAST are applied within the SeaFEM structural model at the rotor's center of mass. For the hydroelastic computation, one-way coupling is used. Figure 6.9 compares

the dynamic energy when using FEM and MMR. Again, the MMR solution agrees with the full FEM one.

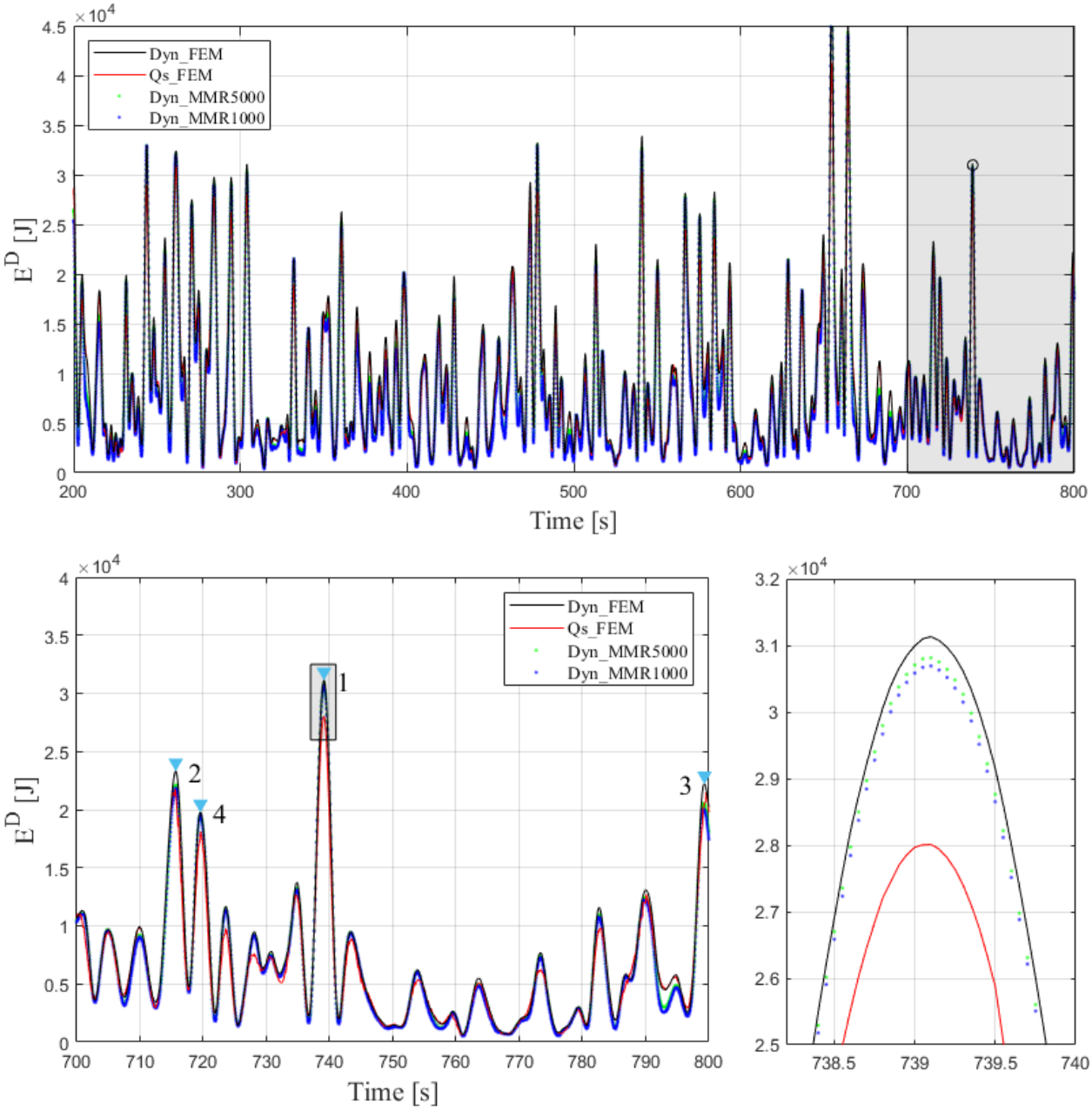

Figure 6.9: Instantaneous E^D plots, left: total time range and right: bounded time range.

Below, Table 6.6 gives the percentages for the four local maximum peaks. The percentages are computed with respect to the dynamic FEM solution. Agreement is found in the modal approximations, retaining over the 90 % of the dynamic structural energy. Even the MMR1000 closely approximates the full FEM solution, while the quasi-static solutions tend to underestimate the dynamic behavior.

Table 6.6: Percentage of the E^D with respect to the dynamic FEM analysis.

Analysis type	Dynamic			Quasistatic		
	FEM	MMR 5000	MMR 1000	FEM	MMR 5000	MMR 1000
Peak 1	100%	98.96%	98.57%	89.92%	88.90%	88.65%
Peak 2	100%	94.78%	93.53%	95.22%	89.90%	88.67%
Peak 3	100%	92.72%	90.43%	91.81%	84.54%	82.21%
Peak 4	100%	99.04%	98.64%	87.75%	86.81%	86.40%

In Figure 6.10 (left) is given a snapshot of the simulation for the wind-wave condition at its maximum structural energy instant. The free surface elevation and stress field in the whole structure are shown. The structure deformations are amplified by 150. The position of the element with maximum stress is pointed in Figure 6.10 (right), coinciding with previously analyzed load case for the element 4423.

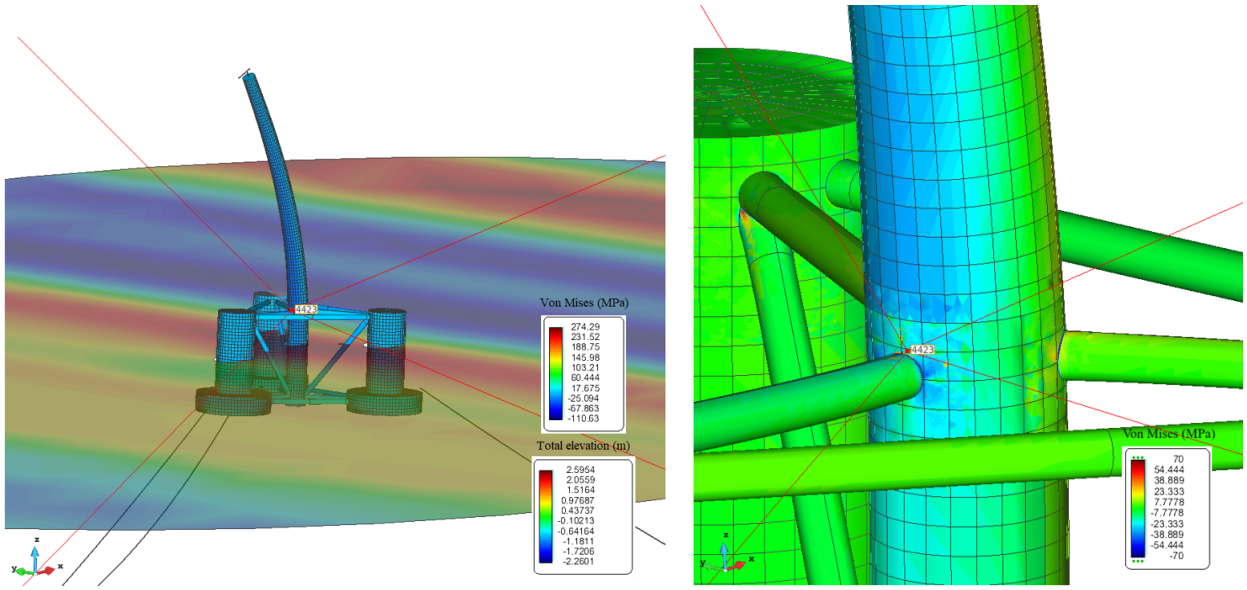

Figure 6.10: Left: stress field and deformation in critical condition (def x150). Right: close-up view of the stress field.

As observed, the potential hotspot is subjected to compressive stresses, consistent with the fore-aft bending mode shape. Additionally, in both analyzed conditions, a region of potential damage was identified in the substructure at the lower intersection between the braces and the main column. This finding suggests that further fatigue research should focus not only on the tower but also on the substructure.

Table 6.7 provides the time-averaged energies of the most energetic modes and their cumulative percentage. The most excited eigenmode has a lower energetic contribution compared to the only-waves condition. However, it is able to retain over the 60% of the FEM structural energy, needing only the 10 most energetic eigenmodes to recover over the 90%. This characteristic concentration of elastic energy in a few low-frequency modes demonstrates the suitability of the MMR approach for analyzing FOWTs. Moreover, it enables further reduction of the MMR hydroelastic problem.

Table 6.7: Energy distribution and cumulative energies from the most energetic modes.

Mode	Modal E^D [J]	E^D [%]	Accumulated E^D [%]
2	5215.50	63.93%	63.93%
11	450.29	5.52%	69.45%
13	379.73	4.65%	74.10%
1	293.47	3.60%	77.70%
17	160.79	1.97%	79.67%

From the stress field at the critical load case condition, it is possible to identify the region associated with the highest fatigue damage, as is the case of the tower base caused by the tower's bending moment [Li et al., 2018] or the intersection between structural members.

A detailed view of the hotspot location, found in the reinforcement between the braces joint and the main column at the tower's base is given in Figure 6.11. The stresses at this point are obtained offline for the time range of 100 seconds. Again, a strong correlation is observed between the stress and structural FEM energy signals.

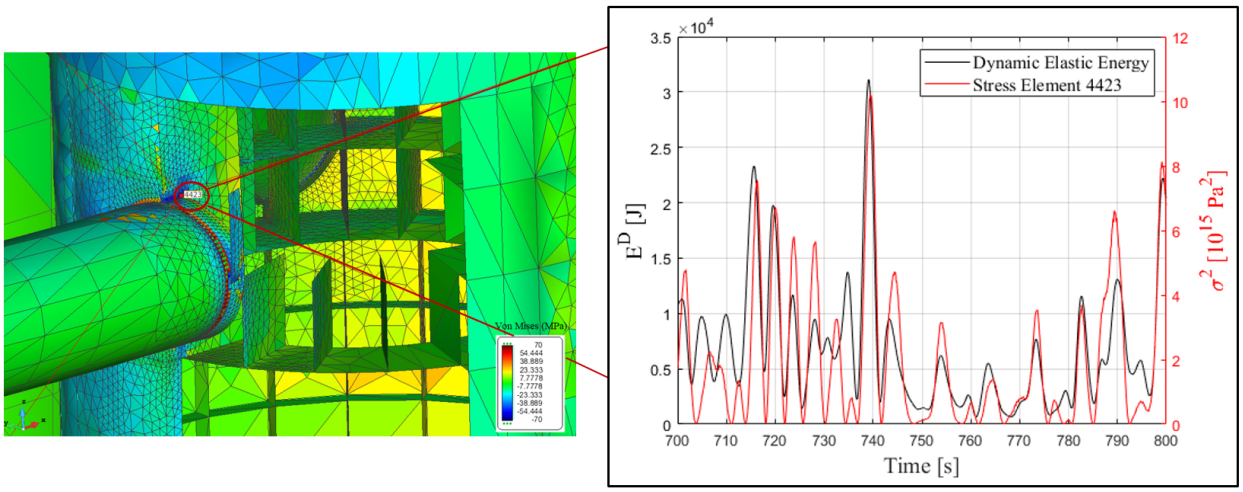

Figure 6.11: Stress filed and location of maximum stress hotspot (left). Instantaneous squared Von Mises stresses at hotspot element and structural energy (right).

6.3.4 Analysis of the most energetic mode

The structural response observed under both analyzed conditions is similar, with the dominant elastic response primarily driven by the wave excitation. This behavior is consistent with the trend seen in Figure 6.8, where the fluctuation in the aerodynamic wind force is considerably smaller than its average static value. Despite its small dynamic contribution, the wind force remains significant and must be accounted for in the simulation. Figure 6.12 presents the dynamic elastic energy, E^D, obtained from the FEM solution and compared between both conditions.

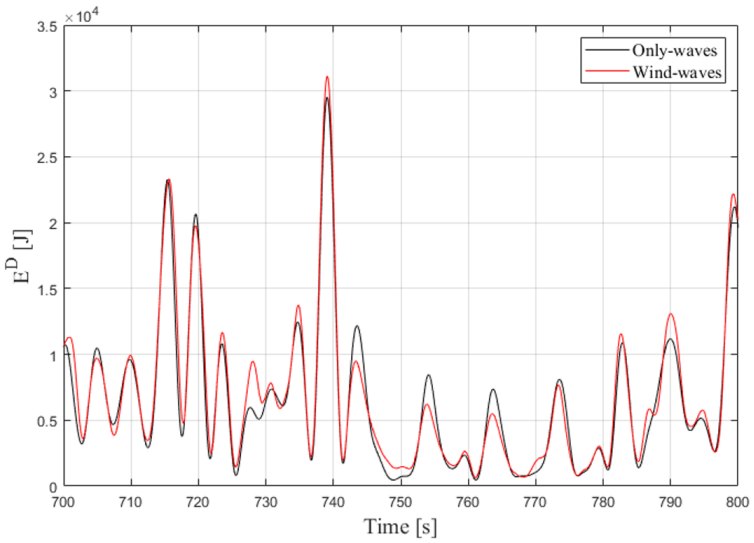

Figure 6.12: Dynamic FEM elastic energy comparison between load cases.

Furthermore, Figure 6.13 (left) plots the maximum and time-averaged modal elastic energies regarding the 5,000 modes. The second eigenmode was identified as the most excited in both analyzed conditions. It is clearly observed that the dynamic condition exhibits a higher concentration of energy in the first modes. In contrast, the energy distribution for the static case, shown in Figure 5.13, displays a more distributed energy across the modes. Figure 6.13 (right) provides a snapshot of the stress field for this dominant mode.

The stress field is given along with the corresponding deformation, characterized by the fore-aft bending of the tower. The element 4423, located at the tower base, is found to be the most stressed. This element consistently experiences critical stress levels in both loadcases, probably due to the significant influence of this mode excitation. According to the existing literature, the structural response of a FOWTs is largely influenced by the fore-after and side-to-side bending modes of the tower. Hence, the natural frequencies of the lower frequency modes are critical to assess the structural dynamics.

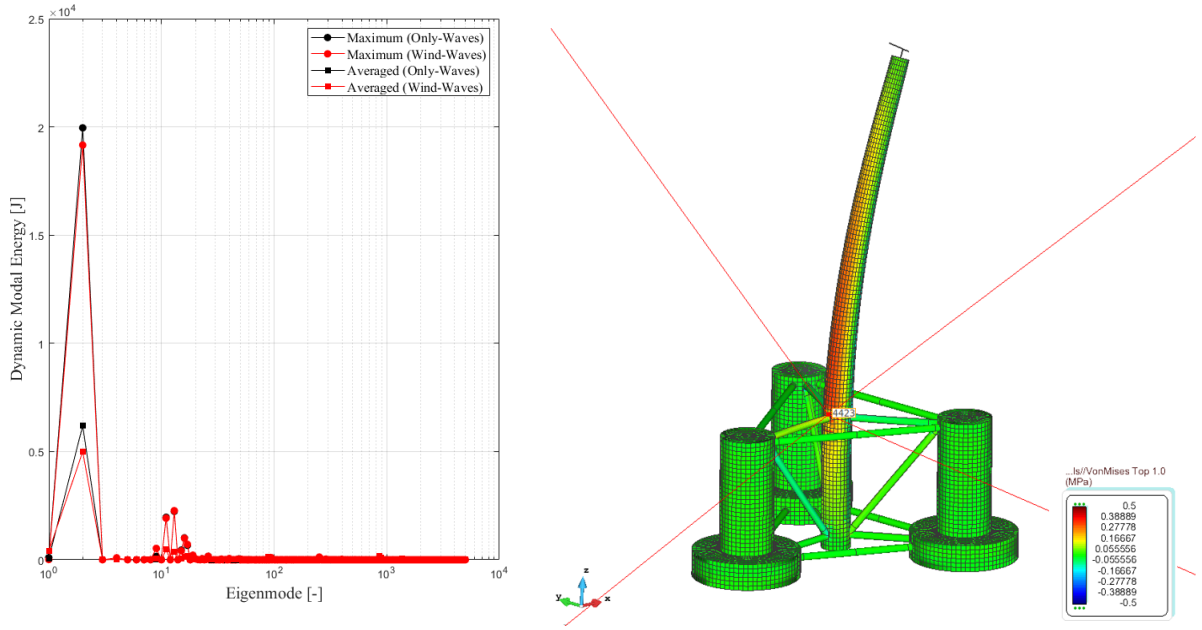

Figure 6.13: Left: dynamic modal energy distribution. Right: stress field corresponding to the second elastic mode.

The correlation between the stresses in element 4423 and the dynamic energy of the second mode is presented in Figure 6.14 for each analyzed condition. A stronger correlation is observed at peak values, where both higher stresses and structural energies are present. Additionally, the dynamic energy of the second mode shows a stronger correlation with the stress compared to the total energy, suggesting that this mode plays a dominant role in the structural damage of the analyzed element. This finding supports the use of the structural energy as indicator of the structural performance.

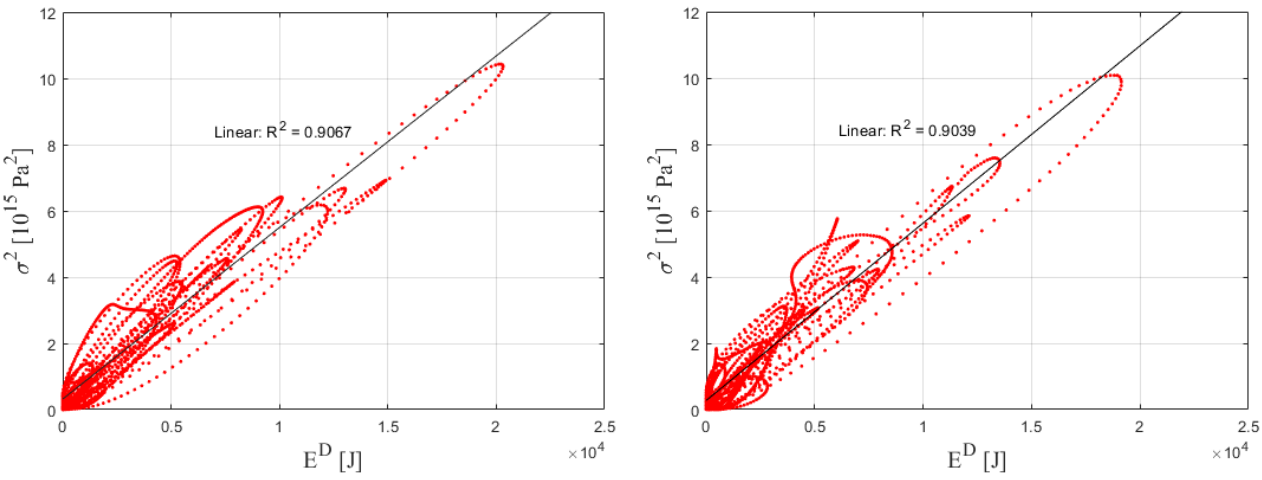

Figure 6.14: Stress correlation with second mode E^D for only-waves (left) and wind-waves (right).

6.3.5 Modal Response Amplitude Operators

When the hydroelastic problem is linear, including structural model and external loads, the response amplitude operators can be computed for each eigenmode. These Modal Response Amplitude Operators (MRAOs) computed for the different modal displacement fields, are obtained for monochromatic waves using a white noise spectrum propagating in the longitudinal direction. The wave periods range from 0.5 to 100 seconds, with a total of 371 wave frequencies computed. The structural damping is set to a 1% of the modal damping.

Hydroelastic couplings can be classified as strong, where the fluid and the structure interact simultaneously, and weak or one-way, where only the fluid influences the structure. The quasi-static coupling refers to a scenario where inertial and damping effects are neglected, and the structural response depends only on the stiffness, remaining independent for each time step. Figure 6.15 compares the MRAOs for the second mode computed using a quasi-static (QS) coupling, one-way (weak) dynamic coupling, and two-ways (strong) dynamic coupling.

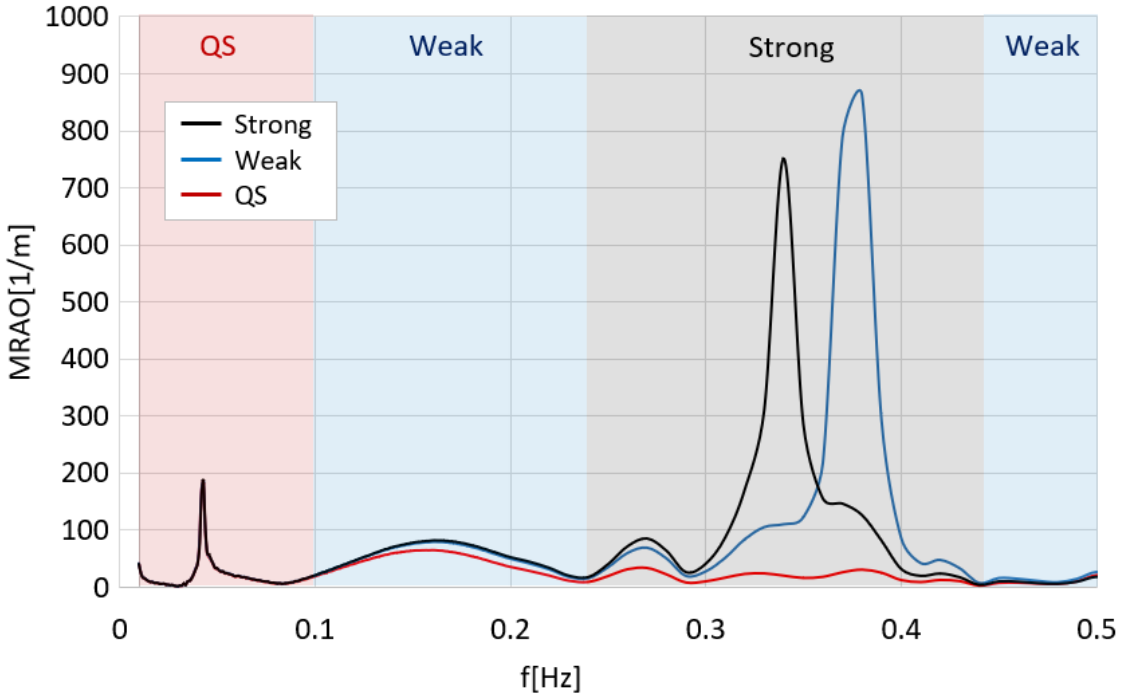

Figure 6.15: MRAOs comparison for 2nd elastic mode in head waves.

The second elastic mode corresponds to the fore-aft bending mode of the tower. Since the waves propagate in the longitudinal direction, this mode is expected to have a relevant contribution to the elastic energy. Hence, although MRAOs have been obtained for all modes, this analysis will focus on this particular mode.

As expected, near the mode resonance frequency, the quasi-static approach fails to recover the dynamic behavior. The QS approach assumes a slow structural response with minimal dependence on time, effectively treating the problem as static. In the low-frequency range, where loads are applied in long time periods, QS models can provide a reasonable approximation. However, in the near resonance region, the strong coupling is required. Otherwise, the resonance will occur at the dry frequency instead of the wet frequency, leading to simulation errors. Between these two scenarios, a weak coupling approach may be sufficient to capture the structural behavior accurately. When using a QS method, it is essential to consider its range of application.

For the dynamic solutions, the resonance peak shifts due to the change in the modal frequency from dry to wet conditions. Additionally, away from the resonance frequency (below 0.1 Hz), the three approximations provide similar results, with a peak at the pitch natural frequency. Given a wave energy spectrum $S_w(\omega)$, one can obtain the structural energy spectrum $S_m(\omega)$ for mode "m" as:

$$S_m(\omega) = \Omega_m^2 S_w(\omega)\,\mathrm{MRAOs}(\omega)^2 \tag{6.8}$$

The zero order moment (E_m^0) of $S_m(\omega)$ is given by:

$$E_m^0 = \int_0^\infty S_m(\omega) d\omega \tag{6.9}$$

E_m^0 is an indicator of how much elastic energy the mode "m" will absorb under a seastate given by $S_w(\omega)$. Figure 6.16 compares $E_{m=2}^0$ for a JONSWAP spectrum with $H_S = 1$ m.

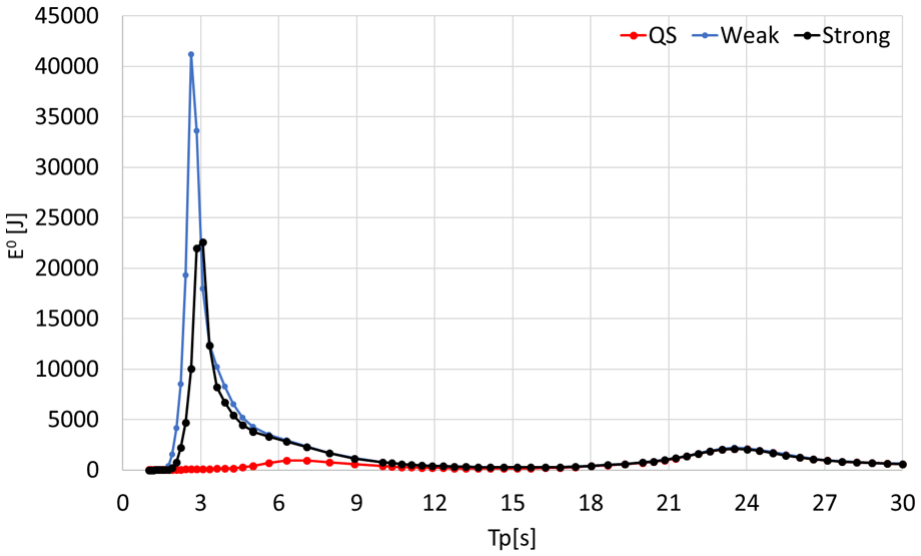

Figure 6.16: Structural energy versus wave peak period for 2nd elastic mode. Wave spectrum: Jonswap Hs = 1m.

It is observed that the modal energy increases significantly for T_p values close to the mode's resonance frequency. However, the quasi-static approach is unable to capture this effect. Moreover, the change in modal frequency from dry to wet conditions also have a significant impact for T_p around the modal resonance. The modal energy E_m^0 can be used also as an indicator to select most excited modes and further reduce the modal basis. Moreover, the total energy $E^0 = \sum_m E_m^0$ can also be used as an indicator to select those extreme wave conditions inducing largest values of E^0.

6.3.6 Second-order wave loading and structural resonance

In marine and offshore engineering, it is a common practice to assume that structures are stiff enough so a quasi-static response to wave loading can be also assumed. However, in floating wind, the presence of the wind turbine on top of a slim tower makes lower modal frequencies to get closer to the wave loading frequencies. The purpose of this study is to compare the structural energy for QS, weak coupling, and strong coupling under first- and second-order hydrodynamic loads.

Monochromatic wave

This section analyzes the structural response under a monochromatic wave with wave period T=6.066 seconds and one meter amplitude. This wave period corresponds to the double of the wet modal period for the second mode. Hence, the second order component of the wave is expected to induce resonance effects. Figure 6.17 shows the instantaneous elastic energy, computed by the MMR5000 model, under first- and second-order wave loading.

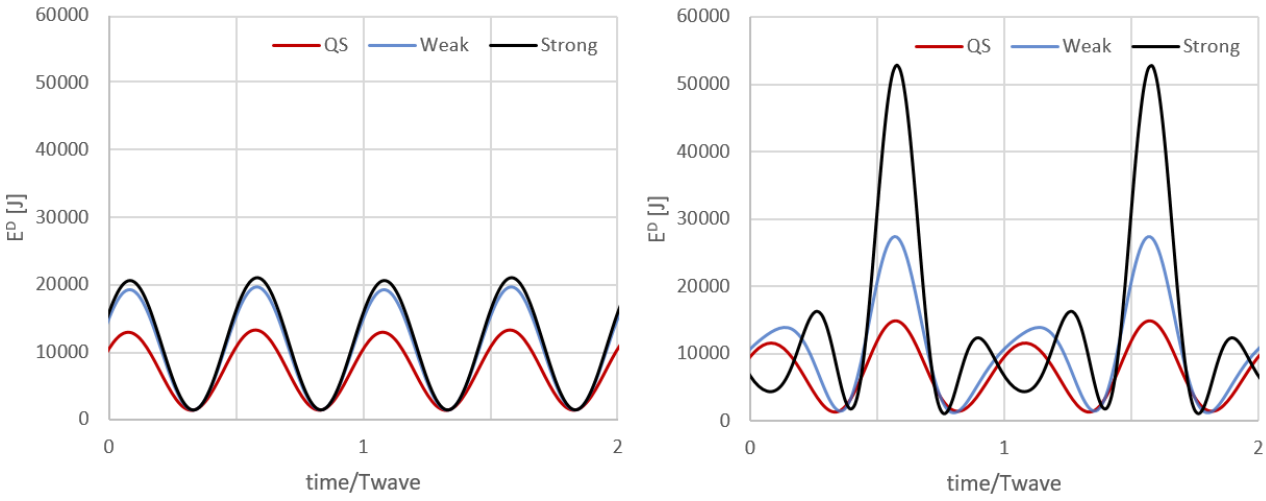

Figure 6.17: Instantaneous elastic energy under first (left) and second (right) order monochromatic wave.

In Figure 6.17 (left), the first-order response demonstrates that the dynamic effect remains significant for this wave period. This makes the QS coupling to underestimate the structural energy, while only a slight difference is observed between the weak and strong dynamic couplings.

Figure 6.17 (right) shows the structural energy also considering the second order loading. In this case, the QS solution is quite similar to the first order response, indicating that no resonance effects are present, as expected. The dynamic weak coupling shows some near resonance effect, but still underpredicts the resonance effect compared to the strong dynamic coupling.

Irregular waves

This section analyzes the structural response under irregular wave conditions. The irregular waves are modeled using a JONSWAP spectrum with a mean wave period $T_m = 6.066$ seconds and a significant wave height $H_S = 3$ meters. This wave period corresponds to the double of the wet modal period for the second mode. Hence, the second order components are expected to induce resonance effects. Figure 6.18 shows the instantaneous elastic energy, computed by the MMR5000 model, under first (top) and second (bottom) order wave loading.

In Figure 6.18 top, the first order response shows that dynamic effects are still relevant for this wave period. This makes the QS coupling to underpredict the structural energy. In addition, significant differences are observed between the weak and strong dynamic couplings.

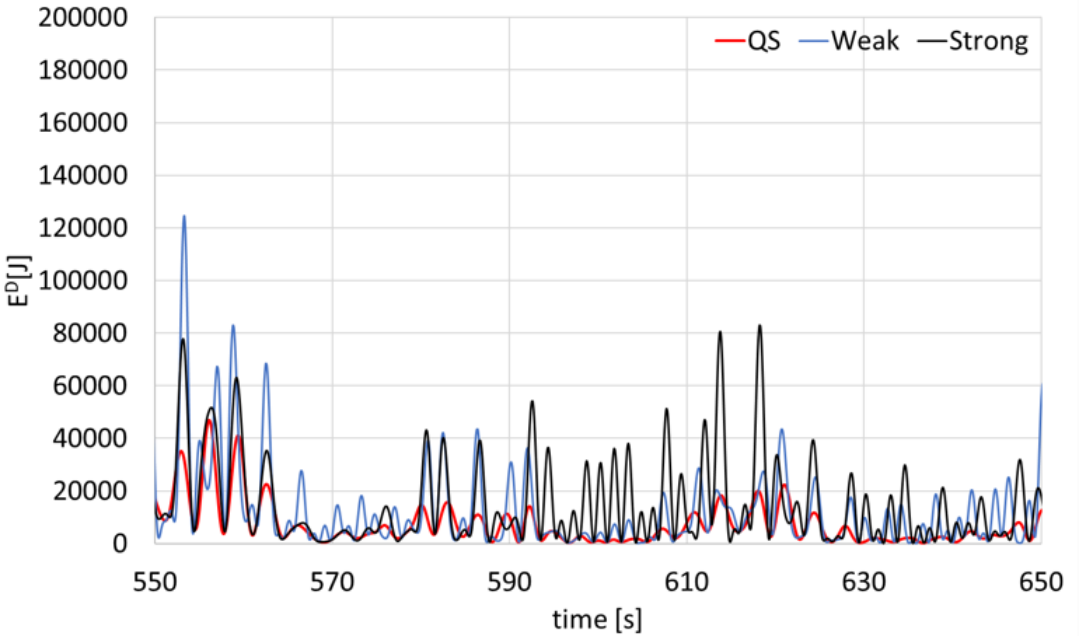

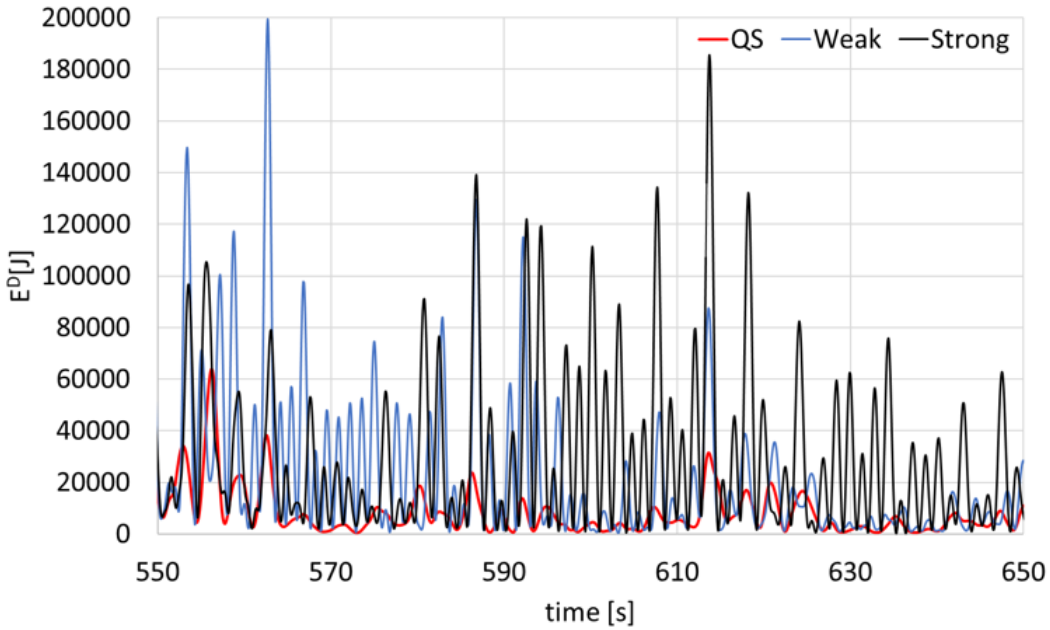

Figure 6.18: Instantaneous elastic energy under first (top) and second (bottom) order irregular waves.

Figure 6.18 bottom presents the elastic energy, also considering the second-order loading. In this case, the QS solution exhibits some differences compared to the first-order response. The dynamic weak coupling exhibits some near-resonance effects, but large differences are observed when compared to the strong coupling.

6.4 Conclusions

This chapter presents the numerical structural assessment of a semi-submersible wind-turbine platform under operation condition. A new strategy is proposed to perform integrated load analysis of FOWTs using a novel hydroelastic solver based on the MMR technique. The consistency of the method has been verified in contrast with a higher fidelity FEM structural solution. Agreement is found in all analyzed conditions. The most energetic eigenmode (second elastic one) is analyzed in detail giving its relevance in the platform structural response.

The optimization of the modal basis following the structural energy criterion, allowed to select the most relevant first modes for an accurate solution. For the present application, a modal basis of 5,000 eigenmodes is considered enough to accurately capture its elastic structural energy and local deformations. This method implies a large reduction in the number of structural degrees of freedom with respect to the 1,026,150 needed in the FEM solver. The MMR solution results in a reduction of approximately a 90 % in the computational time

of the structural solver with respect to the conventional FEM. The detection of the critical conditions and potential hotspots from the offline computation of the stresses, allows to perform a localized analysis reducing the postprocess times.

The use of a whole time-domain FEM framework, allows a more efficient two-way hydroelastic coupling, avoiding the communication among different software. The importance of performing two-way analysis is studied with the modal damping induced by the radiated waves. Showing its relevance when analyzing resonance effects in elastic structures. The dynamic contribution is analyzed versus the traditional quasi-static approach. The limitations of the quasi-static solution are tested, showing to underpredict the MMR dynamic structural response and being unable to capture resonance effects. The ability to compute dynamic effects, which induce cyclic stresses, enables a precise solver for fatigue prevention.

Modal response amplitude operators have been obtained under head waves loading. Since the second elastic mode is the most energetic under these conditions, it has been selected for an energy analysis to compare the quasistatic, one-way, and two-way coupling approaches. Significant resonance effects are observed, inducing notable differences in wave frequencies near the modal resonance, with the quasistatic approach failing, as expected. Moreover, differences between the one-way and two-way coupling approaches are also significant, primarily due to the change in the modal period.

It has been also demonstrated that the modal energy under different irregular waves can be estimated from MRAOs. This information is useful to estimate a priori: the conditions where the structural energy will be higher; to identify most energetic modes (allowing for further reduction of the modal basis); and to check the suitability of the quasistatic, weak and strong couplings.

Chapter 7

Conclusions

This dissertation presents a complete numerical framework to perform integrated load analysis of floating offshore wind turbines. The implemented tool allows to compute the coupled aero-hydro-servo-elastic response of these concepts under combined environmental loads. Structural assessments can be performed with a reduced structural model based on the modal matrix reduction technique. This research is mainly focused on the numerical analysis of the hydroelastic behavior in floating wind platforms.

The solution is based on the hydroelastic solver SeaFEM and the wind turbine simulator OpenFAST. Both codes are coupled: SeaFEM handles the structural, hydrodynamics, and mooring aspects, while OpenFAST manages the aerodynamics, blade elasticity, servomotor, and rigid-body response. The solvers are integrated into a whole time-domain FEM framework. A more representative schema about the solution distribution between both solvers is illustrated in Figure 7.1. The main numerical features in the proposed simulation package for FOWTs are given in Table 7.1.

Structural analyses of marine structures using 3D full-length FEM models are computationally expensive, since they require to solve the structural dynamic equations at each time step. Besides, in the case of two-way coupled hydro-elasticity, this process must be repeated at every iteration. To address this, the MMR technique is applied to reduce this computational cost of the structural solver. The main idea is to largely reduce the number of degrees of freedom in the structural system by retaining only those modes with significant energy. There is still room for further reduction of the modal basis if only the most energetic modes are considered.

Current limitations in existing numerical solvers for simulating the complex multi-physics behavior of floating FOWTs have been addressed. In this regard, higher-fidelity hydrodynamic and structural solutions are implemented, improving their accuracy without significantly compromising the computational effort. The hydrodynamic model solves the time-domain diffraction-radiation problem including second-order effects without needing external BEM solvers for frequency-domain analysis.

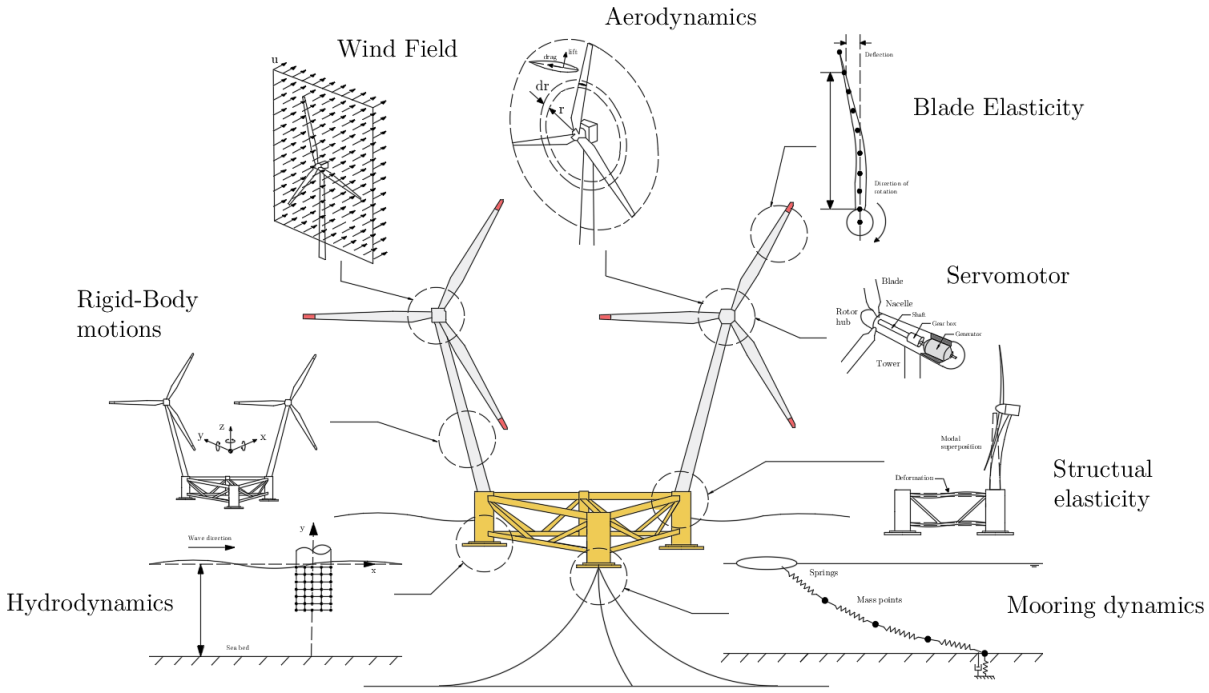

Figure 7.1: ILA framework and solution distribution.

On the structural side, the MMR approach allows for detailed stress analysis at the local level, going beyond linear beam theory and member-level approximations. The entire solution is integrated within a whole FEM framework, enabling strongly coupled two-way hydroelastic interactions. The bottleneck of ILAs is the use of partitioned strategies and quasistatic approaches. With the proposed method this analysis is carried out in a more efficient manner avoiding the use of independent computational tools, while providing a more accurate solution able to capture dynamic elastic effects.

Table 7.1: Capabilities and numerical solution of the ILA framework.

Aerodynamics	BEMT, FVW Multi-Rotor	Hydrodynamics	Potential flow-FEM Second-order
Structural	Rigid-body 3D-FEM-MMR	Mooring	Dynamic-FEM Quasi-static

The MMR approach also allows for the offline computation of the structural displacements and stresses from the modal amplitudes. This implies a more precise analysis and a large reduction in the output data files and postprocess times. A methodology is proposed to identify critical conditions and hotspots based on the structural energy. The validity of this criterion is studied with the correlation between the elastic energy and the stresses. An application case of this methodology is presented for a detailed structural design of the well-known OC4-DeepCwind, showing an efficient handling to perform structural assessments.

Furthermore, a new approach is proposed to extend single-turbine frameworks for the analysis of multi-rotor concepts. To achieve this, a strategy is designed to enhance the SF-OF coupled framework. This approach enables a comprehensive coupled analysis of these platforms, capturing the dynamic interactions between turbines and their impact on power production.

The simulation framework is tested with different full-scale floating turbines configurations, including the spar Hywind, the semi-submersible DeepCwind and the multi-turbine W2Power. The exposed concepts are shown in Figure 7.2. Different analyses have been performed to demonstrate its versatility.

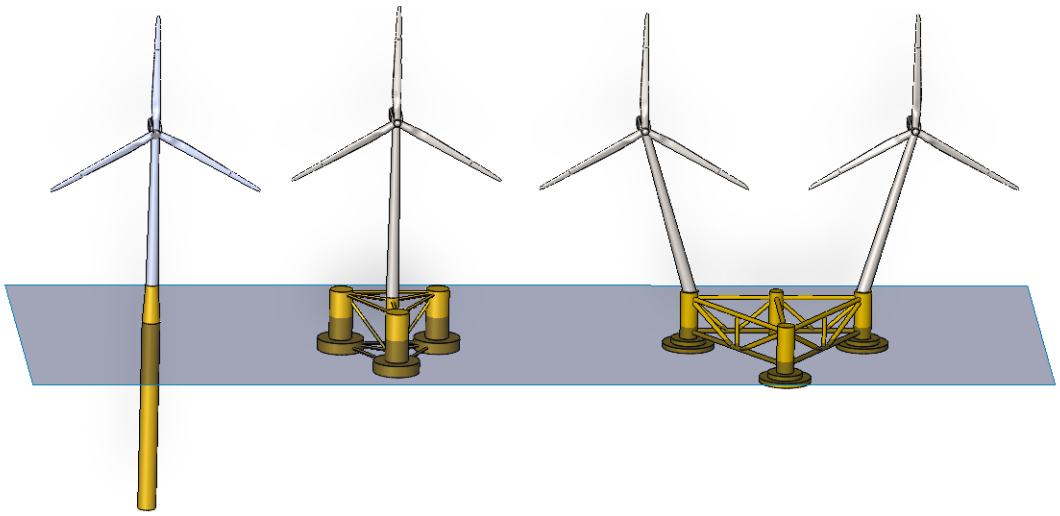

Figure 7.2: (a) Hywind (b) DeepCwind (c) W2Power platforms.

To gain a deeper understanding in the behavior of these concepts, several studies have been performed focusing on different aspects of the multi-physics problem. The reliability of the method is proven with a code-to-code comparison process. The tool has demonstrated to be consistent when compared against other numerical strategies. Agreement is observed in the Response Amplitude Operators and response under wind loads. The reduced order structural solution has shown to converge with higher-fidelity FEM solvers, being able to accurately reproduce the FEM structural response by linear combination of modal responses.

From the ILA performed on the semi-submersible DeepCwind using the proposed ROM, the following key findings have been identified:

- The use of the MMR approach has proven to be convenient for the analysis of FOWTs. The method was able to capture over a 90% of the structural energy with only using a 0.48% of the total degrees of freedom. Additionally, it has demonstrated significantly higher accuracy compared to full FEM-based quasi-static methods.
- A reduction of approximately 90% in computational time is achieved for the MMR structural solver compared to the FEM.
- Its suitability improves when analyzing dynamic load conditions, where the elastic response has shown to be concentrated in the first modes. When analyzing static conditions, it is recommended to solve the full FEM equations.
- The wind component has shown a minor impact on the dynamic response compared to the effects of waves. However, it remains significant and should still be accounted in the analysis.
- The quasi-static approach has been found to underestimate dynamic effects, making it less suitable for the simulation of the entire range of frequency loads. Its application is recommended after assessing its validity range for lower frequencies.
- It is highlighted the importance of performing two-ways hydroelastic couplings, being essential assess the change in the modal periods from dry to wet conditions. This consideration plays a critical role in the elastic response of large-scale flexible floating structures.
- The weak hydroelastic coupling is found to be adequate outside the resonance region.
- A detailed analysis should be conducted on the critical condition where the platform is subjected to head waves with a wavelength twice the length of the platform.
- The elastic response is predominantly concentrated in the tower's fore-aft bending mode, with stress points observed at the intersections between the tower and braces. The tower base is identified as a potential hot-spot area that requires special attention.
- It is recommended to incorporate second-order hydrodynamic effects in order to accurately capture the tower's structural resonance caused by the fore-aft bending mode.

All these findings expect to help in the engineering design and optimization of the structural concepts for floating wind turbines.

7.1 Innovation and impact

This numerical study expects to have an impact on the wind energy research community. The key contributions are outlined below:

Coupled aero-hydro framework:

- The higher-fidelity hydrodynamic and structural solutions used could contribute in the understanding and analysis of the multi-physics problem concerning FOWTs.
- The whole FEM framework provides versatility in the structural designs that can be analyzed, opening to new incoming concepts.
- The framework is implemented using one of the leading wind turbine simulation solvers, OpenFAST, which has a significant impact on the wind energy field.

Multi-Turbine extension:

- The technological development of multi-turbine concepts is at a lower maturity level. Hence, the present extension might help in the study and development of these concepts, which are an interesting alternative to large scale wind turbines.

Hydroelastic MMR method:

- The use of the MMR structural solver allows for the structural assessment of floating offshore structures, addressing critical issues such as fatigue prevention, being a main concern in their design and operation. This might help to ensure the structural integrity of large FOWTs were elastic deformations can be significant.
- The present technique also allows for the structural optimization of a floating wind platform in early design stages, improving its structural performance in operation.

Integrated Load Analysis framework:

- The complete ILA framework avoids to perform partitioned strategies where the problem is solved in several stages. This reduces the use of tools and minimizes potential errors or information loss when performing coupled analysis of FOWTs.
- It offers an alternative to experimental campaigns, avoiding the use of complex monitoring instrumentation and facilities, as well as the time required to adjust the experimental setup between tests to cover a range of operational conditions and load cases.
- Besides, it allows to perform structural analysis and post-processing with optimal computational cost. Being convenient for the certification of FOWTs regarding international

standards, which require the study of long-time simulations under several DLCs.

- In addition, it might be suitable for the implementation of a digital twin for structural health monitoring in operational conditions.
- Finally, since enhancing the structural reliability of ocean energy systems, it might contribute to a reduction in their levelized cost of energy.

7.2 Original contributions

This section outlines the key original contributions in this work, highlighting the numerical implementations introduced throughout this document.

- The main contributions of this work are mainly related to the interaction between SeaFEM and OpenFAST v3.5, particularly in the coupling strategies between both tools.
- A new methodology is proposed for the extension of the numerical framework for the simulation of multi-rotor floating platforms.
- The enhancement of the seakeeping coupling to incorporate second-order hydrodynamic effects.
- The application of a novel hydroelastic method for the analysis of floating wind platforms, with a focus on their detailed structural response.
- A methodology is proposed to identify critical hot-spots for the structural assessment based on the dynamic structural energy.
- An analysis is performed to assess the validity of different hydroelastic methods for the study of fluid-structure interactions.
- The numerical framework for the ILA of floating wind platforms under combined wind and wave environmental loads.

It is important to clarify that the structural ROM used in this work is not an original contribution; rather, its novelty lies in its application to the simulation of FOWTs. Additionally, the implemented framework would not have been possible without the fundamental role of SeaFEM and OpenFAST, as well as the previous work of their developers.

The implementations within OpenFAST v.3.5.0 are updated in the open source repository:

https://github.com/compassis/openfast.

7.3 Future work

This work sets a simulation environment that can be used as starting point for future implementations and analysis. However, there are some aspects in this research that could be open to improvements.

- The current multi-turbine tool is implemented for twin turbine concepts. Its extension to an arbitrary number of turbines would be required to cover incoming floating platforms with several turbines. The present methodology could be easily adapted to this aim.
- Besides, the proposed multi-turbine approach could be improved to account for aerodynamic wake interference between adjacent turbines.
- The aero-elastic coupling between OpenFAST wind turbine loads and SeaFEM's structural MMR is performed allowing only one-way interactions. The rotor loads are received but the structural top-tower deflections are not transferred to the wind turbine. In order to analyze the impact of top-tower deflections in the aerodynamic loads and wind turbine performance, the two-way coupling would be required.
- The use of higher-fidelity computational fluid dynamics solvers could be explored to account for non-linear wave load effects, with particle methods offering an interesting approach.
- The MMR structural solution can be enriched to include the deformation of local modes with high excitation by incorporating the contribution of static modes.
- This methodology can be tested in DLCs required for the certification of FOWTs. Performing long-term fatigue analysis subjected to several combined conditions.
- The Phase II of the incoming Offshore Code Comparison Collaboration 7 project aims to validate member-level loads within a floating substructure, and assess the impact of flexibility on the global dynamics of the system. The present collaboration within this project can serve to perform a validation process of the implemented tool.

This work is mainly focused on implementing numerical tools for the analysis of FOWTs, with the potential for broader applications to enhance the understanding of their behavior.

7.4 Research dissemination

The present research resulted in the following scientific publications:

1. Berdugo-Parada, I.; Servan-Camas, B.; Garcia-Espinosa, J. *Numerical Framework for the Coupled Analysis of Floating Offshore Multi-Wind Turbines.* Marine Science and Engineering. 2024, 12, 85. https://doi.org/10.3390/jmse12010085

2. Servan-Camas, B.; Berdugo-Parada, I.; Garcia-Espinosa, J.; Pastor-Sanchez, A. *Modal matrix reduction for fully coupled integrated load analysis of floating structures.* Under review in Marine Structures.

In addition, this work was presented at the following conferences:

1. Berdugo-Parada, I.; Servan-Camas, B.; Garcia-Espinosa, J. *Numerical tool for the simulation of multi-turbine floating platforms.* 62º International congress of Naval Engineering and Maritime Industry, 2023

2. Berdugo-Parada, I.; Servan-Camas, B.; Garcia-Espinosa, J. *SeaFEM – OpenFAST coupled tool for the simulation of floating offshore multi-wind turbines.* 10$^{\text{th}}$ International Conference on Computational Methods in Marine Engineering, 2023

3. Servan-Camas, B.; Garcia-Espinosa, J.; Berdugo-Parada, I. *Análisis hidroelástico acoplado de estructuras marinas: aplicación a la eólica flotante.* 14$^{\text{as}}$ Jornadas Técnicas ENERMAR, 2024.

Finally, it is highlighted the participation in European and national research projects, which have significantly contributed to the advancements described in this work:

1. *Development, engineering, production and life-cycle management of improved FIBRE-based material solutions for structure and functional components of large offshore wind enerGY and tidal power platform* (FIBREGY). (2021-2024). Proj. Num. 952966. European Union, H2020.

2. *Development of a machine learning strategy for hydroelastic analysis of ships* (MLAMAR). (2022-2025). Proj. Num. PID2021-126561OB-C31. Ministerio de Ciencia e Innovacion.

References

Bae, Y. (2013). Coupled dynamic analysis of multiple unit floating offshore wind turbine. [See Online]. *Texas A&M University*.

Bae, Y., & Kim, M.-H. (2015). The dynamic coupling effects of a MUFOWT (multiple unit floating offshore wind turbine) with partially broken blade. [See Online]. *Ocean Wind Energy*, *2*, 89–97.

Barltrop, N. (1993). Multiple unit floating offshore wind farm (MUFOW). [See Online]. *Wind Engineering*, *17*, 183–188.

Bashetty, S., & Ozcelik, S. (2022). Design and stability analysis of an offshore floating multi-wind turbine platform. *Inventions*, *7*. https://doi.org/10.3390/inventions7030058

Bayati, I., Jonkman, J., Robertson, A., & Platt, A. (2014). The effects of second-order hydrodynamics on a semisubmersible floating offshore wind turbine. *Journal of Physics: Conference Series*. https://doi.org/10.1088/1742-6596/524/1/012094

Berdugo-Parada, I., Servan-Camas, B., & Garcia-Espinosa, J. (2024). Numerical framework for the coupled analysis of floating offshore multi-wind turbines. *Marine Science and Engineering*, *12*. https://doi.org/10.3390/jmse12010085

Bjerg Thomsen, J., Bergua, R., Jonkman, J., Robertson, A., Mendoza, N., & Brown, C. (2021). Modeling the tetraspar floating offshore wind turbine foundation as a flexible structure in orcaflex and openfast. *Energies*. https://doi.org/10.3390/en14237866

Bosnjakovic, M., Katinic, M., Santa, R., & Maric, D. (2022). Wind turbine technology trends. *Applied Sciences*. https://doi.org/10.3390/app12178653

Branlard, E., & Geisler, J. (2021). A symbolic framework for flexible multibody systems applied to horizontal axis wind turbines. *Wind Energy Science Discussions*. https://doi.org/10.5194/wes-2021-46

Brown, K., Cheung, L., Hsieh, A., Maniaci, D., & Hamilton. (2023). Wake interactions behind individual-tower multirotor wind tur-bine configurations. *Journal of Physics: Conference Series*. https://doi.org/10.1088/1742-6596/2505/1/012041

Bureau Veritas. rule note ni 572 dt r02 e [See Online]. (2019).

Butterfield, S., Musial, W., Jonkman, J., & Sclavounos, P. (2007). Engineering challenges for floating offshore wind turbines. [See Online]. *Conference Paper NREL/CP-500-38776*.

Campaña-Alonso, G., Martín-San-Román, R., Méndez-López, B., Benito-Cia, P., & Azcona-Armendáriz, J. (2023). OF^2: Coupling openfast and openfoam for high-fidelity aero-hydro-servo-elastic fowt simulations. *Wind Energy Science*, *8*, 1597–1611. https://doi.org/10.5194/wes-8-1597-2023

Cao, Q., Xiao, L., Cheng, Z., & Liu, M. (2021). Dynamic responses of a 10 MW semi-submersible wind turbine at an intermediate water depth: A comprehensive numerical and experimental comparison. *Ocean Engineering*, *232*. https://doi.org/10.1016/j.oceaneng.2021.109138

Chanprasert, W., Sharma, R. N., Cater, J., & Norris, S. (2022). Large Eddy Simulation of wind turbine wake interaction in directionally sheared inflows. *Renewable Energy*, *201*. https://doi.org/10.1016/j.renene.2022.11.021

Coulling, A. J., Goupee, A. J., Robertson, A. N., & Jonkman, J. M. (2013). Importance of second-order difference-frequency wave-diffraction forces in the validation of a fast semi-submersible floating wind turbine model. *Proceedings of the ASME 32nd International Conference on Ocean, Offshore and Arctic Engineering*. https://doi.org/10.1115/OMAE2013-10308

Del Pozo Gonzalez, H., & Domínguez-García, J. (2022). Non-centralized hierarchical model predictive control strategy of floating offshore wind farms for fatigue load reduction. *Renewable Energy*, *187*. https://doi.org/10.1016/j.renene.2022.01.046

Di Capua, D., Pacheco, R., García-Espinosa, J., & Pastor, A. (2023). OSI4IOT: An advanced open-source platform for sensor-driven iot and digital twins deploymen. https://doi.org/10.13140/RG.2.2.35960.83200

Duarte, T., Sarmento, A. J., & Jonkman, J. (2014). Effects of second-order hydrodynamic forces on floating offshore wind turbines [See Online]. *Conference Paper NREL/CP-5000-60966*.

El Beshbichi, O., Xing, Y., & Ong, M. (2021). Dynamic analysis of two-rotor wind turbine on spar-type floating platform. *Ocean Engineering*, *236*. https://doi.org/10.1016/j.oceaneng.2021.109441

El Beshbichi, O., Xing, Y., & Ong, M. (2023). Modelica-AeroDyn: Development, benchmark, and application of a comprehensive object-oriented tool for dynamic analysis of non-conventional horizontal-axis floating wind turbines. *Wind Energy*, *26*, 538–572. https://doi.org/10.1002/we.2814

Enerocean [https://enerocean.com/w2power/ Accessed on 26 October 2023]. (n.d.).

Fadaei, S., F. Afagh, F., & G. Langlois, R. (2024). A survey of numerical simulation tools for offshore wind turbine systems. *Wind*, *4*. https://doi.org/10.3390/wind4010001

Felippa, C. (2003). A study of optimal membrane triangles with drilling freedoms. *Computer Methods in Applied Mechanics and Engineering*, *192*, 16–18. https://doi.org/10.1016/S0045-7825(03)00253-6

Felippa, C., & Haugen, B. (2005). A unified formulation of small-strain corotational finite elements: I. theory. *Computer Methods in Applied Mechanics and Engineering*, *194*, 21–24. https://doi.org/10.1016/j.cma.2004.07.035

Fibregy project. [See Online Accessed on 26 October 2023]. (2020). *Development, Engineering, Production and Life Cycle Management of Improved FIBRE-Based Material Solutions for the Structure and Functional Components of Large Offshore Wind Energy and Tidal Power Platforms.*

Garcia-Espinosa, J., Di Capua, D., Servan-Camasa, B., Ubach, P.-A., & Oñate, E. (2015). A fem fluid–structure interaction algorithm for analysis of the seal dynamics of a surface-effect ship. *Computer Methods in Applied Mechanics and Engineering*, *295*, 290–304. https://doi.org/10.1016/j.cma.2015.07.010

Garcia-Espinosa, J., & Servan-Camas, B. (2018). A non-linear finite element method on unstructured meshes for added resistance in waves. *Ships and Offshore Structures*, *14*, 153–154. https://doi.org/10.1080/17445302.2018.1483624

Garcia-Espinosa, J., Servan-Camas, B., & Calpe-Linares, M. (2023). High fidelity hydroelastic analysis using modal matrix reduction. *Marine Science and Engineering*, *11*. https://doi.org/10.3390/jmse11061168

Ghaisas, N., Ghate, A., & Lele, S. (2018). Large-eddy simulation study of multi-rotor wind turbines. *Wind Energy Science*. https://doi.org/10.1088/1742-6596/1037/7/072021

Goupee, A., Koo, B., Kimball, R., Lambrakos, K., & Dagher, H. (2014). Experimental comparison of three floating wind turbine concepts. *Offshore Mechanics and Arctic Engineering*, *136*. https://doi.org/10.1115/1.4025804

Gutierrez-Romero, J., J, G.-E., Servan-Camas, B., & Zamora-Parra, B. (2016). Non-linear dynamic analysis of the response of moored floating structures. *Marine Structures*, *49*. https://doi.org/10.1016/j.marstruc.2016.05.002

Hall, M., & Goupee, A. (2015). Validation of a lumped-mass mooring line model with DeepCwind semisubmersible model test data. *Ocean Engineering*, *105*, 590–603. https://doi.org/10.1016/j.oceaneng.2015.05.035

He, J., Men, X., Jiao, B., Lin, H., Sun, H., & Lin, X. (2024). Coupled aero–hydrodynamic analysis in floating offshore wind turbines: A review of numerical and experimental

methodologies. *Marine Science and Engineering*, *12*. https://doi.org/10.3390/jmse12122205

Huang, Y., Zhuang, Y., & Wan, D. (2020). Hydrodynamic study and performance analysis of the OC4-DeepCWind platform by CFD method. *Computational Methods*. https://doi.org/10.1142/S0219876220500206

IEC standard. rule note ni 572 dt r02 e. (2005).

IRENA. (2024). Renewable energy highlights. [See Online]. *International Renewable Energy Agency*.

Irons, B., & Tuck, R. (1969). A version of the aitken accelerator for computer iteration. *Numerical Methods in Engineering*, *1*, 275–277. https://doi.org/10.1002/nme.1620010306

Jamieson, H., & Branney, M. (2012). Multi-rotors; a solution to 20 mw and beyond? *Energy Procedia*, *24*, 52–59. https://doi.org/10.1016/j.egypro.2012.06.086

Jialong, J., Zhenwei, C., Lisi, H., Caixia, J., & Yanchao, G. (2024). Numerical study on hydroelastic responses and bending-torsion coupled loads of a ship in oblique regular waves. *Ocean Engineering*, *315*. https://doi.org/10.1016/j.oceaneng.2024.119904

Jiao, J., Jiang, Y., Zhang, H., Li, C., & Chen, C. (2018). Predictions of ship extreme hydroelastic load responses in harsh irregular waves and hull girder ultimate strength assessment. *Applied Sciences*, *9*. https://doi.org/10.3390/app9020240

Jonkman, J. (2010). Definition of the floating system for phase IV of OC3 [See Online]. *Technical Report NREL/TP-500-47535*.

Jonkman, J., Butterfield, S., Musial, W., & Scott, G. (2009). Definition of a 5-MW reference wind turbine for offshore system development. *Technical Report NREL/TP-500-38060*. https://doi.org/10.2172/947422

Jonkman, J., Damiani, R., Branlard, E., Hall, M., Robertson, A., & Hayman, G. (2019). Flexibility and member-level load capabilities for floating offshore wind turbines in openfast. *Proceedings of the ASME*. https://doi.org/10.1115/IOWTC2019-7566

Jonkman, J., & L. Buhl Jr., M. (2005). Fast user's guide. [See Online]. *Technical Report NREL/EL-500-38230*.

Jonkman, J., & Musial, W. (2010). Offshore Code Comparison Collaboration (OC3) for IEA Task 23 Offshore Wind Technology and Deployment [See Online]. *Technical Report NREL/TP-5000-48191*.

Jonkman, J., & Sclavounos, P. (2006). Development of fully coupled aeroelastic and hydrodynamic models for offshore wind turbines. *Proceedings of the ASME Wind Energy Symposium Reno*, 9–12. https://doi.org/10.2514/6.2006-995

Jonkman, J. (2007). Dynamics modeling and loads analysis of an offshore floating wind turbine. *Technical Report NREL/TP-500-41958*. https://doi.org/10.2172/921803

Jonkman, J., Robertson, A., & Hayman, G. (2014). Hydrodyn user's guide and theory manual [See Online].

Kim, J., Ahn, H., Seo, B., & Shin, H. (2018). Fatigue analysis at the tower of a 12mw floating offshore wind turbine. *ASME 2018 1st International Offshore Wind Technical Conference*. https://doi.org/10.1115/IOWTC2018-1064

Kwangtae, H., Jun-Bae, K., Youngjae, Y., & Hyoung-Seock, S. (2021). Structural modeling and failure assessment of spar-type substructure for 5 MW floating offshore wind turbine under extreme conditions in the east sea. *Energies*. https://doi.org/10.3390/en14206571

Kyong-Hwan, K., Je-Sung, B., Jung-Hyun, K., Yonghwan, K., Seung-Jo, K., & Yooil, K. (2013). Fully coupled BEM-FEM analysis for ship hydroelasticity in waves. *Marine Structures*, *33*, 71–99. https://doi.org/10.1016/j.marstruc.2013.04.004

Lamei, A., Hayatdavoodi, M., & Riggs, H. (2023). Motion and elastic response of wind-tracing floating offshore wind turbines. *Ocean Engineering and Marine Energy*, *9*, 43–67. https://doi.org/10.1007/s40722-022-00250-1

Lei, Y., Binbin, L., Kai, Z., Menglan, D., & Xiaobo, C. (2025). Investigation of global and local structural response of semi-submersible FOWT using hydro-structure interaction in the frequency domain. *Applied Ocean Research*, *154*. https://doi.org/10.1016/j.apor.2024.104318

Li, H., Gao, Z., Bachynski-Polić, E., Zhao, Y., & Fiskvik, S. (2023). Effect of floater flexibility on global dynamic responses of a 15-Mw semi-submersible floating wind turbine. *Ocean Engineering*, *286*. https://doi.org/10.1016/j.oceaneng.2023.115584

Li, H., Hu, Z., Wang, J., & Meng, X. (2018). Short-term fatigue analysis for tower base of a spar-type wind turbine under stochastic wind-wave loads. *Naval Architecture*, *10*. https://doi.org/10.1016/j.ijnaoe.2017.05.003

Malenica, S. (2007). Hydro structure interactions in seakeeping. *International Workshop on Coupled Methods in Numerical Dynamics*.

Marten, D., Saverin, J., Behrens de Luna, R., & Perez-Becker, S. (2022). Qblade documentation. Release 2.0.4. https://doi.org/10.13140/RG.2.2.19363.12326/2

Martin, R. (2022). Coupled dynamics of multi wind turbine floating platforms. [See Online]. *Escuela Técnica Superior de Ingeniería Aeronáutica y del Espacio*.

Martín-San-Román, R., Benito-Cia, P., Azcona-Armendáriz, J., & Cuerva-Tejero, A. (2021). Validation of a free vortex filament wake module for the integrated simulation of multi-rotor wind turbines. *Renewable Energy*, *179*, 1706–1718. https://doi.org/10.1016/j.renene.2021.07.147

Martín-San-Román, R., Benito-Cia, P., Azcona-Armendáriz, J., & Cuerva-Tejero, A. (2022). Influence of lateral rotor spacing on the benefits in power generated by multi-rotor configurations. *Journal of Physics: Conference Series*. https://doi.org/10.1088/1742-6596/2362/1/012024

Matos, V., Simos, A., & Sphaier, S. (2011). Second-order resonant heave, roll and pitch motions of a deep-draft semi-submersible: Theoretical and experimental results. *Ocean Engineering*, *38*, 2227–2243. https://doi.org/10.1016/j.oceaneng.2011.10.005

McCoy, A., Musial, W., Hammond, R., Mulas, D., Duffy, P., Beiter, P., Pérez, P., Ruth, B., Reber, G., & Spitsen, P. (2024). Offshore wind market report: 2024 edition. [See Online]. *Technical Report NREL/TP-5000-90525*.

Mei, X., & Xiong, M. (2021). Effects of second-order hydrodynamics on the dynamic responses and fatigue damage of a 15 MW floating offshore wind turbine. *Marine Science and Engineering*, *9*. https://doi.org/10.3390/jmse9111232

Moriarty, P., & Hansen, A. (2005). Aerodyn theory manual [See Online]. *NREL/TP-500-36881*.

Oberhagemann, J., Shigunov, V., Radon, M., Mumm, H., & Won, S. (2015). Two- and three-dimensional springing analysis of a 16,000 TEU container ship in regular waves. *Ships and Offshore Structures*, *5*, 498–509. https://doi.org/10.1080/17445302.2015.1014255

Orcaflex documentation. [https://www.orcina.com/webhelp/OrcaFlex/Default.htm Accessed on 5 July 2024]. (n.d.).

Otter, A., Murphy, J., Pakrashi, V., Robertson, A., & Desmond, C. (2021). A review of modelling techniques for floating offshore wind turbines. *Wind Energy*, *25*. https://doi.org/10.1002/we.2701

Pacheco-Blazquez, R., Garcia-Espinosa, J., Di-Capua, D., & Pastor-Sanchez, A. (2024). A non-linear finite element method on unstructured meshes for added resistance in waves. *Marine Science and Engineering*. https://doi.org/10.3390/jmse12040573

Park, S., & Choung, J. (2023). Structural design of the substructure of a 10 MW floating offshore wind turbine system using dominant load parameters. *Marine Science and Engineering*. https://doi.org/10.3390/jmse11051048

Partovi-Mehr, N., DeFrancisci, J., Minaeijavid, M., Moaveni, B., Kuchma, D., D.P.Baxter, C., M. Hines, E., & S. Bradshaw, A. (2024). Fatigue analysis of a jacket-supported offshore wind turbine at block island wind farm. *Marine Science and Engineering*, *24*. https://doi.org/10.3390/s24103009

Patalano, S., Mango Furnari, A., Vitolo, F., & et al. (2019). A critical exposition of model order reduction techniques: Application to a slewing flexible beam. https://doi.org/10.1007/s11831-019-09369-1

Ramachandran, G., Robertson, A., Jonkman, J., & Masciola, M. (2013). Investigation of response amplitude operators for floating offshore wind turbines. [See Online]. *Proceedings of the 23rd International Ocean, Offshore and Polar Engineering Conferenc.*

Ran, X., Leroy, V., & Bachynski-Polić, E. (2023). Hydroelastic response of a flexible spar floating wind turbine: Numerical modelling and validation. *Ocean Engineering*, *286*. https://doi.org/10.1016/j.oceaneng.2023.115635

Reddy, L., Milano, D., Walker, J., & Viré, A. (2022). Validation of CFD determined hydrodynamic coefficients for a semisubmersible floating offshore wind turbine. *Physics: Conference Series*. https://doi.org/10.1088/1742-6596/2265/4/042012

Roald, L., Jonkman, J., & Robertson, A. (2014). The effect of second-order hydrodynamics on a floating offshore wind turbine [See Online]. *Technical Report NREL/TP-5000-61452*.

Roald, L., Jonkman, J., Robertson, A., & Chokani, N. (2013). The effect of second-order hydrodynamics on floating offshore wind turbines. *Energy Procedia*, *35*. https://doi.org/10.1016/j.egypro.2013.07.178

Robertson, A., Jonkman, J., Masciola, M., Molta, P., Goupee, A., Coulling, A., Prowell, I., & Browning, J. (2013). Summary of conclusions and recommendations drawn from the deepcwind scaled floating offshore wind system test campaign. *32rd International Conference on Ocean, Offshore and Arctic Engineering*. https://doi.org/10.1115/OMAE2013-10817

Robertson, A., Jonkman, J., Masciola, M., Song, H., Goupee, A., Coulling, A., & Luan, C. (2014). Definition of the semisubmersible floating system for phase II of OC4. *Technical Report NREL/TP-5000-60601*. https://doi.org/10.2172/1155123

Robertson, A., Jonkman, J., Vorphal, F., Popko, W., Qvist, J., Frøyd, L., Chen, X., Azcona, J., Uzunoglu, E., Guedes Soares, C., Luan, C., & Yutong, H. (2014). Offshore code comparison collaboration continuation within IEA wind task 30: Phase II results regarding a floating semisubmersible wind system. *33rd International Conference on Ocean, Offshore and Arctic Engineering*. https://doi.org/10.1115/OMAE2014-24040

Sayed, M., Lutz, T., Krämer, E., Shayegan, S., & Wüchner, R. (2019). Aeroelastic analysis of 10 MW wind turbine using CFD–CSD explicit FSI-coupling approach. *Fluids and Structures*, *87*, 354–377. https://doi.org/10.1016/j.jfluidstructs.2019.03.023

Servan-Camas, B. (2016). A time-domain finite element method for seakeeping and wave resistance problems- doctoral thesis. [See Online]. *Universidad Politécnica de Madrid*.

Servan-Camas, B., Berdugo-Parada, I., & Garcia-Espinosa, J. (2025). Modal matrix reduction for fully coupled integrated load analysis of floating structures. *Under review - Marine Structures*.

Servan-Camas, B., Di-Capua, D., Garcia-Espinosa, J., & Sa-Lopez, D. (2021). Fully 3d ship hydroelasticity: Monolithic versus partitioned strategies for tight coupling. *Marine Structures*, *80*. https://doi.org/10.1016/j.marstruc.2021.103098

Servan-Camas, B., & Garcia-Espinosa, J. (2013). Accelerated 3d multi-body seakeeping simulations using unstructured finite elements. *Computational Physics*, *252*, 382–403. https://doi.org/10.1016/j.jcp.2013.06.023

Servan-Camas, B., Gutierrez-Romero, J., & Garcia-Espinosa, J. (2018). A time-domain second-order fem model for the wave diffraction-radiation problem. *Marine Structures*, *58*, 278–300. https://doi.org/10.1016/j.marstruc.2017.12.001

Serván-Camas, B., Cercós-Pita, J., Colom-Cobb, J., García-Espinosa, J., & Souto-Iglesias, A. (2015). Time domain simulation of coupled sloshing–seakeeping problems by sph–fem coupling. *Ocean Engineering*, *123*, 383–396. https://doi.org/10.1016/j.oceaneng.2016.07.003

Sesam feature description. [See Online]. (2022).

Shengtao, Z., Chao, X., L and Yiqing, Xiaolu, X., W and Wenyuan, & Qing, S. (2023). Evaluation of floating wind turbine substructure designs by using long-term dynamic optimization. *Applied Energy*. https://doi.org/10.1016/j.apenergy.2023.121941

Song, F., Guiyong, Z., Decheng, W., Shengchao, J., Zhe, S., & Zhi, Z. (2021). On the treatment of hydroelastic slamming by coupling boundary element method and modal superposition method. *Applied Ocean Research*, *112*. https://doi.org/10.1016/j.apor.2021.102595

Song, H., Damiani, R., Robertson, A., & Jonkman, J. (2013). A new structural-dynamics module for offshore multimember substructures within the wind turbine computer-aided engineering tool FAST. [See Online]. *Conference Paper NREL/CP-5000-5809*.

Song, X., Bi, X., Liu, W., & Guo, X. (2024). Numerical simulation of a floating offshore wind turbine in wind and waves based on a coupled CFD–FEA approach. *Marine Science and Engineering*. https://doi.org/10.3390/jmse12081385

Steinacker, H., Lemmer, F., Raach, S., Schlipf, D., & Wen Cheng, P. (2022). Efficient multibody modeling of offshore wind turbines with flexible substructures. *Physics: Conference Series*. https://doi.org/10.1088/1742-6596/2265/4/042007

Subbulakshmi, A., Verma, M., Keerthana, M., Sasmal, S., Harikrishna, P., & Kapuria, S. (2022). Recent advances in experimental and numerical methods for dynamic analysis of floating offshore wind turbines — An integrated review. *Renewable and Sustainable Energy Reviews*, *164*. https://doi.org/10.1016/j.rser.2022.112525

Tan, Z., Peng-Nan, S., Nian-Nian, L., Zhe, L., Hong-Guan, L., & Rong-Hua, Z. (2023). SPH simulation and experimental validation of the dynamic response of floating offshore wind turbines in waves. *Renewable Energy*, *205*. https://doi.org/10.1016/j.renene.2023.01.081

Tian, Y., Zhong, Y., Liu, H., Liu, W., Kong, F., & Chen, H. (2024). Modal matrix reduction for fully coupled integrated load analysis of floating structures. *Renewable Energy*, *229*. https://doi.org/10.1016/j.renene.2024.120765

Van der Laan, M., Andersen, S., García, N., Angelou, N., & et al. (2019). Power curve and wake analyses of the vestas multi-rotor demonstrator. *Wind Energy Science*, *4*, 251–271. https://doi.org/10.5194/wes-4-251-2019

Vigara, F., Cerdán, L., Durán, R., Muñoz, S., Lynch, M., Doole, S., Molins, C., Trubat, P., & Guanche, R. (2019). Corewind. d1.2 design basis. [See Online].

Wang, Y., Chen, H.-C., Koop, A., & Vaz, G. (2022). Hydrodynamic response of a FOWT semi-submersible under regular waves using CFD: Verification and validation. *Ocean Engineering*, *258*. https://doi.org/10.1016/j.oceaneng.2022.111742

Wiegard, B., König, M., Lund, J., Radtke, L., Netzband, S., Abdel-Maksoud, M., & Düster, A. (2021). Fluid-structure interaction and stress analysis of a floating wind turbine. *Marine Structures*, *78*. https://doi.org/10.1016/j.marstruc.2021.102970

Xie, S., He, J., Zhang, C., Kan, Y., Ma, J., & Zhang, Z. (2023). Aero-hydro-servo-elastic coupled modeling and dynamics analysis of a four-rotor floating offshore wind turbine. *Ocean Engineering*, *272*. https://doi.org/10.1016/j.oceaneng.2023.113724

Xiong, X.-L., Laima, S., & Li, H. (2023). Experimental study of the wake of multi-rotor turbine. *Ocean Engineering*, *269*. https://doi.org/10.1016/j.oceaneng.2022.113594

Xuemin, S., Xueqing, B., Weiqin, L., & Xiaoxuan, G. (2024). Numerical simulation of a floating offshore wind turbine in wind and waves based on a coupled CFD–FEA approach. *Marine Science and Engineering*, *12*. https://doi.org/10.3390/jmse12081385

Yao, T., Lu, Q., Wang, Y., Zhang, Y., Kuang, L., Zhang, Z., Zhao, Y., Han, Z., & Shao, Y. (2023). Numerical investigation of wake-induced lifetime fatigue load of two floating wind turbines in tandem with different spacings. *Ocean Engineering*, *285*. https://doi.org/10.1016/j.oceaneng.2023.11546

Zhang, W., Calderon-Sanchez, J., Duque, D., & Souto-Iglesias, A. (2024). Computational fluid dynamics (CFD) applications in floating offshore wind turbine (FOWT) dynamics: A review. *Applied Ocean Research*, *150*. https://doi.org/10.1016/j.apor.2024.104075

Annex: CIMNE-DeepCwind Structural Definition

The structural details of the CIMNE-DeepCwind model are presented below, organized by components. This structural model will be made available upon request. The overall structural concept is shown in Figure A1.

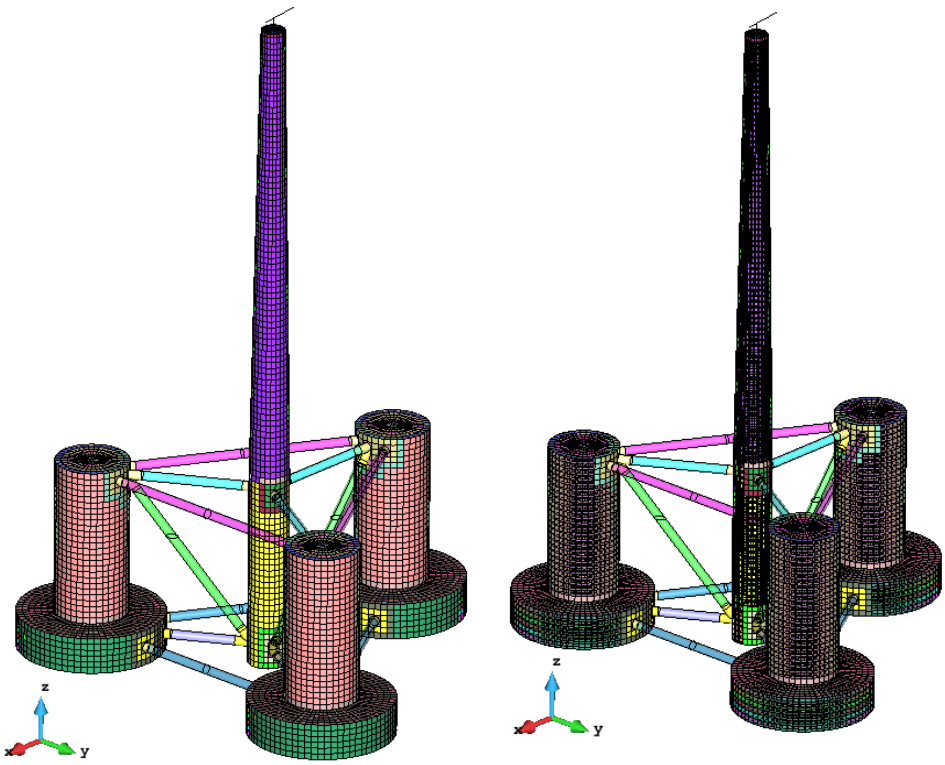

Figure A1: Left: external structural model. Right: inner reinforcements.

The component steel properties as well as stiffeners distribution is given for: the central column, outer columns, heave plates, tower and bracing. The plate thickness is consistent throughout the entire component, including the reinforcements.

Wind turbine: the wind turbine components are included in the model with punctual masses located at their respective center of mass, see Figure A2.

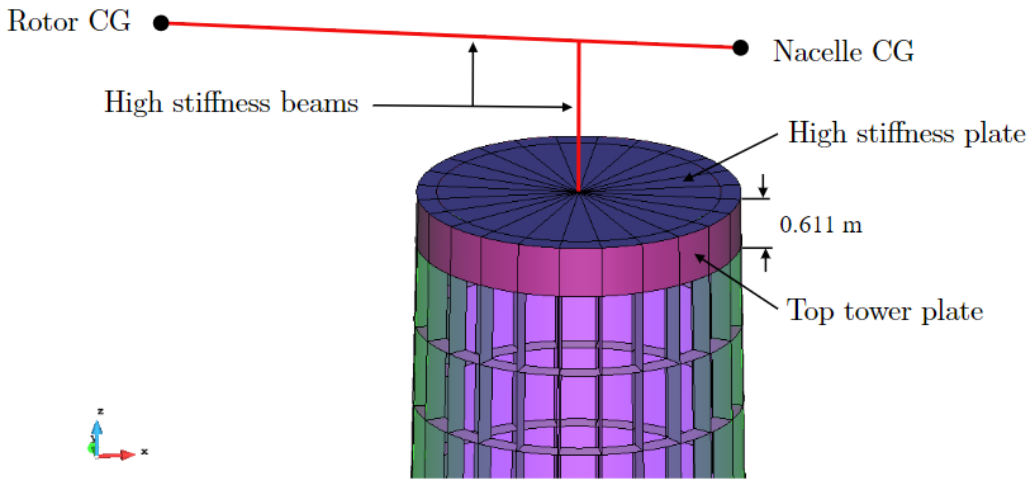

Figure A2: Wind turbine beam structural model.

The point masses are connected to the top of the tower in the model using high-stiffness, low-density beams. The beam properties are provided in Table A1.

Table A1: Turbine beams particulars.

	Beam Steel Data
Width y, z [mm]	1000, 1000
Young modulus [GPa]	210
Torsion modulus [GPa]	81
Density [kg/m^3]	10.2

Additionally, a high-stiffness plate with considerable thickness is used to transfer the turbine loads to the top of the tower. The final plate at the top of the tower has different properties from the rest of the tower to ensure a smoother load transfer. The steel particulars are presented in Table A2.

Table A2: Turbine load transfer components.

	Turbine Steel Plate	Top Tower Steel plate
Thickness [mm]	1000	19
Young modulus [GPa]	2100	210
Poisson coefficient [-]	0.3	0.3
Density [kg/m^3]	0.102	8500

Central column: the cross-sectional view, dimensions, and stiffener details are presented in Figure A3. Additional reinforcement is given to the area near the tower base.

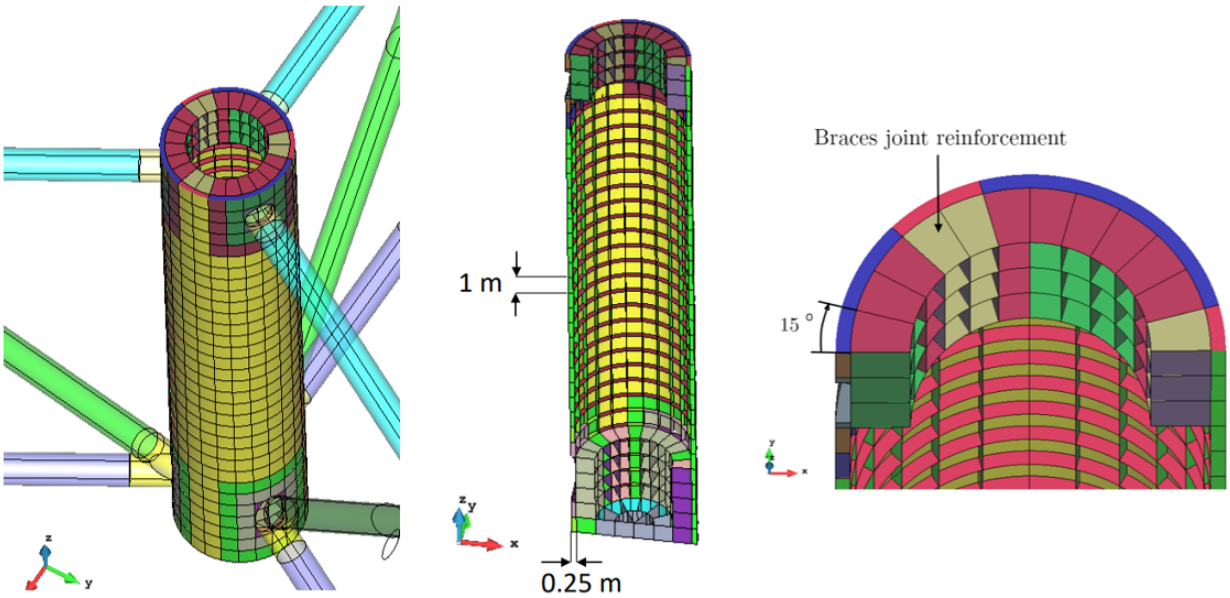

Figure A3: Left: intersection with braces. Middle: cross-section. Right: top close-up view.

The central column steel properties are provided in Table A3, while the stiffeners distribution is detailed in Table A4. The outer columns share the same steel properties.

Table A3: Central column steel properties.

	Central Column Plates
Thickness [mm]	20
Young modulus [GPa]	210
Poisson coefficient [-]	0.3
Density [kg/m^3]	7845

Table A4: Central column stiffeners particulars.

Central Column Stiffeners Data	
Number of rings [-]	31
Number of longitudinals [-]	24
Number of radials [-]	24
Separation between rings [m]	1
Radial separation between longitudinals [º]	15
Stiffeners width [m]	0.25
Braces joint stiffeners width [m]	1

Outer columns: the cross-section view, measures and stiffeners details are provided in Figure A4. The column begins at the double bottom of the heave plate.

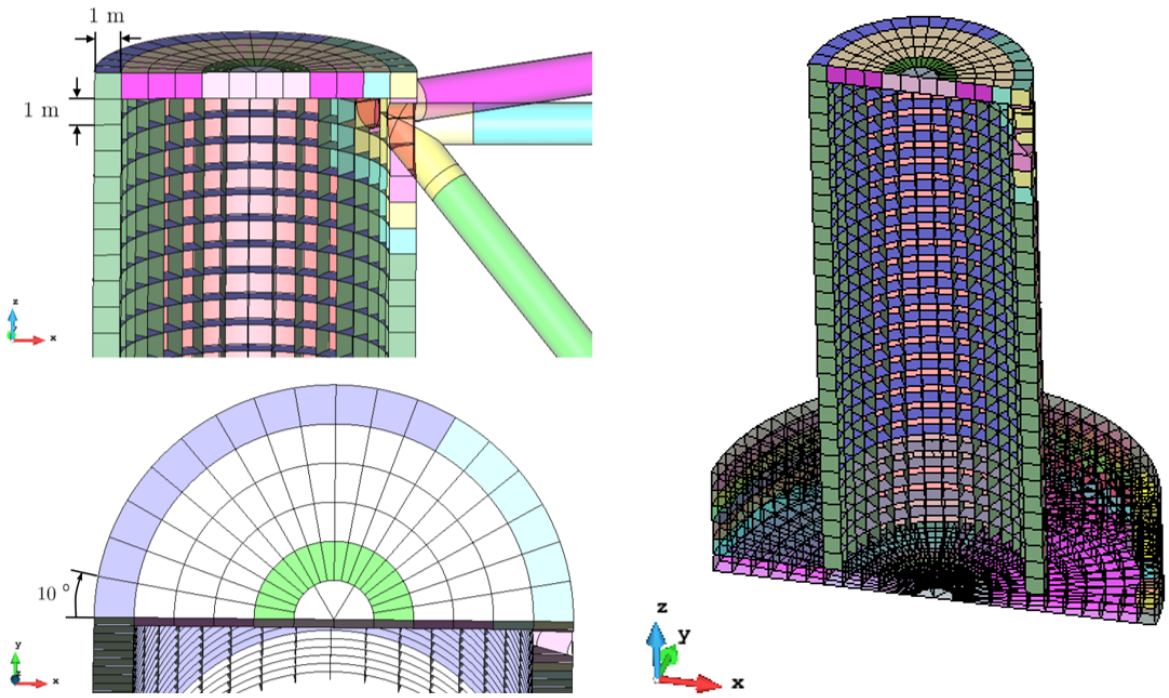

Figure A4: Left: column details and measures. Right: column cross-section.

The steel properties are given in Table A5, and the stiffener distribution in Table A6.

Table A5: Outer columns steel properties.

	Outer Columns Plates
Thickness [mm]	20
Young modulus [GPa]	210
Poisson coefficient [-]	0.3
Density [kg/m^3]	7845

Table A6: Column stiffeners particulars.

Column Stiffeners Data	
Number of rings [-]	30
Number of longitudinals [-]	36
Number of radials [-]	36
Separation between rings [m]	1
Radial separation between longitudinals [º]	10
Stiffeners width [m]	1

Heave plates: the cross-section view, measures and stiffeners details are shown in Figure A5.

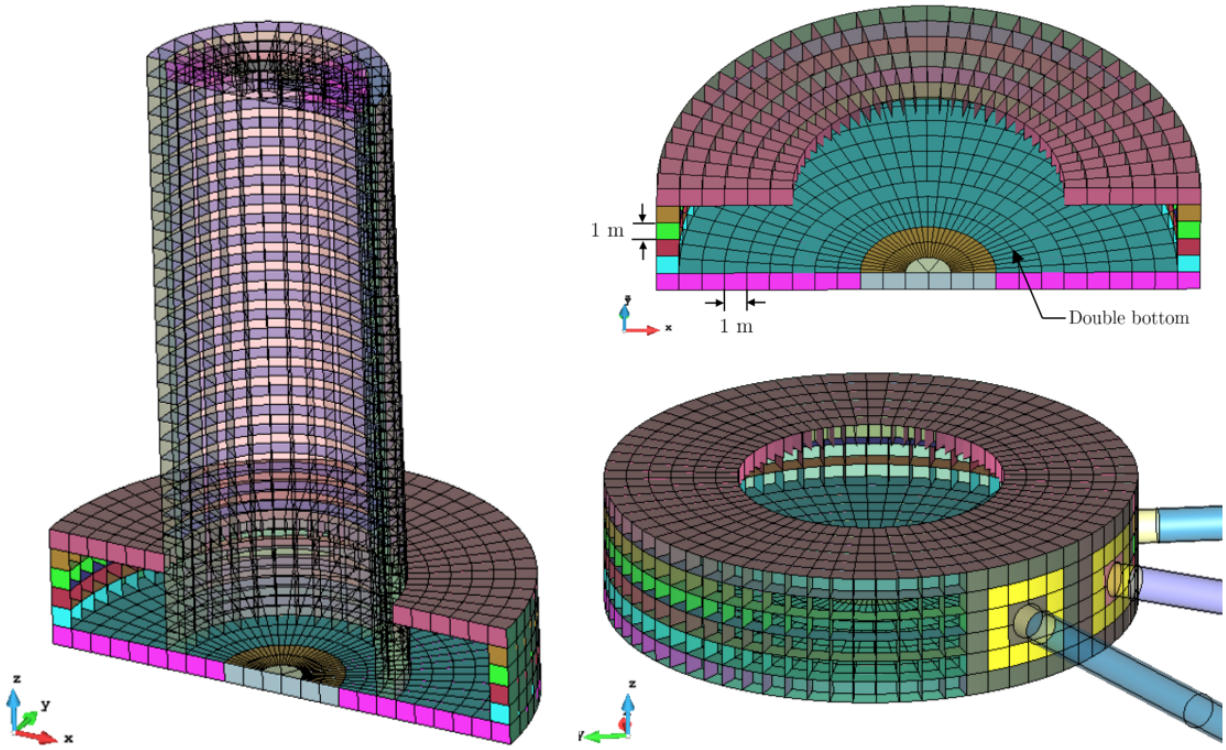

Figure A5: Left: intersection heave plate-column. Right: visibility of the heave plate stiffeners.

The heave plate steel properties are provided in Table A7, while the stiffeners distribution is detailed in Table A8.

Table A7: Heave plates steel properties.

	Heave Plates Data
Thickness [mm]	30
Young modulus [GPa]	210
Poisson coefficient [-]	0.3
Density [kg/m^3]	7845

Table A8: Heave plate stiffeners particulars.

Heave Plate Stiffeners Data	
Number of rings [-]	11
Number of longitudinals [-]	72
Number of radials [-]	72
Separation between rings [m]	1
Radial separation between longitudinals [º]	5
Stiffeners width [m]	1

Tower: the cross-section view and stiffeners details are shown in Figure A6.

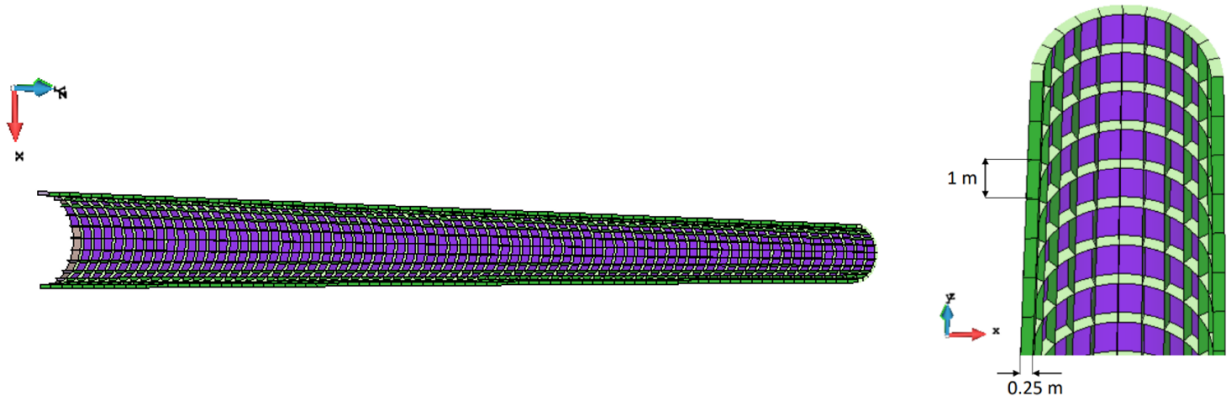

Figure A6: Left: tower cross-section view. Right: tower-top close-up view.

The tower steel properties are provided in Table A9, while the stiffeners distribution is detailed in Table A10.

Table A9: Tower steel properties.

	Tower Plates
Thickness [mm]	14
Young modulus [GPa]	210
Poisson coefficient [-]	0.3
Density [kg/m^3]	8500

Table A10: Tower stiffeners particulars.

Tower Stiffeners Data	
Number of rings [-]	77
Number of longitudinals [-]	24
Separation between rings [m]	1
Radial separation between longitudinals [º]	15
Stiffeners width [m]	0.25

Bracing: the details of the bracing-columns intersections and close-up views are given in Figure A7. Additional reinforcement is given to the intersections between braces and columns.

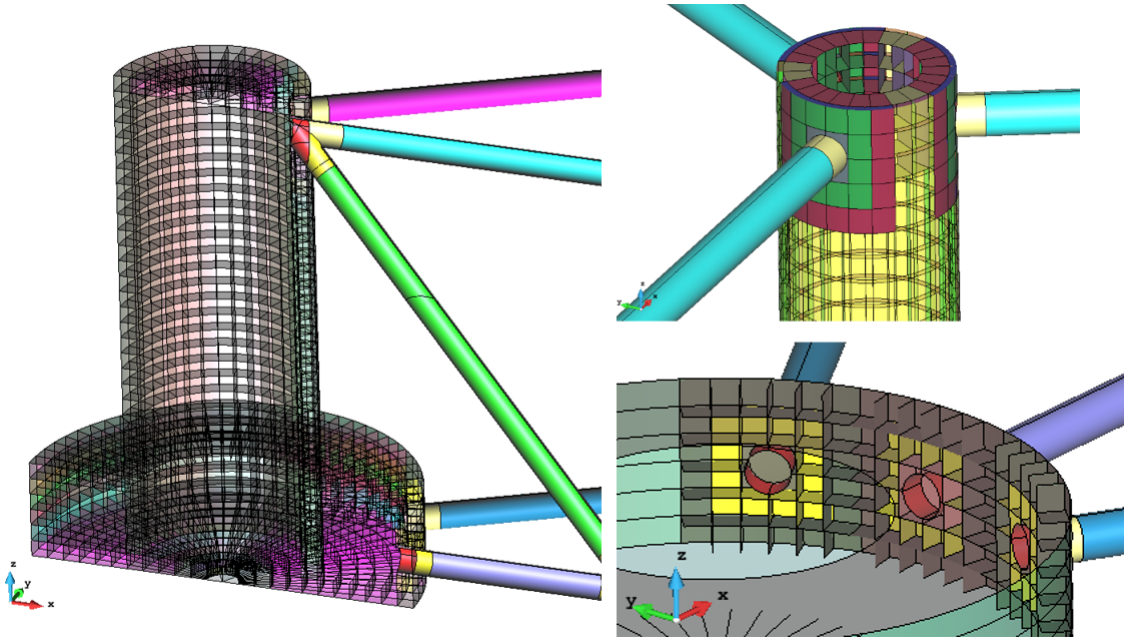

Figure A7: Intersections between braces and columns.

The bracing steel properties are provided in Table A11.

Table A11: Braces steel properties.

	Braces Plates
Thickness [mm]	17.5
Young modulus [GPa]	210
Poisson coefficient [-]	0.3
Density [kg/m^3]	7845